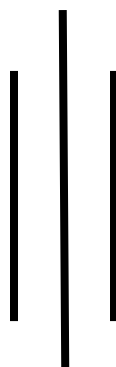




# **Generation and Characterisation of Viral Protease-Dependent Reporter Systems to Monitor Orthoflavivirus Infections in Living Cells**



**By: Susmita Shrestha**

**A thesis submitted for degree of Masters of Biotechnology**

**College of Medicine and Public Health**

**Molecular Virology Group**

**02/06/2025**

**Supervisor: Dr. Nicholas Eyre**

**Co-supervisor: Prof. Jill Carr**

# TABLE OF CONTENTS

<b>Chapter One: Introduction .....</b>	<b>1</b>
1.1 Background .....	1
1.2 Overview on Orthoflaviviruses .....	2
1.2.1 Epidemiology and Disease Burden.....	3
1.2.2 Orthoflavivirus Protease NS2B-NS3 as a Promising Antiviral Drug Target .....	3
1.2.3 Role of NS2B/NS3 in DENV, WNV, and ZIKV .....	5
1.2.4 Dengue Virus Life Cycle .....	6
1.2.5 Transmission Cycle of DENV, WNV, and ZIKV .....	8
1.3 Generation of Viral Protease-Dependent Reporter Systems for DENV, WNV and ZIKV .....	10
1.4 Characterisation of Reporter Systems for DENV, ZIKV and WNV .....	12
1.5 Reporter cell lines to characterise the antiviral activity of small molecule antiviral drug candidates: current approaches for DENV, ZIKV and WNV .....	13
1.6 Dengue Virus Reporter Cell Line for Screening Antiviral Drug Candidate: JNJ-A07 Inhibitor .....	14
1.7 Limitations/Knowledge Gap in generation of engineered reporter systems and antiviral drug discovery.....	16
1.8 Research Question and Rationale .....	17
1.8.1 Aims.....	17
<b>Chapter Two: Materials and Methods.....</b>	<b>18</b>
2.1 Materials.....	18
2.1.1 Cell Culture Media and Composition .....	18
2.1.2 Cell Culture Media and Reagents Used to Maintain Cells .....	18
2.1.3 Reagents used for Lentiviral Packaging and Production.....	19
2.1.4 Reagents and Materials for Routine Laboratory Procedures .....	20
2.1.5 Primary Antibodies Used for Immunofluorescent (IF) Staining and Western Blot Experiments .....	23

2.1.6 Secondary Antibodies Used for Immunofluorescent (IF) Staining and Western Blot Experiments .....	23
2.1.7 Stable Cell Lines .....	24
2.1.8 Primers used for PCR and Sanger Sequencing .....	24
2.1.9 Plasmid Vectors .....	25
2.1.10 Synthetic gBlocks Gene Fragments (Integrated DNA Technologies) Utilized for Construction of pTRIPZ_3XNLS_mScarlet3_DENVpr_mStayGold, pTRIPZ_3XNLS_mScarlet3_WNVpr_mStayGold, and pTRIPZ_3XNLS_mScarlet3_ZIKVpr_mStayGold .....	26
2.2 Methods .....	28
2.2.1 Cell Growth and Maintenance .....	28
2.2.2 Cryopreservation and Resuscitation of Cell Lines .....	29
2.2.3 Seeding cells in 6-well plate, 12-well plate and 96-well plate in Tissue Culture lab .....	29
2.2.4 Cell Transfection .....	30
2.2.5 Lentivirus Production and Transduction of target cells .....	33
2.2.6 FACS (Fluorescence Activated Cell Sorting) to enrich fluorescent (mStayGold-positive) cells .....	35
2.2.7 Live cell imaging to monitor protease-dependent nuclear translocation of mStayGold fluorescent protein using the Incucyte SX5 imaging system.....	35
2.2.8 Immunofluorescent Staining of DENV2 infected and uninfected cells and Confocal Microscopy Imaging using Cytation 5 .....	36
2.2.9 JNJ-A07+Huh7.5+eGFP DENVpr_pTRIPZ_3XNLS_mScarlet3 Incucyte experiment to characterise the antiviral activity of JNJ-A07 drug candidate.....	36
2.2.10 Molecular Cloning .....	37
2.2.11 Cellular protein extraction and Western Blot Analysis .....	42
2.2.12 Bioinformatics Analysis .....	44
<b>Chapter Three: Results .....</b>	<b>45</b>
3.1 Gel Electrophoresis of Plasmid Backbone (pTRIPZ_3XNLS_mScarlet3) after restriction digest .....	45
3.2 Generation of pTRIPZ_3XNLS_mScarlet3_WNVpr_mStayGold and pTRIPZ_3XNLS_mScarlet3_ZIKVpr_mStayGold reporter construct .....	46

3.3 Lentivirus Transfection of pTRIPZ_3XNLS_mScarlet3_WNVpr_mStayGold and pTRIPZ_3XNLS_mScarlet3_ZIKVpr_mStayGold into HEK293FT cells using Lipofectamine 2000 and Lipofectamine 3000 protocol .....	49
3.4 Inefficient production of infectious lentiviral vectors capable of transducing Huh7.5 cells after repeated and careful transfection of pTRIPZ_3XNLS_mScarlet3_WNVpr_mStayGold, and pTRIPZ_3XNLS_mScarlet3_ZIKVpr_mStayGold with lentiviral packaging plasmids into 293FT cells .....	52
3.5 Fluorescent Activated Cells Sorting (FACS) of Huh7.5+ pTRIPZ_3XNLS_mScarlet3_DENVpr_mStayGold reporter proteins for obtaining high fluorescent positive cells .....	53
3.6 Characterization of DENV, WNV, and ZIKV Protease Reporter Construct Design .....	55
3.7 Incucyte live cell imaging of nuclear relocation of the protease-dependent mStayGold reporter proteins following DENV2 infection at different Hours Post Infection (h.p.i) and Multiplicity of Infection (MOI) .....	57
3.8 Immunofluorescence analysis of Dengue Virus Reporter Protease (DENVpr) shows activation of viral protease in infected versus uninfected cells .....	62
3.9 Western Blot Analysis of Huh-7.5+eGFP DENVpr+pTRIPZ_3XNLS_mScarlet3 and Huh-7.5+eGFP ZIKVpr+pTRIPZ_3XNLS_mScarlet3 cell line showed the cleavage properties of reporter construct upon infection with Dengue and Zika viruses .....	63
3.10 Time-course experiments confirms early nuclear translocation of the protease-dependent mStayGold reporter proteins after transient transfection following West Nile and Zika virus infection .....	65
3.11 JNJ-A07 inhibits reporter-detected viral protease activity in infected cells validate the functioning of eGFP DENVpr reporter cell line for antiviral drug screening .....	68
<b>Chapter Four: Discussion .....</b>	<b>71</b>
<b>Bibliography .....</b>	<b>80</b>
<b>Appendices .....</b>	<b>91</b>

# LIST OF FIGURES

<b>Figure 1.2.2:</b> Structure and overview of orthoflavivirus genome and encoded polyprotein.....	5
<b>Figure 1.2.3:</b> Symbolic representation of cleavage sites in polyproteins processed by NS2B-NS3 proteases.....	6
<b>Figure 1.2.4:</b> Lifecycle of Dengue Virus.....	7
<b>Figure 1.2.5:</b> Transmission Cycle of orthoflaviviruses: Dengue, West Nile and Zika Virus.....	9, 10
<b>Figure 1.6:</b> Structure of JNJ-A07 inhibitor targeting DENV non-structural proteins interactions.....	15
<b>Figure 2.2.5:</b> Lentiviral production workflow using second-generation lentiviral packaging plasmids.....	34
<b>Figure 3.1:</b> Agarose gel electrophoresis of pTRIPZ_3XNLS_mScarlet3 plasmid backbone digested with <i>Bsr</i> GI-HF. ....	45
<b>Figure 3.2:</b> Molecular cloning to generate the pTRIPZ_3XNLS_mScarlet3_WNVpr_mStayGold and pTRIPZ_3XNLS_mScarlet3_ZIKVpr_mStayGold plasmid reporter construct.....	46
<b>Figure 3.2.1:</b> Diagnostic digest to verify the vector and insert sizes to determine successful cloning. ....	48
<b>Figure 3.3.1:</b> Lentivirus transfection using Lipofectamine 2000 protocol.....	50
<b>Figure 3.3.2:</b> Lentivirus production via transfection of 293FT cells using Lipofectamine 3000 protocol.....	51
<b>Figure 3.5:</b> Fluorescence Activated Cell Sorting of transduced Huh7.5 cells harbouring DENV reporter (mScarlet3 and mStayGold) cells for high fluorescence.....	54
<b>Figure 3.6:</b> Orthoflaviviruses (DENV, WNV, and ZIKV) reporter construct design.....	56
<b>Figure 3.7.1:</b> Live cell imaging of DENVpr reporter construct for nuclear localization of mStayGold (GFP) following DENV2 at MOI 2 (48h.p.i).....	59
<b>Figure 3.7.2:</b> DENV reporter system under uninfected and DENV2-infected conditions at 24h, 36h, and 48h postinfection (h.p.i). ....	61
<b>Figure 3.8:</b> Immunofluorescence imaging of DENV reporter protease using confocal microscopy to analyse reporter activity within uninfected and WT DENV infected conditions.....	63

**Figure 3.9:** Western Blot Analysis of Huh-7.5+eGFP DENVpr+pTRIPZ\_3XNLS\_mScarlet3 and Huh-7.5+eGFP ZIKVpr+pTRIPZ\_3XNLS\_mScarlet3 cell lysates prepared 48h.p.i (MOI=2) with DENV and ZIKV viruses. ....65

**Figure 3.10:** Quantification of WNVpr and ZIKVpr reporter cell line following infection at different time points, 24hours, 48hours, and 72hours. ....67

**Figure 3.11:** Antiviral effect of JNJ-A07 antiviral drug in a DENV2 infection.....69

# LIST OF TABLES

<b>Table 2.1</b> List of all the Materials.....	18 to 27
<b>Table 2.2.2:</b> Components of Freezing Mixtures.....	29
<b>Table 2.2.4.1:</b> Transfection Reagents prepared for Tube A and Tube B.....	30, 31
<b>Table 2.2.4.2:</b> Transfection Reagents prepared for Tube A and Tube B.....	32
<b>Table 2.2.4.3:</b> Transfection Reagents prepared for Tube A and Tube B.....	33
<b>Table 2.2.10.1:</b> Shows the total volume of reagents for performing restriction digest to linearize the plasmid pTRIPZ_3XNLS_mScarlet3.....	37
<b>Table 2.2.10.5:</b> Represents the NEBuilder DNA Assembly reaction protocol, where total of 10µl volume was used for each reaction.....	39
<b>Table 2.2.10.9:</b> Diagnostic Digest of NEBuilder DNA Assembly product with BamHI-HF..	41
<b>Table 2.2.11:</b> Illustrates the reagents used for RIPA buffer preparation.....	43
<b>Table 3.2:</b> Concentration of WNV protease plasmid construct and ZIKV protease plasmid construct.....	47
<b>Table 3.6:</b> List of DENV, WNV, and ZIKV capsid cleavage site sequences.....	57

# LIST OF ABBREVIATIONS

DENV = Dengue Virus

WNV = West Nile Virus

ZIKV = Zika Virus

DENVpr = Dengue Virus Protease

WNVpr = West Nile Virus Protease

ZIKVpr = Zika Virus Protease

ER = Endoplasmic Reticulum

eGFP = endoplasmic Green Fluorescent Protein

ns = not significant

JNJ = Johnson & Johnson

MOI = Multiplicity of Infection

h.p.i = Hours Post Infection

GFP = Green Fluorescent Protein

RFP = Red Fluorescent Protein

FACS = Fluorescence Activated Cell Sorting

RNA = Ribonucleic Acid

C = Capsid

E = Envelope

prM = Precursor Membrane

NS = Non-Structural

HTS = High Throughput Screening

SRIPs = Single-Round Infectious Particle

NLS = Nuclear Localization Signal

FBS/PBS, BSA = Foetal Bovine Serum/Phosphate Buffered Saline, Bovine Serum Albumin

DAPI = 4'6-diamidino-2-phenylindole

# ABSTRACT

In recent years, pathogenic orthoflaviviruses such as Dengue Virus (DENV), West Nile Virus (WNV), and Zika Virus (ZIKV) have affected millions of people worldwide, resulting thousands of death globally. Despite an urgent need, there are no approved antiviral therapies for these viruses. While live cell imaging represents a powerful approach in antiviral drug discovery and testing, current approaches are limited due to difficulties in manipulation of viral genomes and challenges in generation of reliable reporter systems. To overcome these limitations and address knowledge gaps in our understanding of virus-host interactions and antiviral drug efficacy, we sought to generate and characterise viral protease-dependent reporter systems. These systems comprised expression of a green fluorescent protein (GFP ‘mStayGold’) anchored to endoplasmic reticulum (ER) via a Sec61 $\beta$  transmembrane domain and featuring a nuclear localization signal (NLS) separated by specific cleavage peptide sequences that are cleaved by the virally encoded NS2B/NS3 proteases of DENV, ZIKV and WNV. Accordingly, viral infection and cleavage of the reporter construct by the viral NS2B/3 protease was expected to result in nuclear translocation of mStayGold (GFP), allowing detection of infected cells by live cell imaging. We aimed to generate these reporter cell lines via cloning of lentiviral reporter plasmids specific to DENV, WNV, and ZIKV protease (pr), and preparation of replication-defective lentiviral vectors. Despite successful cloning and transfection, generation of stable reporter cell lines for WNVpr and ZIKVpr reporter constructs could not be achieved. However, we sought to validate the plasmid constructs via transient transfection of HeLa cells using the WNVpr and ZIKVpr reporter plasmids. Additionally, we were able to improve the properties of a previously generated stable reporter cell line for DENVpr via Fluorescence Activated Cell Sorting (FACS) to obtain stronger and more homogenous expression of the fluorescent protein component of the reporter, mStayGold. Virus infection experiments were performed in the DENVpr, WNVpr, and ZIKVpr reporter cell lines and to further test the functionality and reliability of the reporter cell line, studies of the DENVpr system were performed using the antiviral compound JNJ-A07. The analysis of live cell imaging data for transiently expressed WNVpr and ZIKVpr reporter constructs following infection with the respective viruses (24h.p.i, MOI=2) revealed no significant differences in levels of early nuclear translocation of GFP for, WNV (Kunjin strain) infection compared to uninfected cells. However, ZIKVpr data showed a significant difference (\*,  $p < 0.01$ ) between levels of nuclear GFP translocation for ZIKV uninfected and infected cells at

24h.p.i, assuming comparable infection levels and reporter expression levels, this result suggests Zika Virus NS2B/NS3 protease cleavage efficiency is higher than West Nile Virus NS2B/NS3 protease for early detection (24h.p.i) of infection using equivalent reporter constructs. Notably, the DENVpr reporter system enabled reliable analysis of JNJ-A07 antiviral activity in dose-response studies. Similar functioning of our reporter systems through Western blot analysis using previously generated eGFP tagged DENVpr and ZIKVpr reporter construct cell lines showed the expected viral protease-mediated cleavage of the reporter proteins in DENV- and ZIKV-infected cells. Overall, we have successfully developed reporter systems and supportive data towards achieving our aim of detection of virus infection in living cells via viral protease-dependent fluorescent reporter cleavage events. In spite of the challenges, we propose that our reporter systems might have broad applications in antiviral drug development and analysis of viral replication cycles.

# DECLARATION

I certify that:

1. This thesis does not incorporate without acknowledgement any material previously submitted for a degree or diploma in any university
2. The research within will not be submitted for any other future degree without the permission of Flinders University
3. To best of my knowledge and belief, does not contain any material previously published or written by another person except where due reference is made in the text.

A handwritten signature in black ink, appearing to read 'Susmita Shrestha', with a large, sweeping flourish underneath.

Student Name: **Susmita Shrestha**

Date: 2 June 2025

# ACKNOWLEDGEMENT

I would like to acknowledge my supervisor Dr. Nicholas Eyre, and extend my deepest gratitude for his immense guidance and support throughout my Master's thesis year within Molecular Virology Lab. I would also like to thank my co-supervisor Professor Jill Carr, for her invaluable feedback and support throughout my Master's thesis year.

I am further grateful to the present members of Molecular Virology Group (Dr. Eva Hesping, Siena Centofanti, and Tahir Ali) and previous members (Travis Croft, and Aiden Van Zyl) for their technical help and support, throughout the year.

I would also like to thank Dr. Giles Best for his time to perform flow cytometry procedure and analysis of the flow data.

Lastly, I would like to appreciate the moral and emotional support provided by my partner, family and friends. Thank you for your continuous support.

# Chapter One: Introduction

## 1.1 Background

Within the past ten years, pathogenic orthoflaviviruses, like dengue Virus (DENV), West Nile Virus (WNV), and Zika Virus (ZIKV), have infected millions of people worldwide and impacted their lives resulting in thousands of death globally (Liang & Dai, 2024). Orthoflaviviruses, such as DENV, WNV, and ZIKV, represent as some of the most prevalent RNA viruses and hence pose a significant threat to human health across the globe (Wu et al., 2019). Despite continuous studies, no universal vaccines or specific antiviral therapies have been approved for prevention and treatment against infections caused by these viruses. Thus, effective therapeutic strategies are urgently needed to combat these orthoflaviviruses (Pierson & Diamond, 2020).

The Orthoflavivirus genus includes over 70 known species and orthoflaviviruses that infect humans are usually transmitted to humans via arthropod-borne vectors such as mosquitoes and ticks (Wu et al., 2019). Accordingly, orthoflaviviruses are amongst the largest contributors to zoonotic diseases (Williams et al., 2019). The genus includes clinically important mosquito-borne orthoflaviviruses such as DENV, WNV and ZIKV. Because of increased urbanization and climate change-driven expansion of the major mosquito vectors within the past seven decades, orthoflaviviruses have caused increased rates of transmission (Pierson & Diamond, 2020). Besides infecting humans, certain orthoflaviviruses infect a wide array of animal species, which can then act as virus reservoirs and further complicate efforts to control the spread and impact of these viruses (Chen et al., 2012).

As previous studies have mentioned, orthoflaviviruses induce specialized membrane compartments within the endoplasmic reticulum (ER) that harbor viral RNA replication (Van den Elsen et al., 2021). Furthermore, replication organelles protect viral RNA from host immune responses and provide a platform for efficient RNA synthesis (Stancheva & Sanyal, 2024). All these processes are of immense importance in the development of potential antiviral treatments. Traditionally, microscopy-based studies of infection and ER remodelling in infected cells have used imaging of fixed cells, providing only a static view of infection (Liu

et al., 2020). However, viral replication cycles are dynamic and thus additional insights into aspects of the viral replication cycle and virus-host interactions can be revealed by real-time visualization, including via reporter systems that track the activity of a viral protease (Pahmeier et al., 2021). Such reporter systems can enable deeper insights into virus infection kinetics and interaction of a virus with host cells, and thus facilitate the screening of antiviral compounds. A common technique for live cell imaging of viral infections involves the insertion of a genetically encoded fluorescent tag into the virus genome, enabling the monitoring of infected cells (Corliss et al., 2022). However, the major disadvantage of such an approach is that it requires a functional viral genome clone and a large reporter protein insertion that often result in attenuation of viral replication (Wahaab et al., 2021). Accordingly, identification of a suitable site in a viral genome and encoded protein that may tolerate a reporter insertion can be challenging. An alternative approach is to employ the use of engineered reporter fluorescent proteins that are stably expressed in target cells and are responsive to viral infections (Pahmeier et al., 2021).

Building on this, a reporter system was developed based on an ER anchored green fluorescent protein (GFP) with a nuclear localization signal (NLS) and a specific linker region containing an orthoflavivirus NS2B-NS3 protease cleavage sequence. The notion behind this was, such that, upon infection, the viral protease cleaves the linker and thus releases the GFP from the ER, so that it can translocate into the nucleus (McFadden et al., 2018). Such systems can potentially be generated for the detection of DENV, WNV, and ZIKV infection (Medin et al., 2015). Such approaches may help to bridge significant gaps in our understanding of orthoflavivirus-host cell interactions and facilitate screening of antiviral drug activity through real-time monitoring of infection using live-cell imaging systems. The establishment and characterization of viral protease-dependent reporter systems for pathogenic orthoflaviviruses represents a valuable approach that could help to increase our understanding of the replication cycles of these viruses and facilitate the development of therapeutic strategies.

## **1.2 Overview on Orthoflaviviruses**

The genus Orthoflavivirus comprises predominantly vector-borne, positive-sense RNA viruses, that are mainly transmitted by arthropods, but most importantly mosquitoes and ticks (Williams et al., 2019). These viruses are responsible for several severe human diseases,

including dengue fever, yellow fever, congenital Zika syndrome, West Nile encephalitis, Japanese encephalitis, and tick-borne encephalitis (Thomas et al., 2023). Orthoflaviviruses pose significant concern where vector-borne diseases are prevalent and can cause severe outbreaks (Pierson & Diamond, 2020).

### **1.2.1 Epidemiology and Disease Burden**

The frequency of Orthoflavivirus infections have dramatically increased in recent decades, and are estimated to infect up to 400 million people annually (Liang & Dai, 2024). Dengue virus (DENV) alone affects approximately 390 million individuals each year, with around 500,000 experiencing severe complications, such as dengue haemorrhagic fever or dengue shock syndrome, resulting in approximately 25,000 fatalities annually (Guzman et al., 2016). Importantly, epidemics of WNV and ZIKV have been associated with congenital developmental defects, culminating in outcomes like microcephaly and foetal mortality in various parts of the world (Rasmussen et al., 2017). Factors that contribute to increases in the frequency and magnitude of orthoflavivirus epidemics include increases in the extensive distribution of mosquito and tick vectors because of rapid urbanization and climate change, and increased global travel. Seasonal epidemic patterns of DENV, WNV, and ZIKV are observed in tropical and subtropical regions providing ideal sites for mosquitoes, including *Aedes aegypti* as the principal vector of DENV and ZIKV, and *Culex* mosquitoes harbouring WNV (Nguyen-Tien et al., 2019).

### **1.2.2 Orthoflavivirus Protease NS2B-NS3 as a Promising Antiviral Drug Target**

Orthoflaviviruses are small, enveloped viruses that are approximately 50nm in diameter (Chong et al., 2014). The RNA genome consists of single-stranded, positive-sense RNA of approximately 11kb that encodes three structural proteins: capsid (C), precursor membrane (prM), and envelope (E), in addition to seven non-structural (NS) proteins: NS1, NS2A, NS2B, NS3, NS4A, NS4B, and NS5 (Figure 1.2.2) (Diosa-Toro et al., 2020). Although the envelope protein is crucial for the entry of the virus into host cells, the capsid protein forms the icosahedral nucleocapsid within which the RNA genome of the virus is packaged (Wahaab et al., 2021). The NS proteins are critical for the replication of the RNA genome, evading the host's immune system, and the assembly of new virus particles.

The NS2B-NS3 protease complex is involved in both critical steps of viral polyprotein processing and successful replication. The NS3 protein itself is a multifunctional enzyme which possesses both protease and helicase domains and activities. Specifically, the protease domain, together with its cofactor NS2B, cleaves specific sites within the viral polyprotein: a process that ensures the correct processing of the structural and non-structural proteins and supports viral replication and assembly (Arias-Arias et al., 2020). Meanwhile, the helicase possesses properties for unwinding viral RNA secondary structures in replication, thereby allowing the synthesis of new viral RNA strands (Marecki et al., 2021). NS3 contains an RNA triphosphatase subdomain which is utilized in the formation of the type I 5' RNA cap structure that mimics the host mRNA cap, preventing degradation and assuring efficient translation by the cellular ribosome machinery (van den Elsen et al., 2023). Furthermore, the NS2B/NS3 protease complex can modulate immunological signalling pathways and degradation of host proteins that are involved in innate immune signalling, contributing to an optimal environment for viral propagation (Latanova et al., 2022). The NS2B-NS3 protease complex plays a key role in the life cycle of orthoflaviviruses and is considered an attractive target for antiviral drug development.

Figure removed due to copyright restriction.

**Figure 1.2.2: Structure and overview of orthoflavivirus genome and encoded polyprotein.**

(A) Diagrammatic representations of immature and mature orthoflavivirus particle showing its nucleocapsid, lipid membrane, and glycoproteins in the left-panel. The orthoflavivirus genome and encoded polyprotein are schematically represented in the right panel, where structural proteins (C, prM, E) and non-structural proteins (NS1 to NS5) implicated in replication and virion assembly are highlighted (Zhang et al., 2023). (B) Schematic diagram of viral cleavage products and functions of proteins in viral RNA synthesis and assembly within host cells, including the NS2B/NS3 helicase complex (Murugesan & Manoharan, 2020).

**1.2.3 Role of NS2B/NS3 in DENV, WNV, and ZIKV**

The NS2B/NS3 complex plays a pivotal role not only in viral replication and assembly, but also in pathogenic effects, including via suppressing host immunity by degrading cyclic GMP-

AMP synthase (Wahaab et al., 2021). NS2B complexes with NS3 (Figure 1.2.3) and displays considerable structural flexibility, forming a  $\beta$ -hairpin structure with NS3 that is crucial for its proteolytic activity in the case of ZIKV (Dos Santos Nascimento et al., 2022). This NS2B/NS3 complex is responsible for the cleavage of the viral polyprotein and thus takes an important lead in the overall dynamics of proteolysis (van den Elsen et al., 2023).

Figure removed due to copyright restriction.

**Figure 1.2.3: Symbolic representation of cleavage sites in polyproteins processed by NS2B-NS3 proteases.** Here, Dengue Virus cleavage sites in polyproteins processed by NS2B-NS3 proteases are indicated by a black arrow, West Nile Virus by a red dot, and Zika Virus by green x (Wahaab et al., 2021).

#### 1.2.4 Dengue Virus Life Cycle

The dengue virus (DENV) life cycle begins with the virus attaching to host cell surface receptors, such as DC-SIGN, heparin sulphate, and mannose receptors, which facilitate the virus's entry through receptor-mediated endocytosis into a clathrin-coated vesicle (Figure 1.2.4). Following entry of the virus into the host cell, the viral envelope fuses with the endosomal membrane, releasing the viral genome into the cytoplasm, which is then translated by host ribosomes into a single viral polyprotein and cleaved into individual viral proteins essential for replication and assembly (Roy & Bhattacharjee, 2021). Viral RNA replication occurs in virus-induced membrane structures originating from the ER, where the viral RNA-dependent RNA polymerase, along with other non-structural proteins forms the replication complex (Morita & Suzuki, 2021). The replication process involves synthesizing complementary negative-strand viral RNA, which serves as a template for generating new

positive-strand viral genomes. Viral RNA and proteins are assembled into immature virions at the surface of ER, and resulting immature viral particles are then transported through the trans-Golgi apparatus, and further processed by host enzymes, where they undergo maturation, a crucial step for viral infectivity (Van den Elsen et al., 2021). Finally, the mature virions are released from the host cell through exocytosis, ready to infect new cells.

Various stages of the lifecycle represent potential targets for antiviral drug development. These include, inhibiting viral attachment and entry, targeting the NS2B/NS3 protease to prevent polyprotein cleavage, and blocking NS5 RNA polymerase activity to halt viral replication (Fernandes et al., 2020).

Figure removed due to copyright restriction.

**Figure 1.2.4: Lifecycle of Dengue Virus.** The DENV life cycle begins with virus attachment to host receptors. The virus is then internalized via clathrin-mediated endocytosis, culminating in release of the viral genome into cytoplasm where it can be directly translated by the host ribosome machinery to yield the viral polyprotein, which is cleaved by host and viral protease

to liberate the individual viral proteins. Viral RNA replication occurs in ER-derived vesicle packets and progeny RNA can serve additional rounds of viral RNA replication, viral protein translation or be encapsidated into newly formed viral nucleocapsid which buds into ER and collect a prM/E-studded lipid envelope. Particles then mature in the Golgi and are released from the cell by exocytosis (Sinha et al., 2024).

### **1.2.5 Transmission Cycle of DENV, WNV, and ZIKV**

The transmission cycle in DENV begins when an *Aedes aegypti* mosquito bites a person in the viraemic phase (Figure 1.2.5A) (Carrington & Simmons, 2014). During the extrinsic phase, the virus infects the mosquito's midgut and other tissues before spreading to the salivary glands. The infected mosquito can then transmit the virus to multiple humans while feeding (Murugesan & Manoharan, 2020). After a person is infected, it typically takes 4 to 7 days for symptoms to appear and for them to become capable of transmitting the virus back to mosquitoes (Roy & Bhattacharjee, 2021). Both symptomatic and asymptomatic individuals can pass the dengue virus to mosquitoes.

In contrast, the WNV transmission cycle primarily involves birds as the amplifying hosts, where the virus replicates and reaches a significant viral load in their bloodstream, enabling the infection of *Culex* mosquitoes when they feed (Figure 1.2.5B) (Troupin & Colpitts, 2016). While humans and horses can also host the virus, they are classified as dead-end hosts because their blood does not contain a high enough concentration of the virus to infect mosquitoes.

The sylvatic transmission cycle of ZIKV involves transmission of ZIKV between non-human primates, and *Aedes spp.* mosquitoes, whereas, in the epidemic cycle, it involves humans and urban areas where the *Aedes aegypti* and *Aedes albopictus* mosquitoes transmit the virus from infected humans to other humans (Figure 1.2.5C) (Sharma & Lal, 2017).

Figure removed due to copyright restriction.

Figure removed due to copyright restriction.

Figure removed due to copyright restriction.

**Figure 1.2.5: Transmission Cycle of orthoflaviviruses; Dengue, West Nile and Zika Virus.**

(A) The transmission cycle of dengue virus begins with the bite of an infected *Aedes aegypti* mosquito to humans (Murugesan & Manoharan, 2020). (B) The transmission cycle of West Nile Virus, where birds act as an amplifying host and infect *Culex* mosquitoes when they feed (Troupin & Colpitts, 2016). (C) The transmission cycle of Zika Virus which begins with the non-human primates in sylvatic cycle where *Aedes* mosquitoes spread the virus and in the epidemic cycle, *Aedes aegypti* and *Aedes albopictus* transmit virus between humans (Sharma & Lal, 2017).

### **1.3 Generation of Viral Protease-Dependent Reporter Systems for DENV, WNV and ZIKV**

Reporter systems have been an essential tool in virology to monitor viral infection and replication. Viral protease-dependent reporter systems are reliable as they utilize a reporter signal that is only activated through cleavage by a viral protease. It therefore enhances specificity and temporal tracing of infections in living cells (Campeau et al., 2009). They are developed through the incorporation of viral protease cleavage sites in reporter constructs. For instance, the protease NS2B-NS3 can cleave a cleavage site that is coupled to a fluorescent or luminescent reporter to yield a detectable signal during infection (Pahmeier et al., 2021). This type of approach enables real-time observation of infection and can be adapted to specific orthoflaviviruses by including virus-specific cleavage sites.

In the previous study carried out by Arias-Arias *et al.* (2020), the reporter systems, "FlaviA-GFP", "ZIKVA-GFP", and "DENV2A-GFP" were generated by site-directed mutagenesis from a previously constructed caspase-activatable CA-GFP reporter. Thereby changing its linker region, introducing specific cleavage sites for the NS3 protease of orthoflaviviruses, which are a pan-orthoflaviviral cleavage site (AAQRRGRIG), a ZIKV cleavage site (KTGKRSGAL), and a DENV-2 cleavage site (VKKQRAGVL) (Arias-Arias *et al.*, 2020).

Corliss *et al.* (2022) generated a similar reporter system where a GFP reporter was targeted to the cytoplasm unless viral protease cleavage allowed relocation of the GFP reporter into the nucleus via a simian virus 40 (SV40) nuclear localization signal (NLS) (Corliss *et al.*, 2022). Similarly, Wahaab *et al.* (2021) developed a similar Orthoflavivirus NS2B3 protease cleavage dependent reporter system where the fluorescent reporter is anchored to the ER membrane until its cleavage by viral protease triggers the translocation of the reporter to the nucleus (Wahaab *et al.*, 2021).

Several studies have been performed to generate reporter systems using human and animal cell lines, such as Huh7 (human hepatoma-derived cell line), A549 (lung carcinoma epithelial cell), VeroE6 (continuous line of epithelial cells), and HEK-293T (human embryonal kidney cells) cells (Pahmeier *et al.*, 2021); (McFadden *et al.*, 2018); (Medin *et al.*, 2015); (Wahaab *et al.*, 2021). A plasmid-based reporter system was constructed for monitoring infection with ZIKV; it was named ZIKV-NLS-GFP and was utilized in generating stable reporter cell lines through lentiviral transduction, antibiotic selection, and isolation of GFP-positive cells (McFadden *et al.*, 2018). Similarly, a reporter plasmid, p4B5-EGFP, was similarly designed to monitor proteolytic events during DENV infection because it encodes the DENV NS4B protein, followed by a cleavage site between NS4B and NS5, and a fused enhanced GFP protein (Medin *et al.*, 2015). In this system, the NS2B/NS3 protease cleaves the junction of NS4B-NS5 upon DENV infection, releasing the GFP tag to translocate from the cytoplasm to the nucleus, thus enabling visual monitoring of viral infection through localization of GFP. Real-time protease activity or progression of infection could be monitored in live cells (Hsieh *et al.*, 2017). This construct was confirmed by the amplification of the plasmid through PCR, cloning, and DNA sequencing and consequently, the plasmid DNA was transfected into Vero cells for infection experiments (Arias-Arias *et al.*, 2020; Medin *et al.*, 2015).

Recently, Pahmeier *et al.* (2021) engineered a set of enhanced viral protease-dependent reporter systems that allowed for reliable monitoring of infection with DENV, ZIKV, or SARS-CoV-2 through ER-to-nuclear translocation of fluorescent proteins following cleavage by viral proteins themselves (Pahmeier *et al.*, 2021). Whereas, other studies have developed plasmid-based reporters with fluorescent markers like GFP, that depend on viral protease activity, which often only enable detection of infection and do not allow for host cell structures visualization unless additional markers are co-expressed in cells (Arias-Arias *et al.*, 2020; Cihlova *et al.*, 2021).

#### **1.4 Characterisation of Reporter Systems for DENV, ZIKV and WNV**

Various techniques have been employed to describe reporter systems used in tracking orthoflavivirus infection in living cells. For example Pahmeier *et al.* (2021) thoroughly characterised their reporter systems and cell lines by using immunofluorescence and Western blot analyses to confirm the cleavage of the engineered reporter proteins and nuclear translocation of GFP (Pahmeier *et al.*, 2021).

A study performed by Arias-Arias *et al.* (2020) described the expression of such reporter proteins in *Escherichia Coli*, their purification using Co<sup>2+</sup>-affinity chromatography, and *in vitro* cleavage by DENV-2 and ZIKV proteases, as determined by fluorescence analysis and SDS-PAGE (Arias-Arias *et al.*, 2020). The research study carried out by Corliss *et al.* (2022) aimed to validate the utility of their 'FlavER' reporter construct in the detection of protease activity that is unique to Orthoflavivirus infection (Corliss *et al.*, 2022). U2OS cells expressing FlavER were subjected to transfection with an expression plasmid encoding the wildtype or catalytically inactive mutant DENV protease, which showed that only the active form triggers nuclear translocation of the reporter; an observation confirmed through immunofluorescence and immunoblotting. Furthermore, the reporter system was effective in detecting the protease activity from multiple orthoflaviviruses like DENV, ZIKV, and YFV, suggesting its broader application in compared to that of virus-specific reporters. However, this construct could not enable detection of the protease activity of WNV (Samrat *et al.*, 2022). Time-lapse imaging of DENV-infected cells revealed the real-time translocation of the reporter into the nucleus along with associated ER expansion during infection (Barbier *et al.*, 2017). These results established

the utility of the system in monitoring infection kinetics and organelle remodelling in living cells.

In a study by McFadden *et al.* (2018), A549 cell lines stably expressing the ZIKV-NLS-GFP reporter were analysed for GFP translocation subsequent to ZIKV infection, and various microscopy techniques, such as confocal and wide field fluorescence microscopy, were applied for visualization of these GFP translocation events (McFadden *et al.*, 2018). Moreover, Western blotting, and real-time monitoring of infection dynamics by live-cell imaging was performed to validate protease-specific cleavage of the reporter systems as powerful tools to detect viral activity without disrupting normal cellular functions (Caldas *et al.*, 2020).

## **1.5 Reporter cell lines to characterise the antiviral activity of small molecule antiviral drug candidates: current approaches for DENV, ZIKV and WNV**

Despite significant advances in antiviral drug discovery, there are no targeted antiviral therapies available to combat the viruses effectively, underscoring the urgent need for effective treatment options. Reporter cell lines represent valuable tools to help identify and characterize antiviral drug candidates that will ultimately contribute towards the development of new and urgently required antiviral drug-like compounds.

As demonstrated by the research study conducted by Pahmeier *et al.* (2021) in the application of a SARS-CoV-2 reporter system for drug screening, the antiviral drug remdesivir was tested using both reporter-expressing and non-reporter A549-ACE2 cell lines. Following treatment and infection with SARS-CoV-2, a significant and dose-dependent remdesivir-mediated reduction in the nuclear translocation of the viral protease-dependent reporter was demonstrated, confirming remdesivir's antiviral effect (Pahmeier *et al.*, 2021). Antiviral activities (IC<sub>50</sub> values) of remdesivir that were calculated using the reporter system were shown to be comparable with those determined using traditional viral infectivity (plaque) assays, therefore demonstrating that reporter cell lines can be used as tools for antiviral compound screening and testing with a high degree of reliability (Pruijssers *et al.*, 2020; Xie *et al.*, 2020).

The anti-viral activity of small molecule drug candidates can also be effectively screened and tested using replicon-based reporter systems. Self-replicating sub-genomic viral systems in

which the viral structural genes are replaced by a reporter gene and/or selective marker are called sub-genomic replicons (Hannemann, 2020). For example, antiviral screening can be performed by the insertion of a reporter gene, such as luciferase or a fluorescent protein, into a sub-genomic viral replicon construct such that RNA replication-inhibiting small molecule inhibitors will give rise to a diminished reporter signal, therefore enabling quantification of the antiviral activity of compounds (Li et al., 2016). In general, these reporter-based replicon systems offer a number of advantages for high throughput screening (HTS) of antiviral compounds by making possible the rapid identification of inhibitors that interfere with viral RNA replication (Amarilla et al., 2021). In addition, Fernandes *et al.* (2020) demonstrated that replicon system could be adapted to be stably maintained in cells for long-term screening (Fernandes et al., 2020). However, sub-genomic replicons have a drawback of not being suitable for identification of inhibitors of viral entry or assembly as the absence of structural proteins prevents the formation of infectious particles. Despite their disadvantages, replicon-based assays have been widely utilized for screening possible anti-viral drugs against Orthoflavivirus, including DENV, WNV, and ZIKV.

Targeted phenotypic screens and high-throughput imaging have also facilitated antiviral drug development by revealing new antiviral mechanisms of action (De Clercq & Li, 2016). Reporter cell lines can equally serve in follow-up stages of antiviral drug development, including optimization of second and third-generation compounds (Gupta, 2020). For example, such reporter cell lines played an important role in the chemical innovation strategy that led to the discovery of sofosbuvir and etravirine (Matthew et al., 2021).

## **1.6 Dengue Virus Reporter Cell Line for Screening Antiviral Drug Candidate: JNJ-A07 Inhibitor**

Among all of the rapidly expanding mosquito-borne viral diseases worldwide, dengue is one of the most prevalent diseases and represents a major global public health issue (Sinare & Barkade, 2023). Each year there are estimated to be more than 390 million DENV infections, approximately 500,000 dengue-related hospitalizations and up to 25,000 dengue-induced deaths globally (Srisawat et al., 2022; Yang et al., 2021). Antibody-dependent enhancement (ADE) of infection following a secondary DENV infection with a different serotype is a leading cause of risk of developing life-threatening diseases (Aynekulu Mersha et al., 2024). Although

numerous pharmaceutical industry and academic research teams have undertaken drug discovery efforts to identify antiviral drug candidates, the only available treatment option for dengue is supportive fluid therapy (Chauhan et al., 2024; Hadpech & Thongboonkerd, 2024; Mohsin et al., 2023).

In this study, we sought to employ a previously generated DENV protease-dependent reporter cell line (Huh7.5+eGFP DENVpr+pTRIPZ\_3XNLS\_mScarlet3) for testing the antiviral activity of the small molecule inhibitor JNJ-A07. JNJ-A07 is a pan-serotype DENV inhibitor that is highly potent, with nanomolar to picomolar activity against various clinical isolates based on antiviral activity assays (Bouzidi et al., 2024). Addition of the inhibitor soon after onset of viral RNA synthesis resulted in strong inhibition of viral RNA replication (Kaptein et al., 2021). Importantly, further studies using a clinical analogue of JNJ-A07 known as JNJ-1802 demonstrated potent antiviral efficacy against all DENV serotypes, favourable pharmacokinetic profiles and excellent efficacy in animal models (Goethals et al., 2023). Similarly, JNJ-A07 showed outstanding efficacy against DENV infection in infectious animal models and was shown to prevent the critical interaction of DENV NS4B with NS3 (Figure 1.6) (Kaptein et al., 2021). Taken together, these studies have shown that JNJ-A07 and JNJ-1802 are pharmacologically safe and effective against all four DENV serotypes, supporting the progression of JNJ-1802 into clinical trials in humans. Subsequent mechanistic studies have revealed that JNJ-A07 prevents the interaction between the NS4A-2K-NS4B precursor protein and the NS2B/NS3 complex and prevents viral replication organelle formation (Kiemel et al., 2024).

Figure removed due to copyright restriction.

**Figure 1.6: Structure of JNJ-A07 inhibitor targeting DENV non-structural proteins interactions.** (A) Chemical structure of the JNJ-A07 dengue virus inhibitor. (B) Schematic model of action showing that JNJ-A07 blocks the interaction between NS2B/NS3 and NS4B preventing the formation of viral replication organelles (Kaptein et al., 2021).

## **1.7 Limitations/Knowledge Gap in generation of engineered reporter systems and antiviral drug discovery**

Various significant advancements have been reported in the development of reporter systems to monitor orthoflavivirus infections. However, several challenges remain in optimizing these systems for reliable, sensitive, real-time detection and characterization of viral infection in living cells. For example, they can fall short in recapitulating the complexity of viral infections in a living organism, limiting their effectiveness in testing drug efficacy and in studies of host-pathogen interactions, and viral dynamics (Wahaab et al., 2021). Despite the versatility of fluorescence-based reporter systems in the detection of viral infections, knowledge gaps remain in refining their accuracy, specificity and consistency in the monitoring of viral protease activity in living cells. For DENV reporter constructs, non-specific cleavage by cellular proteases has been observed, which complicates the selective identification of viral infections (Pahmeier et al., 2021). Another study performed by Corliss *et al.* (2022) highlighted the differences in cleavage efficiency amongst various orthoflaviviruses, and there is still insufficient understanding of molecular determinants regarding substrate preference and the role of specific amino acid residues in cleavage efficiency (Corliss et al., 2022). The discrepancies between intracellular protease activity and previous biochemical studies indicate that current knowledge does not fully account for how viral proteases interact with host cell machinery in living, virus-infected cells (Arias-Arias et al., 2020). While reporter systems can be utilised for high-throughput screening of antiviral therapeutics, comprehensive methodologies to effectively implement such screening strategies across various virus-host interaction models have not been established.

Reporter systems that are dependent on viral protease activity have the potential to enable real-time visualization of orthoflavivirus infection and may also be used to screen potential antiviral drugs (Lennemann et al., 2020; Pahmeier et al., 2021).

## **1.8 Research Question and Rationale**

Orthoflavivirus infections, such as DENV, WNV, and ZIKV, are estimated to cause over 100 million infections each year and have a significant impact on global health (Wu et al., 2019). In spite of their wide prevalence and impact, there are no universally safe and effective vaccines or effective treatments. The development of safe and effective anti-viral drugs is dependent upon an understanding of the replication cycles and host cell manipulation mechanisms of orthoflaviviruses (Pierson & Diamond, 2020). Current methods for the study of viral infection by microscopy are usually very limited and are based on either static imaging methodologies or the need for genetic manipulations of the virus itself, hindering complete and accurate monitoring (Cassedy et al., 2021). Live cell imaging approaches that allow the monitoring and quantification of viral infection will facilitate research into virus-host interactions and screening of potential antiviral drugs.

### **1.8.1 Aims**

- i. To generate and characterise fluorescent reporter cell lines that enable live cell imaging-based monitoring of viral infection levels for Dengue Virus, West Nile/Kunjin Virus, and Zika Virus
- ii. To employ the dengue virus reporter cell line to characterize the antiviral activity of small molecule compound JNJ-A07: a promising antiviral drug candidate.

# Chapter Two: Materials and Methods

## 2.1 Materials

**Table 2.1 List of all the Materials**

### 2.1.1 Cell Culture Media and Composition

Cell Culture Media	Manufacturer	Catalogue Number	Composition
Dulbecco's Modified Eagle Medium (DMEM) (1X)	Gibco by Life Technologies	12430054	90%V/V Dulbecco's Modified Eagle Medium 4.5 g/L D-Glucose L-Glutamine 25mM HEPES

### 2.1.2 Cell Culture Media and Reagents Used to Maintain Cells

Reagents	Manufacturer	Catalogue Number	Composition
10% Foetal Calf Serum (FCS)	Gibco by Life Technologies	A5670701	Proteins, Fat, Peptides, various Growth Factors and Hormones
Penicillin-Streptomycin	Sigma-Aldrich	P4333	10000 Units/ml Penicillin and 100 mg/ml Streptomycin

Complete DMEM + Puromycin	Gibco by Life Technologies Sigma-Aldrich	12430054 A5670701 P4333	90%V/V Dulbecco's Modified Eagle Medium 4.5 g/L D-Glucose L-Glutamine 25mM HEPES Proteins, Fat, Peptides, various Growth Factors and Hormones 10000 Units/ml Penicillin and 100 mg/ml Streptomycin 3µg/ml Puromycin
1XPBS (Phosphate Buffered Saline)	Sigma-Aldrich	P3818	137mM NaCl, 2.7mM KCl, 10mM Na <sub>2</sub> HPO <sub>4</sub> , 1.8mM KH <sub>2</sub> PO <sub>4</sub>
Trypsin-Disodium Ethylenediamine Tetra Aceticacid (EDTA)	Sigma-Aldrich	T4049	0.25% Trypsin (W/V), 0.02% EDTA (W/V)
Dimethyl Sulfoxide (DMSO)	Sigma-Aldrich	D2650	N/A

### 2.1.3 Reagents used for Lentiviral Packaging and Production

Reagents	Manufacturer	Catalogue Number	Composition
Opti-MEM™ (1X)	Gibco by Life Technologies	31985070	Insulin, Transferrin, Hypoxanthine, and Thymidine

Lipofectamine <sup>R</sup> 2000 Transfection Reagent	Invitrogen <sup>TM</sup>	11668019	Proprietary Formulations
Lipofectamine <sup>TM</sup> 3000 Transfection Reagent + P 3000 <sup>TM</sup> Enhancer Reagent	Invitrogen <sup>TM</sup>	L3000008	3:1 mixture of DOSPA (2,3-dioleoloxymethyl-N-[2(sperminecarboxamido)ethyl]-N,N-dimethyl-1-propaniminium trifluoroacetate) and DOPE
Polybrene Transfection Reagent	Sigma- Aldrich	TR-1003- 50UL	Hexadimethrine bromide

#### 2.1.4 Reagents and Materials for Routine Laboratory Procedures

Laboratory Procedure	Reagents or Materials	Manufacturer	Catalogue Number	Composition
	NEBuilder <sup>R</sup> HiFi DNA Assembly Master Mix	New England Biolabs	E2621S	Proprietary Formulations
	Super Optimal Broth with Catabolite Repression (SOC) Outgrowth Medium	New England Biolabs	B9020S	2% Vegetable Peptone, 0.5% Yeast Extract, 10mM NaCl, 2.5mM KCl, 10mM MgCl <sub>2</sub> , 10mM MgSO <sub>4</sub> , 20mM D-Glucose (100 µl of 20% D-Glucose per 10mL)
	NEB <sup>R</sup> 5- alpha Competent E.coli (High	New England Biolabs	C29871	Derivative of DH5α, T1 Phage Resistant

NEBuilder DNA Assembly and Bacterial Transformation	Efficiency)				
	Cells				
	Luria-Bertani (LB) Broth	Using Sigma-Aldrich Products	N/A	5g/L Sodium Chloride, 5g/L Yeast Extract, 10g/L Bacto Tryptone, 1L dH <sub>2</sub> O	
Luria-Bertani Agar + Ampicillin Plates	Using Sigma-Aldrich Products	N/A	20mL of LB Agar, 2mg/mL Ampicillin		
Agarose Gel Electrophoresis	Gel Red Nucleic Acid Staining (10,000X)	iNtRON	21141	Proprietary Formulations	
	1xTris-Acetate-EDTA (TAE)	In-House	N/A	40mM Tris Base, 20mM acetic Acid, 1mM EDTA (pH 8.0)	
	1% Agarose in TAE (1X Tris-Acetate-EDTA)	BioLine	BIO-41025	1g Molecular Grade Agarose, 1L 1XTAE	
	1kb DNA Ladder	New England Biolabs	N3232	66.6ng/μL of 1kb DNA, Milli-Q H <sub>2</sub> O, 6X Gel Loading Dye	
	6X Purple Loading Dye	New England Biolabs	B7025S	2.5% (w/v) Ficoll <sup>®</sup> -400, 10mM EDTA, 3.3mM Tris-HCl, 0.02% dye 1 (pink/red), 0.001% dye 2 (blue)	

DNA Extraction and Isolation (Miniprep and Maxiprep)	NucleoSpin Gel and PCR Clean-up Mini Kit	Macherey-Nagel	74060950	N/A
	NucleoSpin Plasmid Easy Pure Mini Kit	Macherey-Nagel	740727	N/A
	NucleoBond Xtra Maxi Plasmid Purification Kit	Macherey-Nagel	740414	N/A
Immunofluorescent (IF) Staining	0.2% Gelatine	Sigma-Aldrich	G6144	0.2% (w/v) gelatine powder, sterile H <sub>2</sub> O
	5% Bovine Serum Albumin (BSA) in PBS	Sigma-Aldrich	A7030	1g BSA, 20ml 1XPBS
	1% Bovine Serum Albumin (BSA) in PBS	Sigma-Aldrich	A7030	0.2g BSA, 20ml 1XPBS
	1:1 Methanol: Acetone	Chem-Supply	MA004 and AT008	10mL 100% Methanol, 10mL 100% Acetone
	DAPI	Sigma-Aldrich	D9542	4',6-Diamidino-2-phenylindole dihydrochloride

### 2.1.5 Primary Antibodies Used for Immunofluorescent (IF) Staining and Western Blot Experiments

Name	Target	Source Organism	Immunoglobulin Class	Dilution	Supplier
Anti-E (4G2)	DENV Envelope Protein	Mouse	IgG	1 part anti-E (undiluted) with 1 part 5% BSA/PBS and 3 parts PBS	Dr Nicholas Eyre
Monoclonal Anti-GFP	Green Fluorescent Protein	Rabbit	IgG	1:1000	Sigma-Aldrich
AC-74	$\beta$ -Actin	Mouse	IgG	1:1000	Sigma-Aldrich

### 2.1.6 Secondary Antibodies Used for Immunofluorescent (IF) Staining and Western Blot Experiments

Name	Conjugate	Dilution	Supplier	Catalogue Number
Alexa-Fluor <sup>TM</sup> 647 goat anti-mouse IgG	IgG AlexaFluor647	1:200	Invitrogen	A21236
Licor IRDye <sup>R</sup> 800CW goat anti-mouse	IgG	1:10,000	LI-COR Biosciences	D3072505
Licor IRDye <sup>R</sup> 680CW goat anti-rabbit	IgG	1:10,000	LI-COR Biosciences	C8110605

### 2.1.7 Stable Cell Lines

Cell Line	Origin	Media	Supplier
Huh-7.5	Human Hepatocellular Derived Carcinoma	Complete DMEM	Dr Nicholas Eyre
HEK293FT	Human Embryonal Kidney	Complete DMEM	Dr Nicholas Eyre
Hela cells	Human cervical cancer tumor	Complete DMEM	Dr.Nicholas Eyre
Huh-7.5+ pTRIPZ_3xNLS_mScarlet3_ DENVpr_mStayGold	Human Hepatocellular Derived Carcinoma	Complete DMEM+ 3µg/mL Puromycin	Dr Nicholas Eyre
Huh-7.5+ DENVpr+eGFP+pTRIPZ- 3xNLS_mScarlet3	Human Hepatocellular Derived Carcinoma	Complete DMEM+ 3µg/mL Puromycin+ 3µg/mL Blasticidin	Dr Nicholas Eyre
Huh-7.5+ ZIKVpr+eGFP+pTRIPZ- 3xNLS_mScarlet3	Human Hepatocellular Derived Carcinoma	Complete DMEM+ 3µg/mL Puromycin+ 3µg/mL Blasticidin	Dr Nicholas Eyre
Huh-7.5+ pTRIPZ_3xNLS_mScarlet3_ WNVpr_mStayGold	Human Hepatocellular Derived Carcinoma	Complete DMEM+ 3µg/mL Puromycin	Generated as part of Master's Thesis
Huh-7.5+ pTRIPZ_3xNLS_mScarlet3_ ZIKVpr_mStayGold	Human Hepatocellular Derived Carcinoma	Complete DMEM+ 3µg/mL Puromycin	Generated as part of Master's Thesis

### 2.1.8 Primers used for PCR and Sanger Sequencing

Name	Application	Sequence 5'(Overlap/Spacer/Anneal) 3'
mScar3 FPseq	Sequence	GTGGTGGAACAGTACGAACG
pTRIPZ Seq RP <sub>1</sub>	Sequence	ttgcgccgatccctgtacACTACTAAGTTTGTAGTACA TATTTAACA
pTRIPZ_3XNLS_mS carlet3_fwd	PCR	acttagtagTGGAAGGGCTAATTCCTC
pTRIPZ_3XNLS_mS carlet3_rev	PCR	agccctccaACTACTAAGTTTGTAGTACATATTTA AC

### 2.1.9 Plasmid Vectors

Name	Application	Supplier	Selection Marker
pTRIPZ_3XNLS _mScarlet3	Plasmid Backbone for insertion of synthetic DNA gBlocks mStayGold fluorescent Protein	Dr Nicholas Eyre	Ampicillin (Bacteria) and Puromycin (Mammalian cells)
pTRIPZ_3XNLS_mScarlet3 _DENVpr_mStayGold	Encoding DENV reporter protein with mScarlet and mStayGold Fluorescent Protein	DR Nicholas Eyre	Ampicillin (Bacteria) and Puromycin (Mammalian cells)
pTRIPZ_3XNLS_mScarlet3 WNVpr_mStayGold	Encoding WNV reporter protein with mScarlet and mStayGold Fluorescent Protein	Generated as part of Master's Thesis	Ampicillin (Bacteria)and Puromycin (Mammalian cells)
pTRIPZ_3XNLS_mScarlet3 ZIKVpr_mStayGold	Encoding ZIKV reporter protein with mScarlet and	Generated as part of	Ampicillin (Bacteria)and

	mStayGold Fluorescent Protein	Master's Thesis	Puromycin (Mammalian cells)
psPAX2	2 <sup>nd</sup> Generation Lentiviral Packaging Plasmid	Ampicillin (Bacteria)	Dr.Nicholas Eyre, Addgene
pMD2.G	2 <sup>nd</sup> Generation Lentiviral Packaging Plasmid	Ampicillin (Bacteria)	Dr Nicholas Eyre, Addgene

**2.1.10 Synthetic gBlocks Gene Fragments (Integrated DNA Technologies) Utilized for Construction of pTRIPZ\_3XNLS\_mScarlet3\_DENVpr\_mStayGold, pTRIPZ\_3XNLS\_mScarlet3\_WNVpr\_mStayGold, and pTRIPZ\_3XNLS\_mScarlet3\_ZIKVpr\_mStayGold**

Name	Sequence
P2A_m StayGol d_DEN Vpr_gBl ock	ggcggctcc ggtggctccttgtacaa gggatcc ggc gcaacaa acttctctctctgaaacaa gcc gga gat gtc gaagagaatcctggacc ggtgtctaca ggc ga gga gc tgttacc ggc gtggtgc cctcaa gtcca gct gaag ggcaccatcaacggcaa ga gcttcacc gt ggaa ggc ga gggc ga gggc aata gcc ac ga gggca gccac aa aggcaagtacgtgtgcacc agc ggcaaatgccaatgtcttgggcc gccctgggaacta gcttc ggctatggcat gaagtactacaccaagtaccca gc ggcc t gaa gaact ggtccac ga ggt gat gcc ga gggcttacc tac g acagacacatccagtacaagggc gac ggca gcatccac gcc a gcacca gcac tcat gaa gaac ggcaccta ccacaacatcgtgga gttcacc ggcc a ggacttcaa gga gaac a gcccc gtgctgacc ggc gacat gGAC gt gagcctgccaacga ggtgca gca catc CCCATC gat gac ggc gt gga gtgc ACCgtgaccctgC A Gtaccctctgctgagc gac GAGa gca agtgc gtgga ggcctacca gaacacca tcatca gcccc tgaca atcagccagcccc gatgtgcca TTCactggatca gaaa gca gtacacca ga gcaaggac gacacc gag gagagagaccacatcatcca gac ga gacctgga ggcccacc tgggaa gtgga gca gc gat gat gaa gc g accgcggatagcca gcata gcacccc gcc gaa gaa aaa gc gcaaa gtgac gc gta gga gac gca gat ctgcc ggcatgggatcc gttc ca gta tt ggtta tga gtc ttc tgttcac gc ttc t gta ttat gtt gca catttggggcaa gtac actcgttcgtagtgtac aa gtaaac gc gt gccc tcc g

<p>P2A_m StayGol d_WNV pr_gBlo ck</p>	<p>ggcggctcc ggtggctcc ttgtacaa gggatcc ggc gcaacaa acttctc tct gct gaaacaa gcc c gga gat gtc  gaagagaatcct ggacc ggtgtctaca ggc ga gga gct gttacc ggc gt ggt gcc tca a gtcca gct gaag  ggcaccatcaac ggcaa ga gcttcacc gt ggaaggc ga gggc ga gggc aata gcc ac ga gggca gccac aa  aggcaagtacgtgtgcacc agc ggcaaac tccaatgtcttgggcc gccctgggaacta gcttc ggctatggcat  gaagtactacaccaagtacccca gc ggctgaa gaactggtccac ga ggtgatgcc ga gggcttacc tac g  acagacacatccagtacaagggc gac ggca gcatccac gcc a gcacca gcac tcat gaa gaac ggcaccta  ccacaacatcgtgga gttcacc ggcc a ggactca a gga gaac a gcccc gtgctgacc ggc gacatgGAC gt  gagcctgcccaacga ggtgca gca catcCCCATC gat gac ggc gt gga gtgc ACCgtgaccctgC A  Gtacccttctgctga gc gac GAGa gca a gtgc gtgga ggcctacca gaacacatca tca a gcccc tgca a  atcagccagcccc gatgtgcca TTCactg gatca gaaa gca gtacacca ga gcaaggac gacac c ga g  gagagagaccacatcatcca ga gc ga gacctgga ggcccacc tggaa gtgga a gca gc gat gat gaa gc g  accgcggatagcca gcata gcacccc gcc gaa gaa aaa gc gcaaa gtgac gc gtAAGAAGAGAGG  AGGAAAGACCGG A g gatcc gttcc a gtattggtat ga gtc ttc t gtt catc gc ttc t gta tttat gtt gca  catttggggcaa gtacactc gttc gta gtgtacaa gtaaac gc gtggcctcc g</p>
<p>P2A_m StayGol d_ZIKV pr_gBlo ck</p>	<p>ggcggctcc ggtggctcc ttgtacaa gggatcc ggc gcaacaa acttctc tct gct gaaacaa gcc c gga gat gtc  gaagagaatcct ggacc ggtgtctaca ggc ga gga gct gttacc ggc gt ggt gcc tca a gtcca gct gaag  ggcaccatcaac ggcaa ga gcttcacc gt ggaaggc ga gggc ga gggc aata gcc ac ga gggca gccac aa  aggcaagtacgtgtgcacc agc ggcaaac tccaatgtcttgggcc gccctgggaacta gcttc ggctatggcat  gaagtactacaccaagtacccca gc ggctgaa gaactggtccac ga ggtgatgcc ga gggcttacc tac g  acagacacatccagtacaagggc gac ggca gcatccac gcc a gcacca gcac tcat gaa gaac ggcaccta  ccacaacatcgtgga gttcacc ggcc a ggactca a gga gaac a gcccc gtgctgacc ggc gacatgGAC gt  gagcctgcccaacga ggtgca gca catcCCCATC gat gac ggc gt gga gtgc ACCgtgaccctgC A  Gtacccttctgctga gc gac GAGa gca a gtgc gtgga ggcctacca gaacacatca tca a gcccc tgca a  atcagccagcccc gatgtgcca TTCactg gatca gaaa gca gtacacca ga gcaaggac gacac c ga g  gagagagaccacatcatcca ga gc ga gacctgga ggcccacc tggaa gtgga a gca gc gat gat gaa gc g  accgcggatagcca gcata gcacccc gcc gaa gaa aaa gc gcaaa gtgac gc gtaa gaa ga gac ga ggc gc  agatactggatcc gttcca gtattggtat ga gcttctgttca tgc ttc t gta tttat gttgcacatttggggcaa gtac  actcgttcgtatgtac aa gtaaac gc gtggcctcc g</p>

## 2.2 Methods

### 2.2.1 Cell Growth and Maintenance

Huh-7.5 (Hepatocyte derived Carcinoma Cells), HEK293FT (Human Embryonic Kidney Cells), and HeLa (Cervical Cancer Cells) cells were cultured in Corning 75cm<sup>2</sup> cell culture flasks. These cells were cultured in complete media containing Dulbecco's Modified Eagle Medium (DMEM) (Gibco) supplemented with foetal Bovine Serum (10%) (Gibco), and 100 U/ml Penicillin and 100 µg/ml Streptomycin(Sigma-Aldrich) (Invitrogen, 2014). The Huh7.5 cells that were stably transduced with the doxycycline-inducible pTripz lentiviral vector retaining DENV, WNV/Kunjin, and ZIKV reporter proteins were cultured in complete media containing 3 µg/ml Puromycin. Cells were maintained at 37°C in a humidified 5% CO<sub>2</sub> incubator and were checked every 2-3 days for confluence. Once the cells reach ~80% confluence, they were passaged at a 1:6 ratio into 75 cm<sup>2</sup> or 175cm<sup>2</sup> cell culture flasks depending on the requirement of the experiment. For cell passaging, the media was aspirated, cells were washed with 1X Phosphate Bovine Serum (PBS) which was then aspirated, followed by trypsinization using Trypsin-EDTA (supplied by Sigma-Aldrich) to detach the cells following incubation at 37°C at 5% CO<sub>2</sub> for 3-4 minutes. Warm complete DMEM culture media was added to stop the trypsin reaction. The desired cell suspension was then collected for evaluation using a haemocytometer (Hirschmann, Neubauer improved bright line) based on following calculation:

$$\text{cells/ml} = \frac{\text{Number of cells counted}}{\text{Number of large corner squares}} \times \text{Dilution Factor} \times 10,000$$

Using Trypan blue assay, a 1:2 ratio of dye and cell suspension was mixed and applied between the coverslip and then cells on all large four corner squares were counted for both upper and lower chamber and averaged. The cell concentration (cells/ml) was then determined using the above equation. The cell suspension was then diluted to the desired cell concentration and seeded or transferred into a new cell culture flask containing complete medium. The passaged cells were kept at 37°C at 5% CO<sub>2</sub> in a humidified incubator.

## 2.2.2 Cryopreservation and Resuscitation of Cell Lines

Cells at ~80% confluence in a 175cm<sup>2</sup> flask were used for cryopreservation (Burlison et al., 2014). Following harvesting of cells by trypsinization (described in 2.2.1), cells were centrifuged at 200 x g for 8 minutes. During this period, about 6 cryovials were labelled with cell line, date and initials and 5ml of 2 X freezing mixture was prepared following the Table 2.2.2:

**Table 2.2.2: Components of Freezing Mixture**

Name of mixture	Volume (ml)
DMEM (no additives)	2.5
FBS	1.5
DMSO	1.0
Total	5

Subsequently, all the components were mixed in a 5 ml tube and filtered sterilised using a 0.2 µm sterile filter and 5 ml syringe. Following centrifugation, the medium was carefully aspirated and cell pellets were resuspended in 2 ml of complete DMEM. Next, 2 ml of filtered 2 x freezing mixture was added to the cell suspension and cells were mixed by pipetting. This cell suspension was then aliquoted into labelled cryovials (1 ml per tube). The cryovials were transferred into controlled-rate freezing chamber (Mr. Frosty, Thermo Fisher Scientific) at -80°C (containing 250 ml isopropanol, which was replaced after every 5<sup>th</sup> freezing cycle) for up to 1-2 weeks. The cryovials were then transferred to liquid nitrogen (Cryopreservation) for long-term storage. In regards to resuscitation, the cells were taken out from the liquid nitrogen, transported on dry ice and then thawed in a 37°C bead bath for about 1-2 minutes and then transferred to a 75cm<sup>2</sup> cell culture flask with fresh complete DMEM media. Afterwards, cells were cultured, maintained and seeded as described in 2.2.1.

## 2.2.3 Seeding cells in 6-well plate, 12-well plate and 96-well plate in Tissue Culture lab

### 2.2.3.1 Seeding cells in 6-well plate

For seeding the cells in a 6-well plate, cells were harvested as described in 2.2.1. Cells were counted using haemocytometer and average cell concentrations were calculated, as described

in 2.2.1 (O’Kelly, 1998). Cells were seeded at  $3 \times 10^5$  or  $1.2 \times 10^6$  cells per well for HEK293FT cells and  $2 \times 10^5$  cells per well for Huh-7.5 cells in a 6-well plate (Costar<sup>R</sup> 6-well clear TC-treated multiple well plate) and returned to incubation at 37°C, 5% CO<sub>2</sub> for 24hrs.

### 2.2.3.2 Seeding in 12-well plate

For seeding the cells in a 12-well plate, cells were harvested and counted, as described in 2.2.1. Cells were seeded at  $1 \times 10^5$  cells per well for HeLa cells in a 12-well plate and returned to incubation at 37°C, 5% CO<sub>2</sub> for 24hrs (O’Kelly, 1998).

### 2.2.3.3 Seeding in 96-well plate

For seeding the cells in a 96-well plate, cells were harvested and counted, as described in 2.2.1. Cells were seeded at  $1.5 \times 10^4$  cells per well in black-walled 96-well imaging plates (Revvity PhenoPlate 96-well microplate) and returned to culture at 37°C, 5% CO<sub>2</sub> for 24hrs (O’Kelly, 1998).

## 2.2.4 Cell Transfection

### 2.2.4.1 Transfection using Lipofectamine 2000 for 6-well plate

For the lentiviral vector-mediated delivery of WNV and ZIKV reporter constructs into Huh-7.5 cells, HEK293FT cells were used for lentiviral packaging (Dalby et al., 2004). To begin, 293FT cells were seeded in a 6 well plate at  $3 \times 10^5$  cells per well as described in 2.2.3.1. Following incubation for 24hrs, Opti-MEM (Invitrogen) and Lipofectamine 2000 (Invitrogen) were brought into room temperature and transfection complexes were prepared in two separate microcentrifuge tubes according to Table 2.2.4.1.

**Table 2.2.4.1: Transfection Reagents prepared for Tube A and Tube B**

Tube A	Tube B
Opti-MEM = 100µl	Opti-MEM = 100µl

Lipofectamine 2000 = 3µl	DNA = 2µg (containing 0.66µg of each lentivirus packaging plasmid (psPAX2 and pMD2.G) and 0.66µg of transfer plasmid (WNVpr and ZIKVpr plasmid))
--------------------------	--

Both Tube A and Tube B were gently flicked to mix properly. Then Tube A was combined in Tube B and mixed well. Then Tube B was incubated at room temperature for approximately 15-20 minutes to allow them to form a stable efficient transfection complex. Subsequently, 200 µl of this mixture was added dropwise carefully to the appropriate well being transfected and then incubated at 37°C, 5% CO<sub>2</sub> overnight. After incubation for 24hrs, media was removed from all the wells and replaced with 2 ml of complete DMEM into each well followed by another incubation period at 37°C, 5% CO<sub>2</sub> for 24hrs.

Following incubation, media from each well was collected into a 15 ml labelled yellow cap tube, the tubes were sealed with parafilm and all the wells were replaced with 2 ml of fresh complete DMEM supplemented with 1µg/ml Doxycycline (as we were working with doxycycline-inducible vector). A single well was transfected with pTRIPZ\_3xNLS\_mScarlet3 and treated with doxycycline at 1 µg/ml for induced expression to determine the transfection efficiency, which also serve as a negative control. These transfected plates were imaged using an EVOS M5000 (Invitrogen by Thermo Fisher Scientific) fluorescent microscope to confirm doxycycline-induced expression and transfection efficiency. The 6-well plate was returned to incubation at 37°C, 5% CO<sub>2</sub> for another 24hrs and the tubes were stored upright in labelled and double-contained at 4°C for 24hrs. This procedure was followed by another media collection in the same 15 ml tubes 24hrs later, such that a total of 4 ml collected cell supernatant was obtained.

#### **2.2.4.2 Transfection using Lipofectamine 3000 for 6-well plate**

Lipofectamine 3000 transfection reagent (Thermo Fisher Scientific) was also used as an alternative to Lipofectamine 2000 (2.2.4.1) for lentiviral vector packaging (gene, 2025). For this, HEK293FT cells were seeded in a 6-well plate at  $1.2 \times 10^6$  cells per well as described in 2.2.3.2. Following incubation for 24hrs, Opti-MEM (Invitrogen) and Lipofectamine 3000 (Invitrogen) were brought to room temperature and the mixtures for the transfection were prepared in two separate microcentrifuge tubes according to Table 2.2.4.2 (Scientific).

**Table 2.2.4.2: Transfection Reagents prepared for Tube A and Tube B**

Tube A	Tube B
Opti-MEM = 250µl	Opti-MEM = 250µl
Lipofectamine 3000 = 7µl	P3000 Enhancer = 6µl DNA = 0.75µl of each plasmid prepared from 1µg/µl (containing 0.75µl of each lentivirus packaging plasmid (psPAX2 and pMD2.G) and transfer plasmids ( WNVpr and ZIKVpr))

Both Tube A and Tube B were flicked to mix properly. Then the contents of Tube A was combined with that of Tube B and samples were mixed well. The resulting mixture was incubated at room temperature for approximately 20 minutes to allow formation of a transfection complex. Before adding the lipid-DNA complex, 1ml of medium was removed from each well with 1 ml of total media left in each well. Subsequently, 500 µl of the transfection mixture was added dropwise carefully to the appropriate well being transfected and the plate was gently agitated to ensure even distribution. Then the plate was incubated at 37°C, 5% CO<sub>2</sub> for 6hrs. At 6hrs post-transfection, media was removed from all the wells and replaced with pre-warmed 2 ml of complete DMEM into each well followed by another incubation period at 37°C, 5% CO<sub>2</sub> for 24hrs.

Following incubation, media from each wells were collected into a 15 ml labelled yellow cap tube, tubes were wrapped with parafilm and 2ml of fresh complete DMEM was added to each well. A single well was transfected with pTRIPZ\_3xNLS\_mScarlet3 and treated with 2 µl of doxycycline (1 µg/ml final concentration) for induced expression to determine the transfection efficiency. These transfected plates were imaged using an EVOS M5000 (Invitrogen by Thermo Fisher Scientific) fluorescent microscope to confirm doxycycline-induced expression and transfection efficiency. The 6-well plate was returned to incubation at 37°C, 5% CO<sub>2</sub> for another 24hrs and the tubes were stored upright in labelled and double-contained at 4°C for 24hrs. This procedure was followed by another media collection in the same 15 ml tubes 24hrs later, such that a total of 4 ml collected cell supernatant was obtained.

### 2.2.4.3 Transfection using Lipofectamine 3000 for 12-well plate

Where indicated, transfections were performed using Lipofectamine 3000, essentially as described in 2.2.4.2, using cells plated in 12-well plates according to Table 2.2.4.3 (gene, 2025).

**Table 2.2.4.3: Transfection Reagents prepared for Tube A and Tube B**

Tube A	Tube B
Opti-MEM = 50µl	Opti-MEM = 50µl
Lipofectamine 3000 = 2µl (Here, Tube A was incubated for 5 minute while making up Tube B )	P3000 Enhancer = 2µl DNA = 1µl (containing transfer plasmids (WNVpr, and ZIKVpr))

### 2.2.5 Lentivirus Production and Transduction of target cells

Before lentiviral integration, Huh-7.5 cells were seeded at  $2 \times 10^5$  cells per well in a 6-well plate, incubated at 37°C, 5% CO<sub>2</sub> for 24hrs as described in 2.2.3.1 (Ding & Kilpatrick, 2013). The lentivirus produced from 2.2.4 in 15 ml conical tubes were centrifuge at 1000 x g for 5 minutes at room temperature to remove cell debris (Figure 2.2.5). Afterwards, using a 0.45 µm sterile filter and 5 ml sterile syringe, the lentivirus medium was filtered carefully and transferred into a fresh 15 ml conical tube. The filtered lentivirus was aliquoted into 1.5 ml screw cap tubes for storage under -80°C for further use or used directly for transduction as described in 2.2.5. Subsequently, the lentivirus preparations were diluted at 1/3 with complete DMEM + 8µg/ml Polybrene (Sigma-Aldrich), where 800µl of the diluted lentivirus was transferred into each appropriate well containing Huh-7.5 cells being transduced.

The plate was then incubated at 37°C, 5% CO<sub>2</sub> for 3 days. At 3 days post-incubation, the media was removed, cell monolayers were washed with 1 x PBS and 2 ml of fresh complete DMEM supplemented with 3µg/ml Puromycin media was added into each well. The plate was returned to the incubator at 37°C, 5% CO<sub>2</sub> and checked every 2 days with media replacement to enable the removal of all floating dead cells and retain viable attached cells. As soon as the cells were confluent, they were harvested and transferred to a 25 cm<sup>2</sup> cell culture flask, as described in 2.2.1. An overview of the procedure for the lentiviral production and transduction has been

presented in Figure 2.2.5. Once the cells were confluent, the cells were harvested and transferred to a 25 cm<sup>2</sup> cell culture flask and then grown to confluency and harvested and transferred to a 75 cm<sup>2</sup> cell culture flask, where they were maintained as described in 2.2.1.

Figure removed due to copyright restriction.

**Figure 2.2.5: Lentiviral production workflow using second-generation lentiviral packaging plasmids (gene, 2025).** Schematic diagram of lentiviral production and transduction showed generation of stable cell lines using lentiviral plasmids and second-generation packaging plasmids (Figure generated using BioRender).

#### **2.2.5.1 Transient Transfection of WNVpr and ZIKVpr plasmids into HeLa cells**

To perform transient transfections, HeLa cells were harvested as described in section 2.2.1. Cells were counted and  $1 \times 10^5$  cells were seeded in each well of a 12-well plate and incubated at 37°C, 5% CO<sub>2</sub> (Wright, 2009). After 24-hour incubation, cells were transfected using Lipofectamine 3000 protocol as described in 2.2.4.3 using only the WNVpr and ZIKVpr expression plasmids. Doxycycline (1µg/ml final concentration) was added to the respective wells and the plate was incubated for 24 hours at 37°C, 5% CO<sub>2</sub>. At 24h post incubation, media was removed and replaced with fresh complete DMEM medium and then West Nile and Zika

Virus infections (MOI: ~1) were performed on the respective West Nile and Zika Virus protease construct-transfected cells. After infection, plates were incubated for 24 hours and then imaged using an Incucyte SX5 imaging system over a period of 2 days.

### **2.2.6 FACS (Fluorescence Activated Cell Sorting) to enrich fluorescent (mStayGold-positive) cells**

For FACS-mediated enrichment of cells that were transduced with pTRIPZ-3xNLS-mScarlet3-2A-DENVpr-mStayGold or pTRIPZ-3xNLS-mScarlet3-2A-ZIKVpr-mStayGold lentiviral vectors and grown under selection with puromycin for over three weeks, cells were grown in 175 cm<sup>2</sup> flasks and cultured in the presence of doxycycline (1 µg/mL) for 24 hours prior to sorting to induce fluorescent protein expression. As described in 2.2.5, cells were harvested by trypsinization, counted and diluted to a concentration of 1-1.5 x 10<sup>6</sup> cells/ml. Cells were sorted for strong mStayGold fluorescence by Dr. Giles Best and Alana White at the Flinders Flow Cytometry Facility using a FACS Aria Fusion Flow Cytometer (BD Biosciences). Huh-7.5 cells were used as negative control to set appropriate levels for gating and sorting fluorescent cells. After the sorting session, cells were seeded into 25 cm<sup>2</sup> cell culture flasks and returned to culture. Following culture and progressive expansion into 75 cm<sup>2</sup> and then 175 cm<sup>2</sup> cell culture flasks, cells were cryopreserved for future experiments.

### **2.2.7 Live cell imaging to monitor protease-dependent nuclear translocation of mStayGold fluorescent protein using the Incucyte SX5 imaging system**

To perform live cell imaging to monitor protease-dependent nuclear relocation of the mStayGold reporter following the virus infection, Huh-7.5+ pTRIPZ\_3xNLS\_mScarlet3\_DENVpr\_mStayGold cells (described in 2.2.6) were seeded in a 96-well imaging plate as described in 2.2.3.3. The cells were treated with doxycycline throughout the experiment. The plate was incubated for 24 hr at 37°C, 5% CO<sub>2</sub> incubator, then infected with wild-type (WT) DENV2 at two-fold serial dilutions (from MOI=2) and then further incubated at 37°C, 5% CO<sub>2</sub> incubator overnight. At 24hrs post-infection, the plate was imaged using an Incucyte SX5 imaging system for 48hrs to monitor levels of infection as determined by nuclear relocation of mStayGold fluorescence (Dehghani et al., 2024; Lanigan et al., 2020).

### **2.2.8 Immunofluorescent Staining of DENV2 infected and uninfected cells and Confocal Microscopy Imaging using Cytation 5**

Following live cell imaging (as described in 2.2.7), cells were fixed by removing and replacing the media with 100  $\mu$ l/well of ice-cold methanol: acetone (1:1) ratio inside a Class II biosafety cabinet (Beutner, 1961; Donaldson, 2015). The plate was incubated for 5 minutes at 4°C. After incubation, fixative was removed, cell monolayers were washed with 150  $\mu$ l/well PBS inside the biosafety cabinet and then replaced with 50  $\mu$ l/well 5% BSA in PBS at the benchtop. For blocking, the samples were incubated for 30 minutes at room temperature and during this period, primary antibody was prepared details as mentioned in 2.1.5. Following blocking, 40  $\mu$ l/well primary antibody was added to each well using a multichannel pipette and incubated overnight at 4°C. The samples were then removed and replaced carefully with 150  $\mu$ l/well PBS. Further, PBS was removed and replaced with 40  $\mu$ l/well secondary antibody, which was prepared as detailed in 2.1.6, and samples were incubated for 1hr at 4°C in dark. After successive primary and secondary antibody staining, the samples were removed and replaced with PBS at 150  $\mu$ l in each wells and further removed and stained with 50  $\mu$ l/well DAPI diluted to 1  $\mu$ g/ml (1:1000) in PBS. Samples were again incubated at 4°C in the dark for 10 minutes. DAPI stained was then removed and washed with 150  $\mu$ l/well PBS and then stored at 4°C in the dark. The samples were imaged by fluorescence microscopy (Bio-Tek Cytation 5 imaging system).

### **2.2.9 JNJ-A07+Huh7.5+eGFP DENVpr\_pTRIPZ\_3XNLS\_mScarlet3 Incucyte experiment to characterise the antiviral activity of JNJ-A07 drug candidate**

To perform this Incucyte experiment, the Huh7.5+eGFP DENVpr\_pTRIPZ\_3XNLS\_mScarlet3 cell line that was previously generated by Dr. Nicholas Eyre was used. Cells were carefully seeded at  $1 \times 10^4$  cells per well into a 96-well plate and incubated at 37°C, 5% CO<sub>2</sub> overnight (Gong, 2013). After overnight incubation, cells were infected (50  $\mu$ l/well) with wild type DENV2 (prepared by dilution in complete medium, 1 in 5 for approximately MOI of 0.1) for 2 hours. Concurrently, 5-fold serial dilutions of JNJ-A07 were prepared in a separate 96-well plate. For this, 250  $\mu$ l/well of complete DMEM containing JNJ-A07 at 2  $\mu$ M (DMSO 0.1% [v/v] final concentration) was aliquoted into wells in column 12 and then the 5-fold dilution series were prepared using complete DMEM containing 0.1% [v/v] DMSO. Controls included ‘uninfected’ cells (column 1), and ‘DMSO 0.1% [v/v] carrier control’ cells (column 2). After 2 hours of

infection, the virus-containing media was replaced with diluted JNJ-A07 from the dilution plate. Afterwards, plate was loaded into the Incucyte SX5 imaging system and imaged every 2 hours for 48 hours.

## 2.2.10 Molecular Cloning

### 2.2.10.1 Restriction Enzyme Digestion

To construct viral protease-dependent reporter system, the pTRIPZ\_3XNLS\_mScarlet3 plasmid was linearized by digestion with *Bsr*GI-HF (restriction endonuclease high fidelity enzyme). 2  $\mu$ l of Plasmid DNA (1 $\mu$ g/ $\mu$ l), 2 $\mu$ l of rCutsmart buffer (10X New England Biolabs), 1  $\mu$ l of restriction enzyme and nuclease-free water that makes total volume up to 20  $\mu$ l were added to the bottom of 0.2 ml sterile PCR tube as presented in Table 2.2.10.1. The reaction mixture was mixed by pipetting up and down or by flicking the tube 5 times followed by a quick spin-down in a benchtop microcentrifuge. The sterile tube was transferred to a thermocycler (S1000<sup>TM</sup> Thermal Cycler, Bio-Rad) under the digest protocol for 16hrs at 37°C for complete digestion and then transferred back on ice. The samples were subjected to agarose gel electrophoresis, as described in Table 2.2.10.1.

**Table 2.2.10.1: Shows the total volume of reagents for performing restriction digest to linearize the plasmid pTRIPZ\_3XNLS\_mScarlet3**

Reagents	Volume
Plasmid DNA (1 $\mu$ g/ $\mu$ l) pTRIPZ_3XNLS_mScarlet3	2 $\mu$ l
rCutsmart buffer (10X)	2 $\mu$ l
dH <sub>2</sub> O (water)	15 $\mu$ l
Restriction enzyme ( <i>Bsr</i> GI-HF)	1 $\mu$ l
<b>Total</b>	<b>20<math>\mu</math>l</b>

### 2.2.10.2 DNA Extraction following Agarose Gel Electrophoresis

An appropriate 1% agarose gel was prepared, stained with iNtRON Red Safe (2.5  $\mu$ l) diluted 1:20,000, which was used to separate restriction digest product or visualize the linearized

plasmid presence under UV light, alongside with 1kb DNA ladder. Initially, the restriction digest product (20 µl) was mixed with 6 X Purple Loading Dye (New England Biolabs #B7025) at 1:5 dilution to reach 1X concentration (total 24 µl). A Mini-Sub cell GT cell with powerpac basic power supply (Bio-Rad) was used to perform electrophoresis for 60 minutes at 100 Volts in 1 X Tris-acetate-EDTA (TAE) running buffer. Afterwards, for imaging, the gel was imaged carefully using GelDoc Go Imaging System (Bio-Rad) under UV transilluminator (ChemiDoc MP) to visualize the DNA fragments. Once the band corresponding to the appropriate DNA size was observed, it was cut out using scalpel and then placed into a microcentrifuge tube. The tube was weighed and gel was cleaned up following a NucleoSpin Gel and PCR Clean-up Mini Kit (Macherey-Nagel) manufacturer's protocol as described in 2.2.10.3.

#### **2.2.10.3 PCR clean up (NucleoSpin Gel Mini Kit)**

As described in 2.2.10.2, DNA fragments were purified using the NucleoSpin Gel and PCR Clean-up Mini Kit (Macherey-Nagel) manufacturer's instructions. Where the protocols was followed with the exceptions that an initial centrifugation was performed at 2000 x g for 1 minutes to bind DNA to the column and 10 µl of nuclease-free water was used for the elution, instead of 30 µl, to achieve a higher concentration of DNA. The purity and concentration of purified DNA samples were determined using a Nanodrop One Spectrophotometer (Thermo Fisher Scientific).

#### **2.2.10.4 Synthetic gBlocks gene fragments resuspension**

The synthetic gBlocks (IDT) described in 2.1.10 were resuspended by brief micro centrifugation and dissolving in 100 µl of molecular-grade water to reach a final concentration of 10 ng/µl. Samples were then mixed briefly using a vortex. The tube was then vortexed and briefly centrifuged using a benchtop centrifuge and the concentration of DNA was measured using a Nanodrop One Spectrophotometer (Thermo Fisher Scientific).

#### **2.2.10.5 NEBuilder DNA Assembly for High-Efficiency Cloning**

To perform DNA assembly reactions using linearized vector (pTRIPZ\_3XNLS\_mScarlet3 digested with *Bsr*GI-HF) and DNA inserts (P2A\_mStayGold\_ZIKVpr\_gBlock and P2A\_mStayGold\_ZIKVpr\_gBlock), NEBuilder HiFi DNA Assembly Master Mix (New

England Biolabs) was used, as per manufacturer's instructions. The following online tools were used to determine the appropriate DNA amounts and volumes to use to achieve a 1:3 vector: insert ratio using 50 ng of digested vector: <https://nebuildercalculator.neb.com/> and <https://nebiocalculator.neb.com#!/ligation>. DNA fragments were added to a PCR tube with nuclease-free water to make a final volume of 5 µl. To mediate efficient DNA assembly, 5 µl of NEBuilder HiFi DNA Assembly Master Mix (New England Biolabs) was also added and samples were vortexed briefly and pulse-centrifuged. The below Table 2.2.10.5 shows the reaction volume components. Samples were transferred to a S1000 thermocycler (Bio-Rad) and incubated for 60 minutes at 50°C. The reaction product was then stored at -20 °C.

**Table 2.2.10.5: Represents the NEBuilder DNA Assembly reaction protocol, where total of 10µl volume was used for each reaction**

Assembly Reaction Tube A	Volume (µl) Tube A	Assembly Reaction Tube B	Volume (µl) Tube B
Vector Aliquot (25ng/µl)	2.5	Vector Aliquot (25ng/µl)	2.5
Insert Aliquot (7.5ng/µl)	0.75	Insert Aliquot (7.9ng/µl)	0.79
Nuclease-free H <sub>2</sub> O	1.75	Nuclease-free H <sub>2</sub> O	1.71
2x NEBuilder HiFi DNA Assembly Master Mix (New England Biolabs)	5	2x NEBuilder HiFi DNA Assembly Master Mix (New England Biolabs)	5
Total	10	Total	10

### 2.2.10.6 High Efficiency Transformation with NEB Stable Competent E.coli cells

Following the manufacturer's protocol from New England Biolabs High efficiency transformation (C3040I), plasmid DNA prepared from NEBuilder DNA Assembly as described in 2.3.7 and NEB 5-alpha competent high-efficiency E.coli (NEB) cells were thawed until liquefy (Biolabs, 2013). Ensuring everything was done on ice, 50 µl of competent cells was gently mixed and pipette into a transformation tube along with 2 µl of plasmid DNA. Tube was slightly flicked about 5 times to gently mix the cells and DNA. The tube was then incubated on ice for 30 minutes and heat shocked at exact 42°C for exactly 30 seconds and back into the ice for 5 minutes. During this period Stable Outgrowth Medium (SOC) was stored at room

temperature. After the incubation, 950 µl of NEB 10-beta/SOC media was pipette and then added to the mixture and the tube was placed at 37°C with shaking at 250 rpm for 60 minutes. Following the completion of 60 minutes incubation, the sample was centrifuged at benchtop at 3000 x g for 5 minutes. Luria Bertani (LB) Agar plates with 100 µg/ml Ampicillin were incubated at 37°C for 10-15 minutes. Upon completion of centrifugation, 900 µl of supernatant media was removed and the pellet was resuspended in the remaining 100 µl of media. Among the 100 µl media, 20 µl and 80 µl was aliquoted to be used for spreading onto the warm selected Luria Bertani agar plates. The plates were incubated at 37°C overnight.

#### **2.2.10.7 Preparation of Bacterial Culture for Mini-Prep/Maxi-Prep**

Single isolated and well transformed colonies were picked from each plates prepared as mentioned in 2.3.8 and inoculated into 10 ml LB broth supplemented with 100 µg/ml ampicillin for mini-prep. Whereas, 200 ml LB broth supplemented with 100 µg/ml ampicillin was used to inoculate for Maxi-prep. 16hrs incubation was performed for the Mini-prep cultures with shaking at 250rpm at 37°C and 180rpm at 37°C for Maxi-Prep cultures.

#### **2.2.10.8 Mini-Prep Plasmid Protocol using NucleoSpin Plasmid EasyPure (Machery-Nagel) kit**

The incubated cultures for Mini-prep from 2.2.10.9 were centrifuged at 2500 x g for 10 minutes in a Multifuge X Pro series (Thermo Fisher Scientific) to pellet the cells (Machery-Nagel, 2019). Supernatant was discarded and bleached in a Schott bottle containing sodium hypochlorite. Cells were then resuspended in a 150 µl Buffer A1 by vortexing and pipetting up and down. 250 µl of A2 buffer was added and mixed gently by inverting tube and then incubated at room temperature for 2 minutes until lysate gets clear. 350 µl of buffer A3 was added and mixed properly by inverting tube and transferred into a labelled microcentrifuge tube. The sample was centrifuged at >12,000 x g for 3 minutes and then the NucleoSpin column was placed into a 2 ml collection tube. Clear supernatant was loaded onto the spin column and centrifuged at 1000-2000 x g for 30 second and follow-through was discarded. Following the follow-through, 450 µl of buffer AQ was added to spin column and centrifuge for 1 minute at >12000 x g. The collection tube was discarded and spin column was placed into new microcentrifuge. To get a more concentrated pure plasmid, 20 µl of buffer AE was added and incubated for 1 minutes at room temperature. Upon addition of elution buffer, spin column was

centrifuged for 1 minutes at >12000 x g and the eluted plasmid concentration was then measured in Nanodrop One Spectrophotometer (Thermo Fisher Scientific).

### 2.2.10.9 Diagnostic Digest and Gel electrophoresis to confirm the Cloning

The samples obtained from 2.2.10.10 after Mini-prep procedures were collected to perform diagnostic digest with BamHI-HF (High Fidelity restriction enzyme, supplied by New England Biolabs). The resulting reaction product was run under digest protocol in PCR for 16hrs at 37°C as according to method described in 2.2.10.1. The reagents used for this diagnostic digest is listed in Table 2.2.10.9.

**Table 2.2.10.9: Diagnostic Digest of NEBuilder DNA Assembly product with BamHI-HF**

Reagents	Volume
Plasmid DNA ( $\mu\text{g}/\mu\text{l}$ )	5 $\mu\text{l}$
1) pTRIPZ_3XNLS_mScarlet3	
2) pTRIPZ_3XNLS_mScarlet3_P2A_mStayGold_WNVpr_gBlock	
3) pTRIPZ_3XNLS_mScarlet3_P2A_mStayGold_ZIKVpr_gBlock	
rCutsmart buffer (10X)	2 $\mu\text{l}$
dH <sub>2</sub> O (water)	12 $\mu\text{l}$
Restriction enzyme (BamHI-HF)	1 $\mu\text{l}$
Total	<b>20<math>\mu\text{l}</math></b>

Gel electrophoresis was run according to method described in 2.2.10.2 to analysed the product results and to check the expected size of vector and insert via ChemiDoc imaging system (Bio-Rad).

### 2.2.10.10 Sanger Sequencing to confirm cloning after Mini-prep

Clones product after Mini-prep procedures were set up for Sanger sequencing. 1  $\mu\text{g}$  of plasmid DNA from each product was added to appropriate 1  $\mu\text{l}$  of forward (mScar3 FPseq) and 1  $\mu\text{l}$  of reverse primers (pTRIPZseq RP1) (IDT) as mentioned in 2.1.8 to make a final volume of 13  $\mu\text{l}$  with nuclease-free water. Products were sent for sequencing through AGRF and were

analysed with expected sequences using Benchling. Plasmid map and chromatogram were obtained to assess sequence quality.

#### **2.2.10.11 Maxi-Prep Plasmid Protocol using NucleoBond Xtra Maxi Plasmid (Machery-Nagel) kit**

The overnight cultures for Maxi-prep as outlined in 2.2.10.9 were transferred into 200 ml Nalgene centrifuge tubes (Machery-Nagel, 2019). For cultivation and harvest, tubes were centrifuged in Multifuge X pro series (Thermo Fisher Scientific) for 30 minutes at 4°C 4000 x g to pellet cells. Cell resuspension was performed in 12 ml buffer RES and 12 ml buffer LYS was added and gently inverted to check for precipitation. Then afterwards, samples were incubated for 5 minute at room temperature. During this incubation period, columns and filter were equilibrated with 25 ml of buffer EQU and allowed to dry properly. For neutralization, 12ml buffer NEU was added and inverted gently and mixed thoroughly until turned colourless. The lysate was then loaded to the NucleoBond Xtra column filter and later filter was washed with 15 ml buffer EQU and discarded.

Similarly, the column was washed second time with 25 ml buffer wash and permitted to empty before DNA was eluted. 15 ml buffer ELU was added to elute DNA and 10.5 ml of isopropanol was added to the DNA. After the precipitation, samples were centrifuged for 30 minutes at 4°C 15000 x g (Multifuge X pro series (Thermo Fisher Scientific)). From the supernatant 1 ml was scrapped and rest were resuspended and transferred to a microcentrifuge tube and again centrifuged for 5 minutes at 15000 x g room temperature (PICO 17, Thermo Fisher Scientific). Afterwards, supernatant was discarded and 4 ml of 70% ethanol was added to the remaining pellet and again centrifuged for 5 minutes at 15000 x g room temperature (PICO 17, Thermo Fisher Scientific). This process of washing was again repeated and pellet was air dried for 15 minutes. Following the washing and drying, sample was restored in 50 µl of buffer TE (5mM Tris/HCL) and concentrations were measured using Nanodrop One Spectrophotometer (Thermo Fisher Scientific). Samples were then stored at -20°C.

#### **2.2.11 Cellular protein extraction and Western Blot Analysis**

To extract proteins,  $2 \times 10^5$  cells per well were harvested in a 6-well plate as according to 2.2.3.1. Where cells were labelled as according to infected and uninfected conditions. After

48hrs post infections, media was replaced and gently washed with 1 x PBS and 100 µl of RIPA buffer with 1 µl Proteinase inhibitor (1 in 100) which are prepared as shown in Table 2.2.11, was added to each well and incubated for 20 minutes on ice (Meads & Medveczky, 2009; Ocegüera et al., 2007; Qiu et al., 1992).

**Table 2.2.11: Illustrates the reagents used for RIPA buffer preparation**

Buffer Recipe	Volume
150mM NaCl	1.5ml (4M)
0.5% deoxych	0.2g
0.1% SDS	0.4ml (10%)
1% NP-40	0.4ml
50mM Tris	2ml (1M)
dH <sub>2</sub> O	37.5ml

The cell monolayer was scraped using the pipette tip and transferred into Eppendorf tubes. Cell lysates were pipette up and down using needle and syringe in the RIPA buffer and then centrifuged at 14000 x g for 10 minutes at 4°C. The cell supernatant was then transferred into new labelled eppendorf tubes. An adequate volume of 5 µl of 4 X loading buffer was added with 15 µl of sample to load the sample in polyacrylamide gel. Before loading the sample in precision plus protein Kaleidoscope pre-stained protein standards (Bio-Rad) to a polyacrylamide gel, the samples were boiled in a thermal cycler at 95°C for 5 minutes. Afterwards, 1 X GTS running buffer was added to tank as from the protocol as per the manufacturer's and samples were separated by SDS-PAGE for 90 minutes at 100 volts. As per manufacturer's instructions, proteins after the SDS-PAGE separation were shifted to the nitrocellulose membrane using Trans-Blot TURBO system (Bio-Rad). The membrane was then probed with primary antibodies overnight as seen in 2.1.5 at concentration of 1% skim milk at 4°C shaking overnight. Following primary antibody, membrane was washed with TBS-T 5 times in 5 minutes intervals and probed with secondary antibodies as seen in 2.1.6 at room temperature in 1% skim milk for 1 hour. Afterwards process again involves washing with TBS-T 5 times in 10 minutes intervals or even increased washing to get rid of unbound secondary antibody. Following washing, the membrane was then imaged under LI-COR Biosciences Odyssey imaging system.

### **2.2.12 Bioinformatics Analysis**

All the images obtained were analysed using Incucyte 2023A software (located at the FHMRI building, level 8). The graph generation and statistical analysis using paired t-test was performed using GraphPadPrism Version 4.0 software package (Motulsky & GraphPad Software, 2003).

## Chapter Three: Results

### 3.1 Gel Electrophoresis of Plasmid Backbone (pTRIPZ\_3XNLS\_mScarlet3) after restriction digest

The pTRIPZ\_3XNLS\_mScarlet3 plasmid is a pTRIPZ lentiviral inducible expression vector that encodes three nuclear localization signal (NLS) sequences fused in-frame to a red fluorescent protein (mScarlet3). The plasmid was linearized by digestion with *Bsr*GI-HF (high-fidelity restriction endonuclease). To visualize and extract the digested plasmid backbone, gel electrophoresis was performed and the gel was observed using a UV transilluminator. This revealed a single ~13 kb band consistent with the expected band size of 13,057 bp, as represented in Figure 3.1. This indicated that the restriction enzyme (*Bsr*GI-HF) had effectively linearized the plasmid.

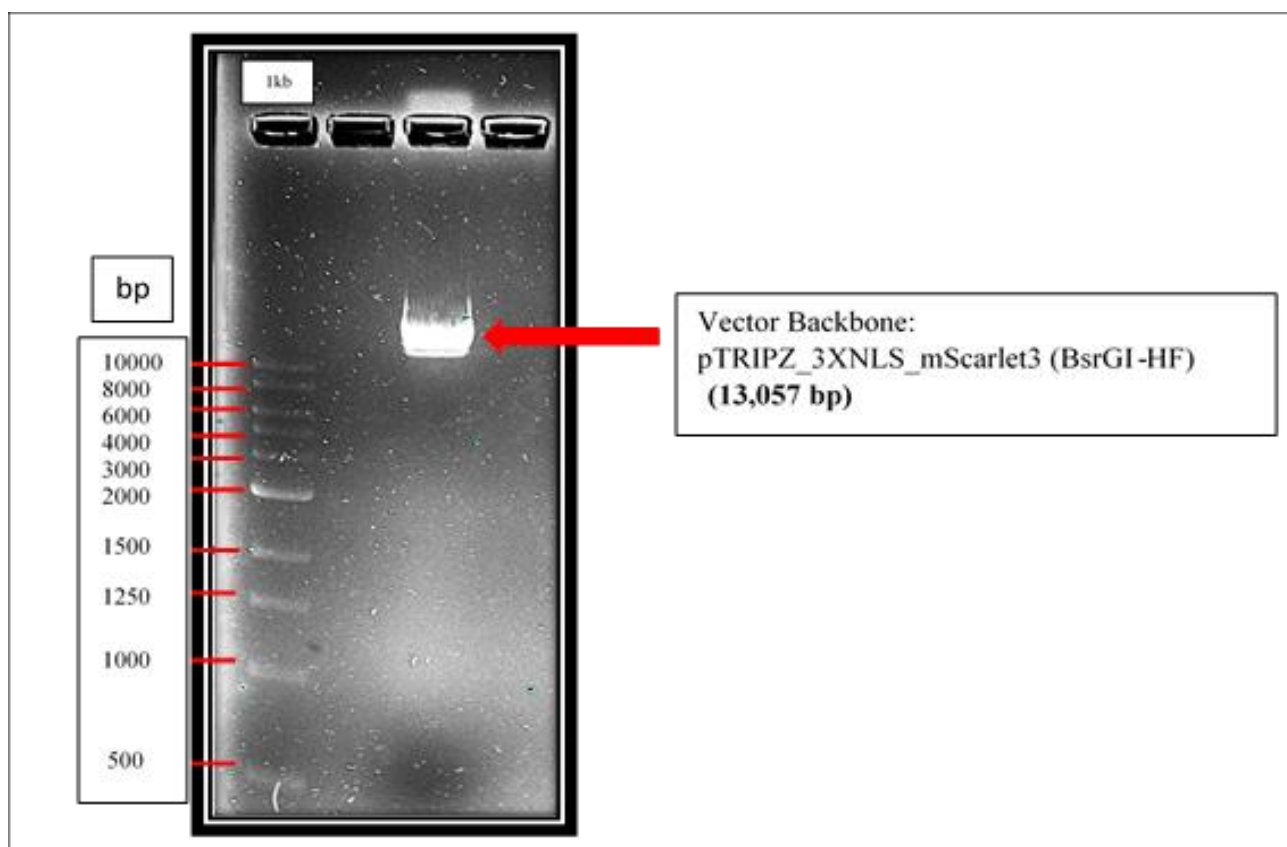


**Figure 3.1:** Agarose gel electrophoresis of pTRIPZ\_3XNLS\_mScarlet3 plasmid backbone digested with *Bsr*GI-HF. 1Kb DNA ladder was used to see appropriate corresponding band

size of the plasmid. As presented, the expected band size of the vector backbone was 13,057bp as per the plasmid map shown in Figure Appendices 1 (generated using Benchling).

### 3.2 Generation of pTRIPZ\_3XNLS\_mScarlet3\_WNVpr\_mStayGold and pTRIPZ\_3XNLS\_mScarlet3\_ZIKVpr\_mStayGold reporter construct

To begin with generating WNVpr and ZIKVpr reporter construct plasmids, synthetic DNA fragments (gBlocks) were assembled with pTRIPZ\_3XNLS\_mScarlet3 vector backbone using NEBuilder HiFi DNA assembly as mentioned in 2.2.10.2 and 2.2.10.3. The resulting assembly products were transformed into NEB 5-alpha component *E. coli* cells (New England Biolabs), as per manufacturer's instructions, as described in 2.2.10.5 and 2.2.10.6. This resulted in numerous colonies for both pTRIPZ\_WNVpr, and pTRIPZ\_ZIKVpr reporter constructs. A brief summary explained with the process to generate the construct is presented in Figure 3.2 with specific details generated using BioRender. Notably the cloned plasmids along with the control (pTRIPZ\_3XNLS\_mScarlet3) were digested with BamHI to verify the vector and insert size which was compared against the virtual digest gel image created using Benchling as shown in Figure 3.2.1.

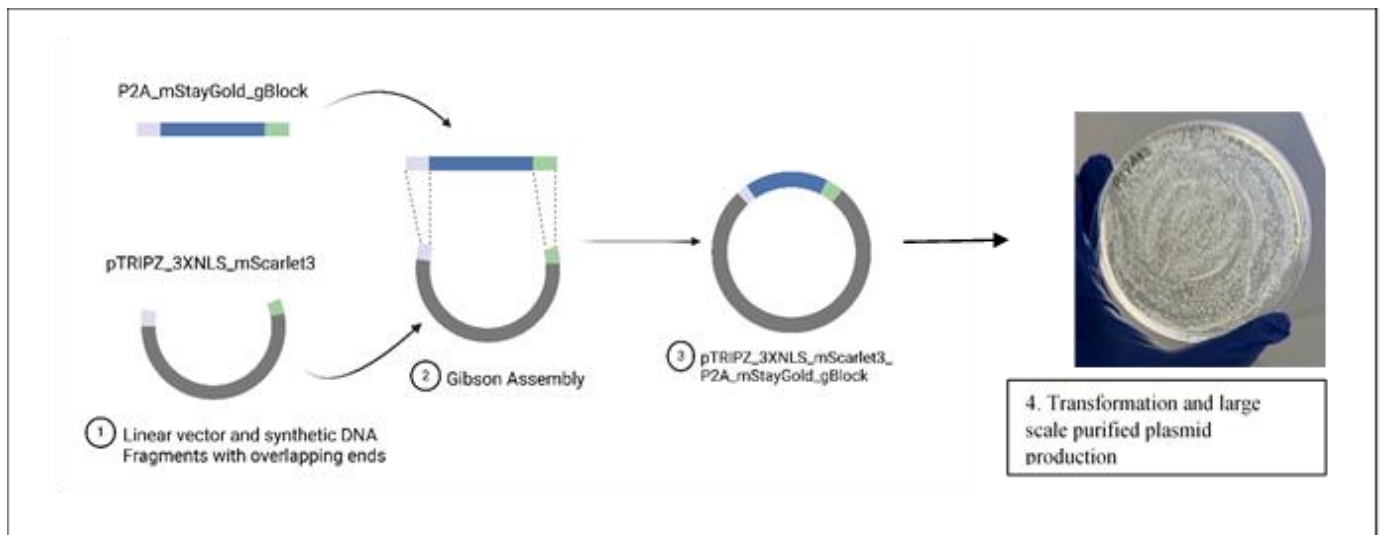


**Figure 3.2: Molecular cloning to generate the pTRIPZ\_3XNLS\_mScarlet3\_WNVpr\_mStayGold and pTRIPZ\_3XNLS\_mScarlet3\_ZIKVpr\_mStayGold plasmid reporter construct.** The high efficiency transformation of NEBuilder reaction products into chemically component *E. coli* (NEB –Alpha Component cells) was performed for all plasmids reporter construct and 5

medium-sized colonies were picked and inoculated in each tubes containing Luria Bertani (LB) broth (+ Ampicillin).

Mini and Maxi prep plasmid DNA extraction was performed as described in 2.2.10.8. Concentrations were measured using a Nanodrop as shown in Table 3.2A. Each highly concentrated sample was sent for Sanger sequencing. The high concentrated samples were further transformed, inoculated and performed maxi prep plasmid procedure as mentioned in 2.2.10.8 to obtain purified large amount of plasmid DNA. Concentrations were measured using Nanodrop as represented in Table 3.2B.

**Table 3.2: Concentration of WNV protease construct and ZIKV protease construct.** (A) represent the concentration of 5 colonies picked from each sample after Mini prep plasmid

A			
Sample Name	Nucleic Acid(ng/uL)	A260/A280	A260/A230
WNVpr 1	311.942	1.879	2.221
WNVpr 2	283.113	1.885	2.222
WNVpr 3	327.089	1.854	2.107
WNVpr 4	164.75	1.871	2.21
WNVpr 5	132.849	1.839	1.884
ZIKVpr 1	290.459	1.879	2.255
ZIKVpr 2	392.863	1.885	2.255
ZIKVpr 3	110.938	1.293	1.434
ZIKVpr 4	373.38	1.881	2.257
ZIKVpr 5	400.929	1.879	2.209

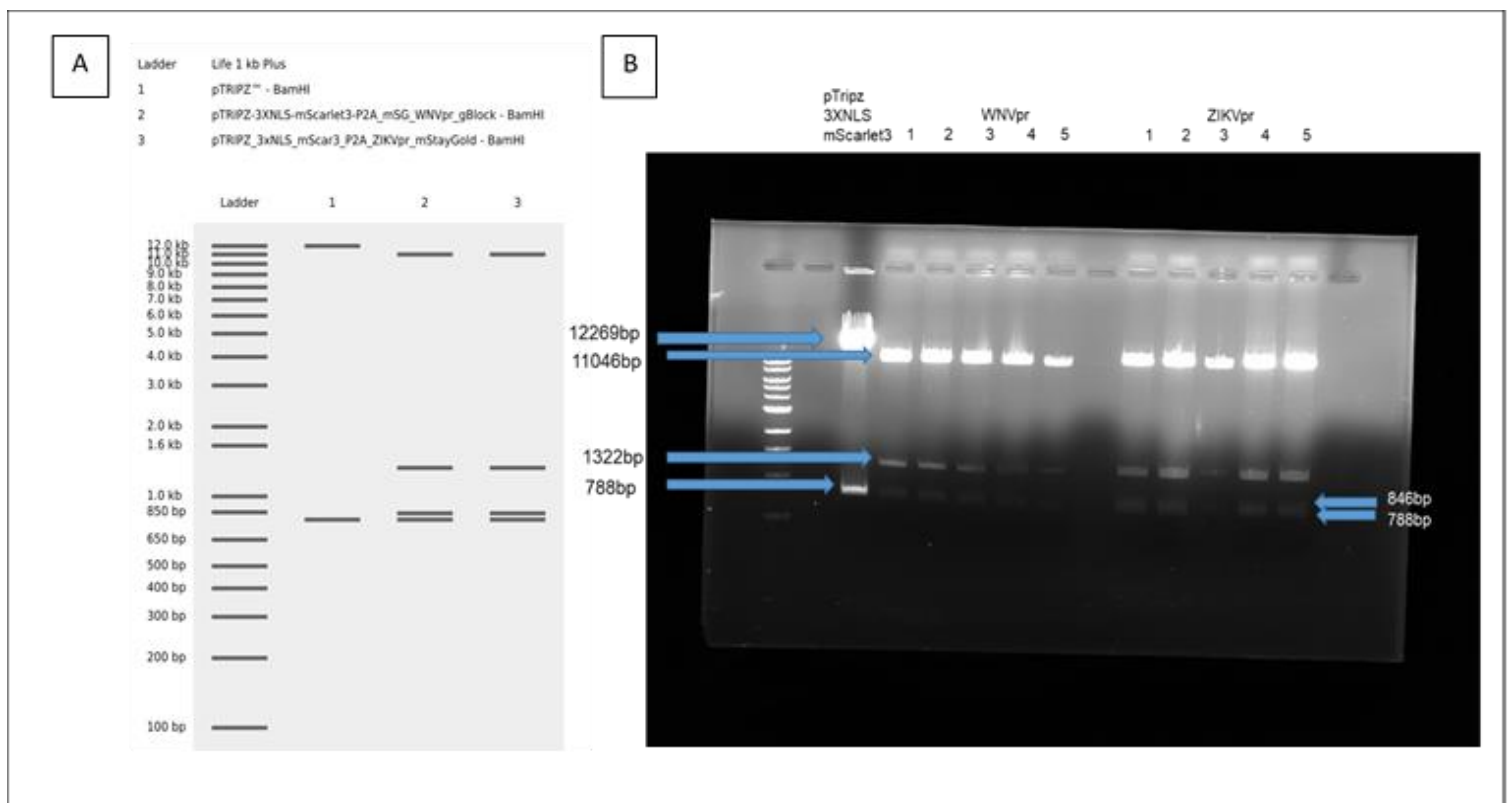
  

B		
Sample Name	Nucleic Acid (ng/μl)	A260/280
WNVpr (3)	3374	1.92
ZIKVpr (5)	3100	1.89

extraction and (B) showed the highly concentrated plasmid DNA of each sample after maxi prep plasmid extraction and purification.

### 3.2.1 Diagnostic Digest to verify the size (bp) of insert in cloned plasmid DNA

As described in 2.2.10.9, plasmid DNA was digested with BamHI-HF and to interpret the expected band size of the insert in the gel image, virtual digest was performed in Benchling as shown in Figure 3.2.1 (A). In Figure 3.2.1 (B), pTRIPZ\_3XNLS\_mScarlet3 serve as a control and we can see an expected the single linearized band size of 788bp, whereas the WNVpr and ZIKVpr samples digested with BamHI releases the expected band sizes of 11048bp, 1322bp, 846bp and 788bp which confirms successful cloning. The differences between the band sizes of 846bp and 788bp was small so could be the reason for these two bands to be appears as one as shown in Figure 3.2.1 (B)



**Figure 3.2.1: Diagnostic digest to verify the vector and insert sizes to determine successful cloning.** (A) Represent the virtual digest with expected insert sizes created using Benchling. (B) shows the gel image presenting the successful incorporation of gBlocks in the

pTRIPZ\_3XNLS\_mScarlet3 vector (control), where we can see an expected 4 band sizes of 11048bp, 1322bp, 846bp and 788bp in WNVpr and ZIKVpr plasmid construct which confirms successful cloning.

### **3.3 Lentivirus Transfection of pTRIPZ\_3XNLS\_mScarlet3\_WNVpr\_mStayGold and pTRIPZ\_3XNLS\_mScarlet3\_ZIKVpr\_mStayGold into HEK293FT cells using Lipofectamine 2000 and Lipofectamine 3000 protocol**

#### **3.3.1 Transfection using Lipofectamine 2000 to check qualitative transfection efficiency**

Reporter plasmid construct and packaging plasmid generated as described in 2.2.4 were transfected into HEK293 FT cells using Lipofectamine 2000 protocol as described in section 2.2.4.1. At 24-hour post-transfection incubation, cells were treated with doxycycline (1 $\mu$ g/ $\mu$ l) to induce the expression of fluorescence reporter protein. To further check the transfection efficiency, cells were imaged after 24 hours under EVOS M5000 (Invitrogen by Thermo Fisher Scientific) to confirm doxycycline-induced expression and qualitative transfection efficiency, Cells were imaged using a 10 X objective as shown in Figure 3.3.1. Here, cells transfected with pTRIPZ\_3XNLS\_mScarlet3 serve as a positive control for mScarlet fluorescence that also assess background green fluorescence and as well to compare the relative transfection efficiency from that of cells expressing reporter construct mScarlet3\_WNVpr\_mStayGold, and mScarlet3\_ZIKVpr\_mStayGold. We could see fairly lower expression of fluorescence reporter proteins (mStayGold and mScarlet3), which represent lower transfection efficiency using Lipofectamine 2000 with our generated plasmid DNA reporter construct as compared to image obtained using Lipofectamine 3000 (Figure 3.3.2).

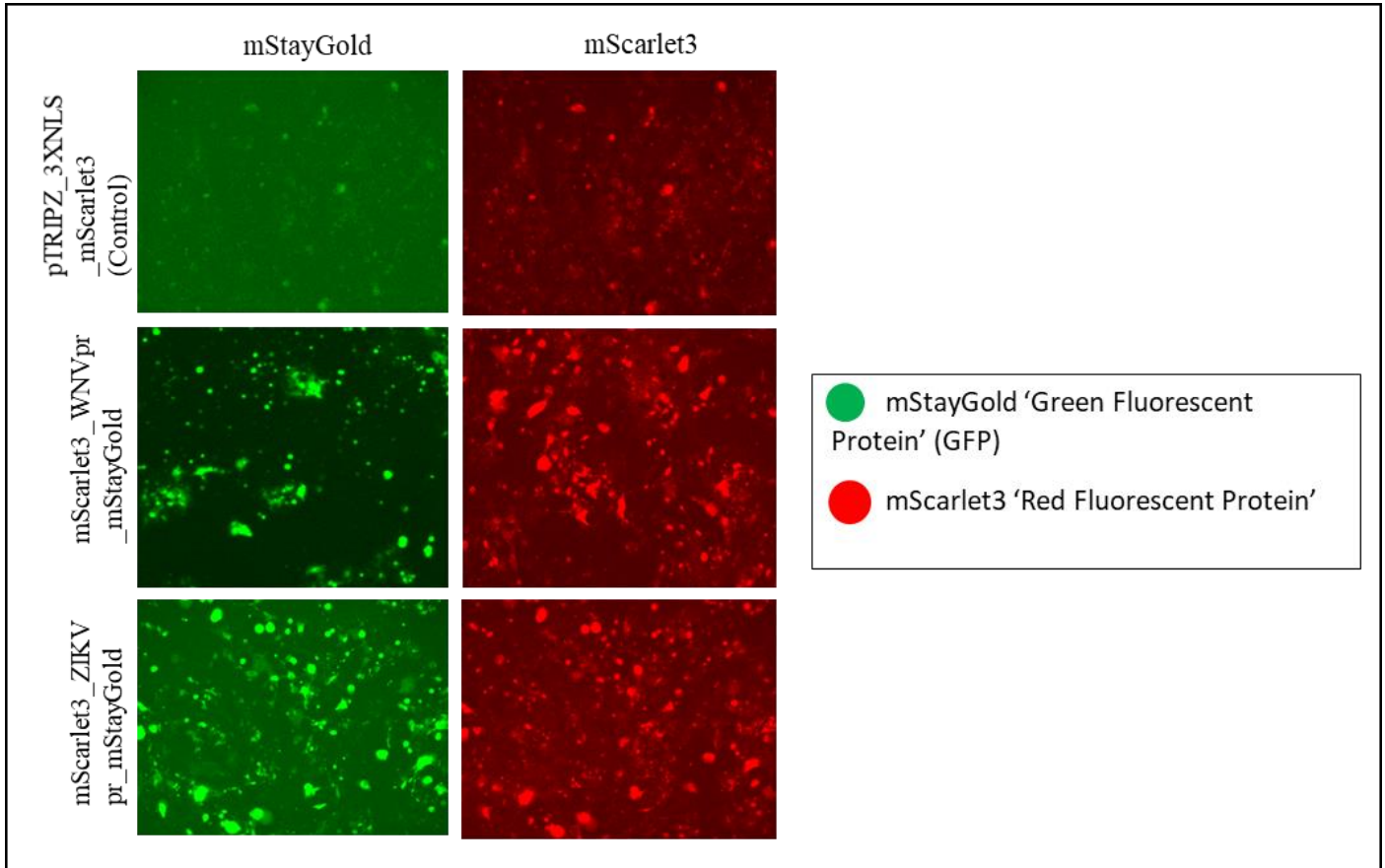


**Figure 3.3.1: Lentivirus transfection using Lipofectamine 2000 protocol.**

Reporter plasmids (pTRIPZ\_3XNLS\_mScarlet3\_WNVpr\_mStayGold, pTRIPZ\_3XNLS\_mScarlet3\_ZIKVpr\_mStayGold) and Packaging Plasmids (psPAX2, and pMD2.G) were transfected with HEK293 FT cells using Lipofectamine 2000 protocol as described in 2.2.4.1. We could see inhomogeneous and lower doxycycline-induced expression of mStayGold (Green) and mScarlet3 (Red) which was not expected and resulted from lower transfection efficiency while using Lipofectamine 2000 reagent.

### 3.3.2 Transfection using Lipofectamine 3000 and assessment of transfection efficiency

As mentioned in 2.2.4.2, 293FT cells were transfected using Lipofectamine 3000 transfection reagent since Lipofectamine 2000 yielded a qualitatively lower transfection efficiency, as described in 3.3.1. Cells were treated with doxycycline and imaged under EVOS M5000 (Invitrogen by Thermo Fisher Scientific) to confirm doxycycline-induced expression and transfection efficiency as shown in Figure 3.3.2. In order to achieve high transfection efficiency, Lipofectamine 3000 reagent was used in combination with an optimized 293FT cell

transfection protocol (Thermo Fisher Scientific; <https://assets.thermofisher.com/TFS-Assets/BID/Application-Notes/lentiviral-production-lipofectamine-reagent-app-note.pdf>) that involved a higher cell density and optimized transfection reagent and DNA volumes. This resulted in enhanced transfection efficiency as compared to Lipofectamine 2000 (Figure 3.3.2). This higher transfection efficiency could be due to optimal cell density and the improved properties of the Lipofectamine 3000 reagent. Here, cells transfected with pTRIPZ\_3XNLS\_mScarlet3 serve as a control to assess background fluorescence and as well to compare the relative transfection efficiency from that of cells expressing reporter construct mScarlet3\_WNVpr\_mStayGold, and mScarlet3\_ZIKVpr\_mStayGold.

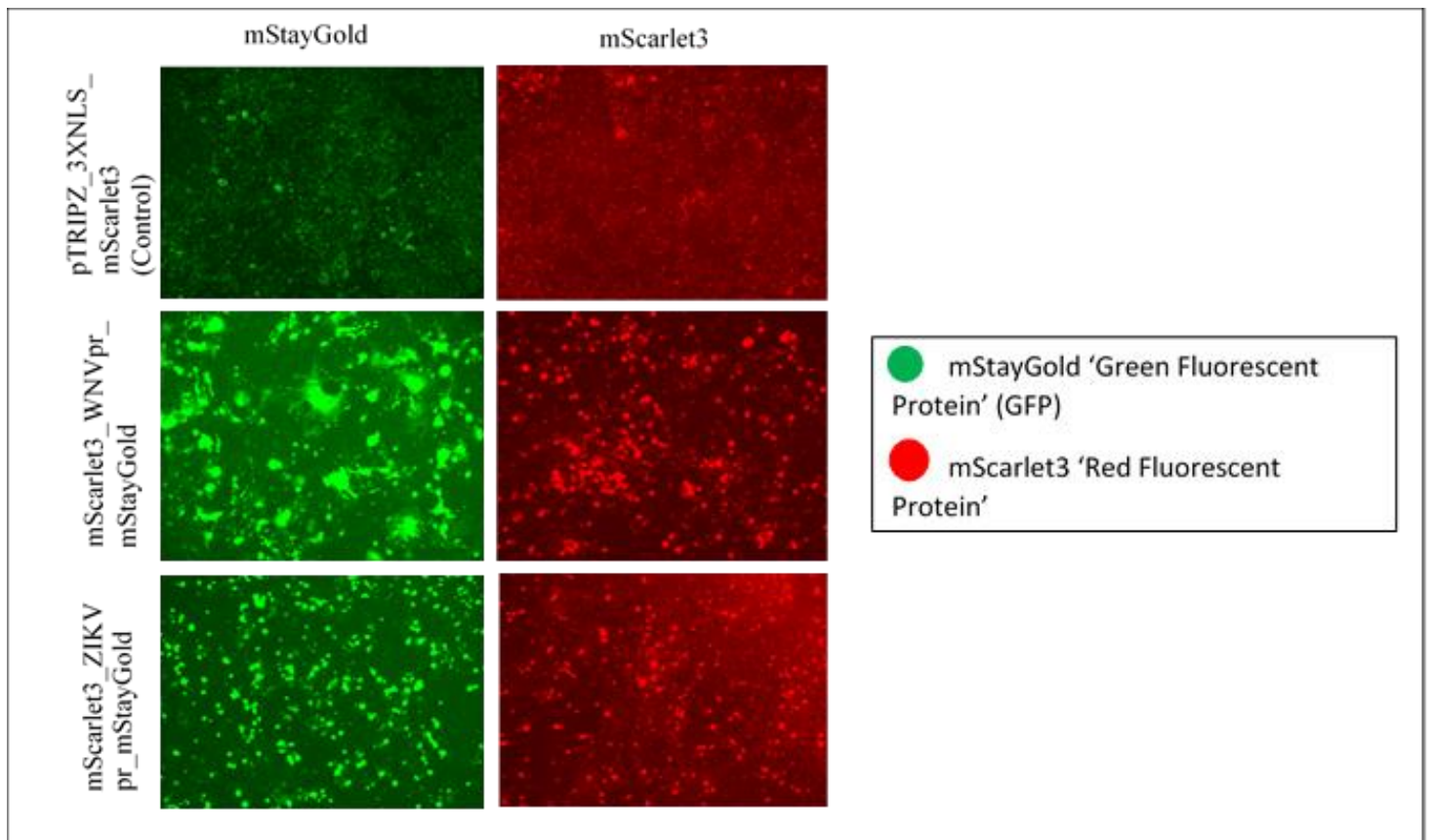


**Figure 3.3.2: Lentivirus production via transfection of 293FT cells using Lipofectamine 3000 protocol.** Reporter plasmids (pTRIPZ\_3XNLS\_mScarlet3\_WNVpr\_mStayGold, and pTRIPZ\_3XNLS\_mScarlet3\_ZIKVpr\_mStayGold) and Packaging Plasmids (psPAX2, and pMD2.G) were transfected into HEK293FT cells using Lipofectamine 3000, as described in 2.2.4.2 and 2.2.4.3. We could see a homogenous higher doxycycline-induced expression of mStayGold (Green) and

mScarlet3 (Red) as compared to images of the cells transfected using Lipofectamine 2000 transfection reagent (Figure 3.3.1).

### **3.4 Inefficient production of infectious lentiviral vectors capable of transducing Huh7.5 cells after repeated and careful transfection of pTRIPZ\_3XNLS\_mScarlet3\_WNVpr\_mStayGold, and pTRIPZ\_3XNLS\_mScarlet3\_ZIKVpr\_mStayGold with lentiviral packaging plasmids into 293FT cells**

As described in 3.3.2 the transfection efficiency was higher while using Lipofectamine 3000 resulting in more homogenous expression of fluorescent protein induced with doxycycline. Based on this, the produced lentivirus encoding for WNVpr\_mStayGold and ZIKVpr\_mStayGold (see section 2.2.4.2) was used to transduce target Huh-7.5 cells. After overnight incubation at 37°C at 5% CO<sub>2</sub>, the lentivirus media was removed and replaced with fresh media containing 3µg/ml puromycin to select the cells that harboured the fluorescent reporter construct (mScarlet3\_WNVpr\_mStayGold, and mScarlet3\_ZIKVpr\_mStayGold). After incubation for 3 days at 37°C at 5% CO<sub>2</sub>, however, the number of viable cells was very low. The media was again removed and replaced with fresh media containing puromycin at every 2-3 days depending upon the requirement for the cells. After continuous cultured puromycin-resistant cells, they were expanded into 25cm<sup>2</sup> flasks. Despite the strong 293FT cell transfection during lentiviral packaging and successful growth of puromycin-resistant cells in 6-well plates, nearly all of the cells died after expansion into 25 cm<sup>2</sup> flasks. Although the lentivirus packaging and transduction process was repeated and completed several times, the generation of puromycin-resistant stable Huh-7.5 cell lines after lentiviral transduction and puromycin selection was unsuccessful. Despite an apparently high transfection efficiency of 293FT cells during lentiviral packaging (see 3.3.2), as determined by fluorescence of cells transfected with packaging vectors and the pTRIPZ\_3XNLS\_mScarlet3, pTRIPZ\_3XNLS\_mScarlet3\_WNVpr\_mStayGold, and pTRIPZ\_3XNLS\_mScarlet3\_ZIKVpr\_mStayGold plasmids, the inefficient transduction of Huh-7.5 cells suggested that there may have been problems with efficient lentiviral packaging. This may be attributable to partial degradation of the lentiviral packaging plasmids (psPAX2 and pMD2.G). In order to perform subsequent experiment to show progress of the generated reporter construct, Huh7.5 cells stably expressing an analogous DENVpr eGFP or ZIKV-pr-eGFP fusion protein and a separate

3x-NLS\_mScarlet construct (which were previously generated by Dr. Nicholas Eyre) were resuscitated and utilized for infection and nuclear translocation experiments.

### **3.5 Fluorescent Activated Cells Sorting (FACS) of Huh7.5+ pTRIPZ\_3XNLS\_mScarlet3\_DENVpr\_mStayGold reporter proteins for obtaining high fluorescent positive cells**

The previously generated Huh7.5 + pTRIPZ\_3XNLS\_mScarlet3\_DENVpr\_mStayGold cells were harvested and seeded as described in 2.2.1 and 2.2.2. Cells were treated with 1 µg/ml doxycycline one day before cell sorting to induce expression of the fluorescent reporter construct.. The parent cells “Huh7.5 cells” served as a negative control (Figure 3.5A), while the Huh7.5 cells harbouring DENV reporter cells were 95% positive for mStayGold (Green Fluorescent Protein) fluorescence (Figure 3.5B). It is important to note that strong and relatively homogenous expression of the fluorescent reporter construct was desirable for further experiments involving DENV, WNV and ZIKV infection.

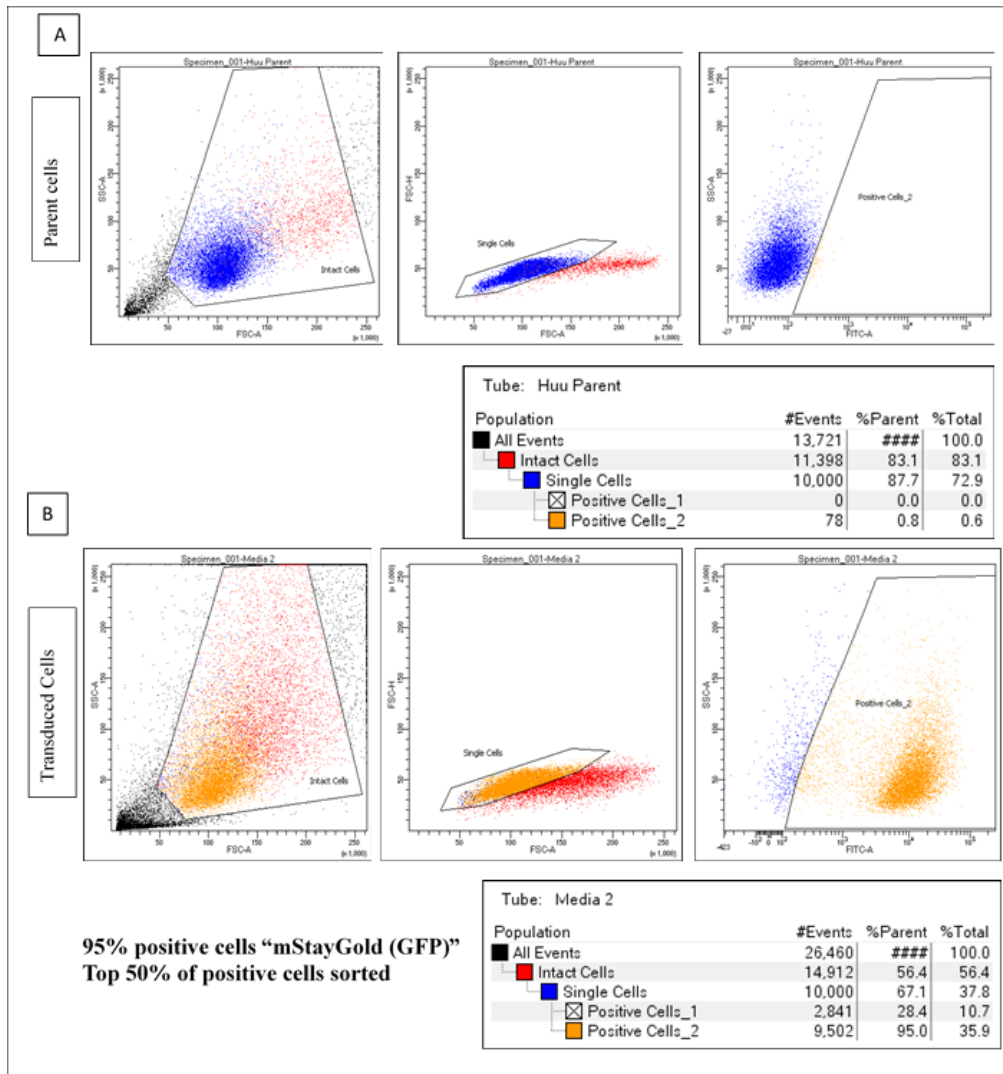


**Figure 3.5: Fluorescence Activated Cell Sorting of transduced Huh7.5 cells harbouring DENV reporter (mScarlet3 and mStayGold) cells for high fluorescence.** Here plot 1 in both A and B identifies majority of intact cells containing cell debris based on their cell sizes, plot 2 represents individual cells by excluding the doublets and plot 3 further analysed for fluorescent marker expression (FITC = mStayGold Fluorescence). (A) Showed the parent “Huh7.5” cells which serve as a negative control and we could see the distribution of intact, single cells and extent of green fluorescence in the sample (‘Background Fluorescence’). (B) Indicates the similar selection of intact cells, isolation of them from doublets and further analysed for high positive fluorescence cells, where 35.0% of all events showed high fluorescence representing that they are expressing the 95% of mStayGold fluorescent proteins.

### **3.6 Characterization of DENV, WNV, and ZIKV Protease Reporter Construct Design**

In order to monitor the live cell in orthoflavivirus infection, a reporter construct expressing GFP fused with the respective orthoflavivirus protease system was designed which can be cleaved by the presence of viral NS2B/NS3 proteases at a cleavage site. The construct design as shown in Figure 3.6A shows GFP containing three nuclear localization signal (NLS) sequence anchored with the transmembrane domain (TM) of the endoplasmic reticulum (ER) protein sec61 $\beta$  to target the fluorescent reporter protein to ER membranes through a linker. Various protease cleavage sequences specific to respective orthoflavivirus like DENV, WNV, and ZIKV can be inserted in the linker. The viral protease cleavage of the linker region would then result in translocation of GFP from cytoplasm of the ER to the nucleus (Figure 3.6B), revealed the presence of viral infection, which can be easily monitored and detected using live cell imaging software like Incucyte SX5 imaging system (Sartorius).

The DENV, WNV, and ZIKV polyprotein which is cleaved by viral NS2B/NS3 protease into individual viral proteins ((Arias et al., 1993; Medin et al., 2015; Preugschat et al., 1990)), NS2B/NS3 protein anchors it to ER membranes depending upon the cleavage sequences which were inserted into the reporter construct for DENV, WNV, and ZIKV. The specific DENV, WNV, and ZIKV capsid cleavage site sequences is shown in Table 3.6.

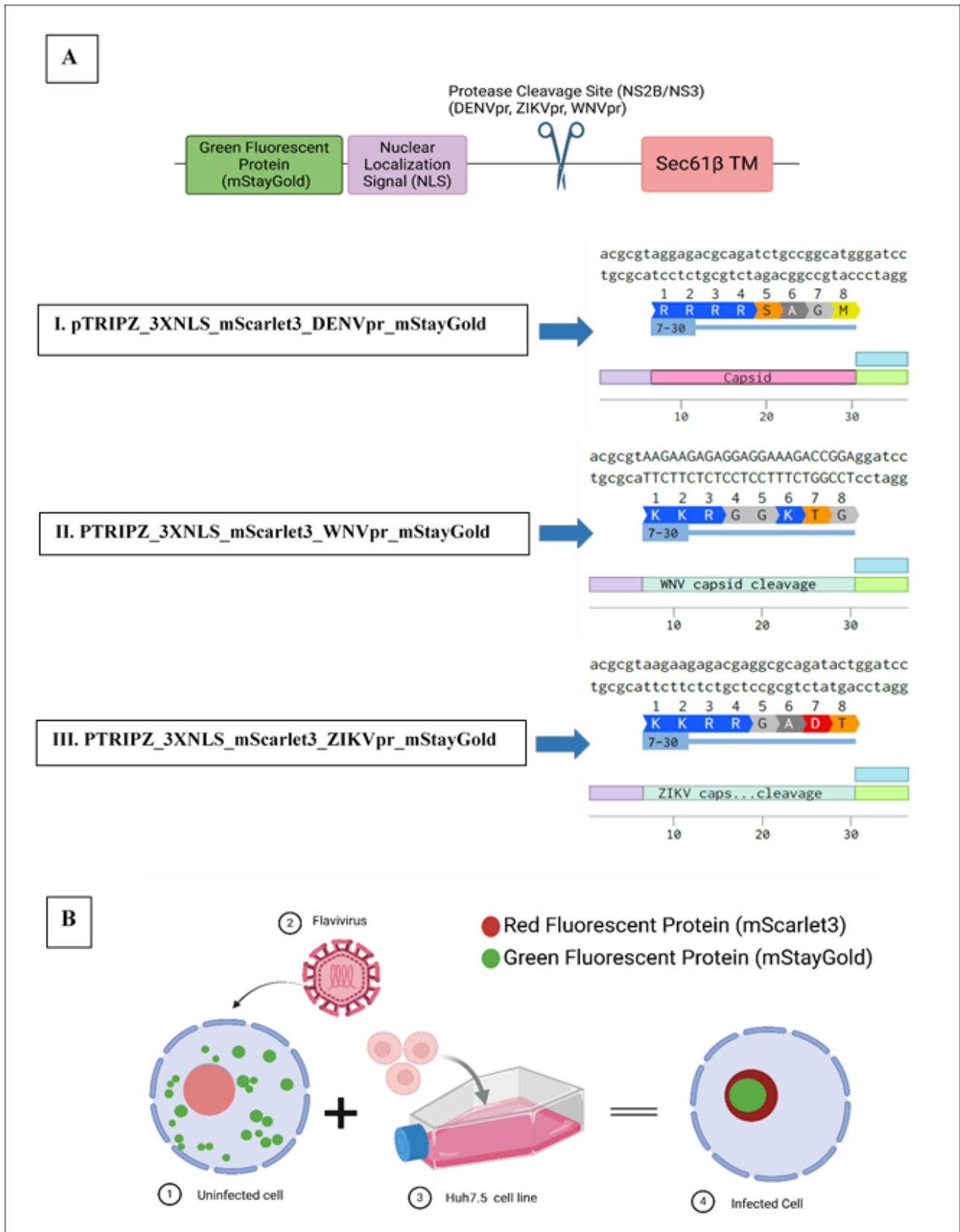


**Figure 3.6: Orthoflaviviruses (DENV, WNV, and ZIKV) reporter construct design.** (A) Shows the GFP anchored with TM of ER membrane protein sec61β and the cleavage site

specific sequences for each reporter plasmid constructs (full sequences is shown in Figure Appendices 5). (B) Shows the schematic of translocation of GFP from cytoplasm to nucleus upon infection as viral protease cleaved the linker region at the protease cleavage site shown in (A). Red and Green fluorescent protein are coloured as indicated on top right of the panel in B.

**Table 3.6: List of DENV, WNV, and ZIKV capsid cleavage site sequences inserted into reporter construct for each corresponding orthoflaviviruses**

Capsid	Cleavage Site Sequence
Dengue Virus Capsid Cleavage Site	RRRR ↓SAGM
West Nile Virus Capsid Cleavage Site	KKRG ↓GKTG
Zika Virus Capsid Cleavage Site	KKRR ↓GADT

### **3.7 Incucyte live cell imaging of nuclear relocation of the protease-dependent mStayGold reporter proteins following DENV2 infection at different Hours Post Infection (h.p.i) and Multiplicity of Infection (MOI)**

#### **3.7.1 Incucyte live cell imaging of nuclear relocation of the protease-dependent mStayGold reporter following MOI 0 to 2 of DENV2**

The stable cell lines for the DENV protease reporter construct (Huh 7.5 + pTRIPZ\_3XNLS\_mScarlet3\_DENVpr\_mStayGold) which were previously generated by Dr. Nicholas Eyre through lentiviral production were harvested and seeded in a 96-well imaging plate as described in methodology section 2.2.3.3. Cells were treated with 1 µg/ml doxycycline to induce expression of the fluorescent reporter protein and after 24-hour incubation at 37°C at 5% CO<sub>2</sub>, cells were infected with wildtype dengue virus (DENV2) at 2-fold serial dilution of Multiplicity of Infection (MOI) from 2 to 0.002. Here, uninfected cells served as a negative control.

In uninfected cells (Figure 3.7.1A), we can see the ER-like pattern represented by mStayGold (GFP) in the cells expressing at MOI 0 (not infected), while mScarlet3 localized to the nucleus. As almost all of the mStayGold fluorescence was found in the cytoplasm, this was consistent

with the absence of DENV2 infection. As shown in images at MOI 0.125, MOI 0.25, MOI 1, and MOI 2, the majority of cells were double positive (Green and Red proteins) for nuclear fluorescence in DENV2 infected cells, with a noticeable increase in the GFP translocation from cytoplasm into the nucleus begun at MOI 0.125 (Figure 3.7.1A). A very similar pattern and even higher nuclear GFP accumulation was observed in the reporter cell lines expressing the reporter constructs at MOI 0.25, with most prominent at MOI 1 and MOI 2. A very clear difference in nuclear GFP following the DENV2 was seen in increasing infection levels. Among all the reporter constructs that were tested for DENV2 at high infection dose (MOI 2), showed relatively higher nuclear GFP localization, which also shows that the nuclear localization of GFP is dose dependent and upon infection, GFP translocate into nucleus from cytoplasm indicating the activation of viral protease. In Figure 3.7.1B, this evidence has been further illustrated by plotting the total percent of cells expressing the reporter construct (mStayGold + mScarlet3) at different MOIs. Here, it is can be seen as, at MOI 0 (uninfected), some cells already showed some nuclear GFP signal whereas, at MOI 2 almost all of the cells expressing the reporter construct showed nuclear GFP localization and very lower cytoplasmic GFP. This showed a good indication to validate our generated reporter constructs performed upon orthoflavivirus infection. Similarly, a drastic GFP translocation with relatively higher peak indicating more GFP translocation into nucleus was seen at an MOI 0.25 (Figure 3.7.1C). Consequently, complete GFP translocation in the nucleus was observed at MOI 2, thereby confirming that the detection of infection was dose dependent.

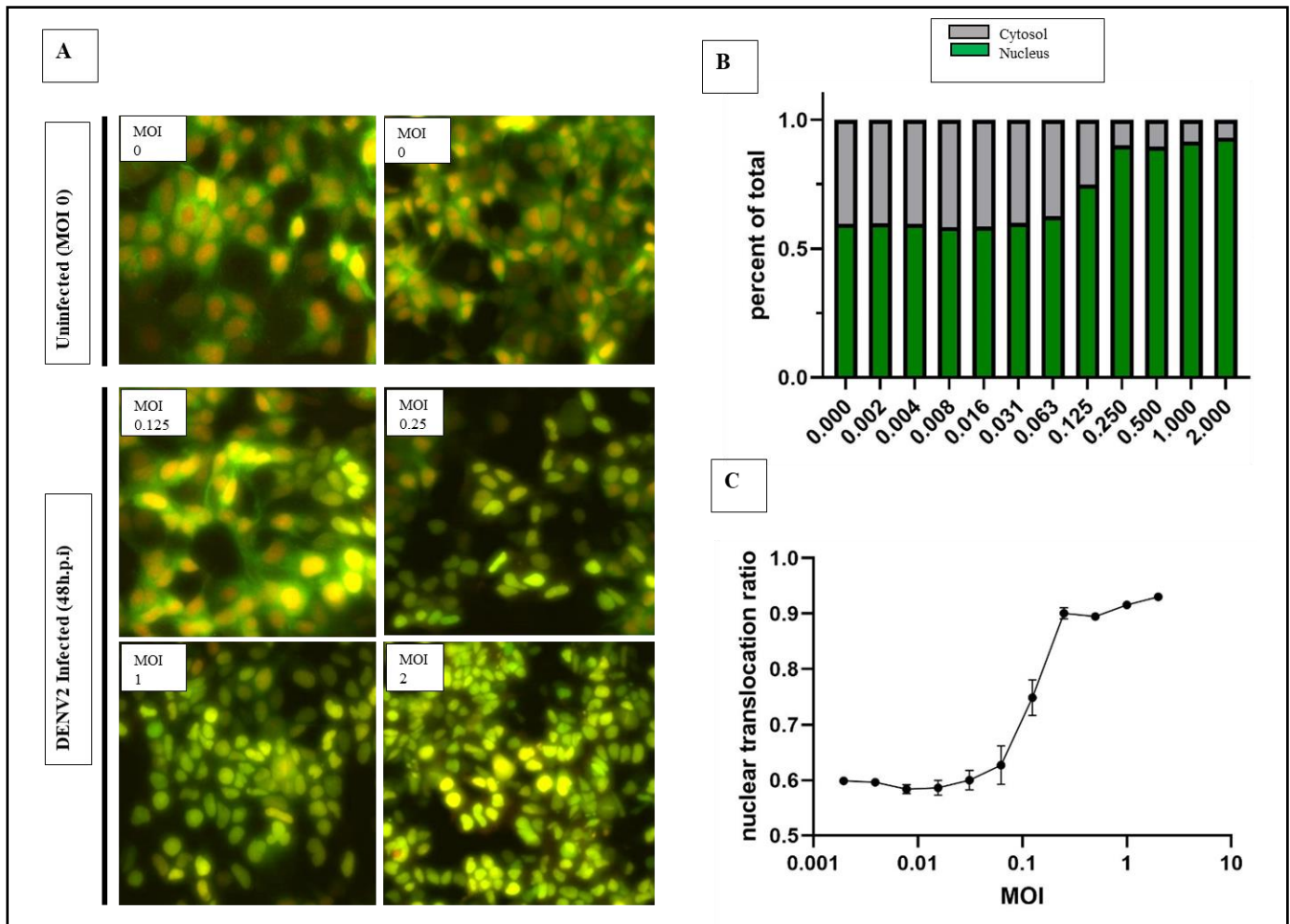


**Figure 3.7.1: Live cell imaging of DENVpr reporter construct for nuclear localization of mStayGold (GFP) following DENV2 at MOI 2 (48h.p.i).** (A) Huh7.5 cells stably expressing the 2xNLS\_mScarlet3\_2A\_DENVpr-mStayGold reporter construct were infected with DENV2 at a range of concentrations (2-fold serial dilutions of DENV2; MOIs: 0.125, 0.25, 1, and 2) or uninfected (MOI 0). Representative live cell images of uninfected cells (MOI 0) and cells infected with a range of high MOIs (0.125, 0.25, 1, and 2) at 48h.p.i. (B) Quantitation of nuclear localization of mStayGold under various DENV-2 infection conditions. The bar graph shows the total percentage of green/red double positive cells that display a green fluorescent nuclear. (C) The line graph shows GFP nuclear translocation ratios plotted against different DENV2 MOIs. Scale bar = 200µm. Cells were imaged using an Incucyte SX5 (Sartorius) live cell imaging system. Note that DENV2 infections were performed by Dr. Nicholas Eyre and assistance in imaging analysis was provided by Dr. Eva Hesping.

### **3.7.2 Confirmation of early identification of protease-dependent reporter cells expressing mStayGold nuclear relocation following hours post infection of DENV2**

As described in 3.7.1, cells were infected with wild-type (WT) DENV2 and incubated at 37°C at 5% CO<sub>2</sub>. Doxycycline was present throughout the experiment. At 24h.p.i, cells were imaged in Incucyte SX5 imaging system for further 24 hours at 20 x objective with 3-4 images per well. As we can see, the double positive mStayGold + mScarlet3 (green and red) fluorescent cells expressed the reporter constructs, uninfected cells represent the GFP localized like ER pattern (Figure 3.7.2A). As compared to infected cells at 24h, 36h, and 48h postinfection, cells showed increased in nuclear GFP localization with early detection at 24 hours postinfection (Figure 3.7.2A). The overall number of the double positive cells expressing GFP nuclear localization was higher at 48h postinfection as compared to infected cells after 24h and 36 hours postinfection (Figure 3.7.2B). The increment in mScarlet3 suggests viral replication and growth in a time course manner in case of cells infected with wild-type DENV2. This also predicts mScarlet3 showed higher nuclear translocation of GFP with increase in hours postinfection, respectively (Figure 3.7.2B).

As shown in Figure 3.7.2C, the total nuclear translocation ratio which indicates the cells expressing reporter constructs in nucleus showed higher ratio i.e. 0.90 at 48h.p.i and lower ratio i.e. 0.75 at 24h.p.i, providing evidence for nuclear GFP translocation from cytoplasm to nucleus with increase in green fluorescent signal in a time dependent manner. Additionally, nuclear translocation ratio of 0.75 at 27h.p.i has also suggest early detection of nuclear GFP translocation in reporter constructs cells infected with wildtype dengue virus. Further, this result gives an overall well correlation of total percentage of double-positive cells (Figure 3.7.2B) with the nuclear translocation ratio at different time points upon infection (Figure 3.7.2C).

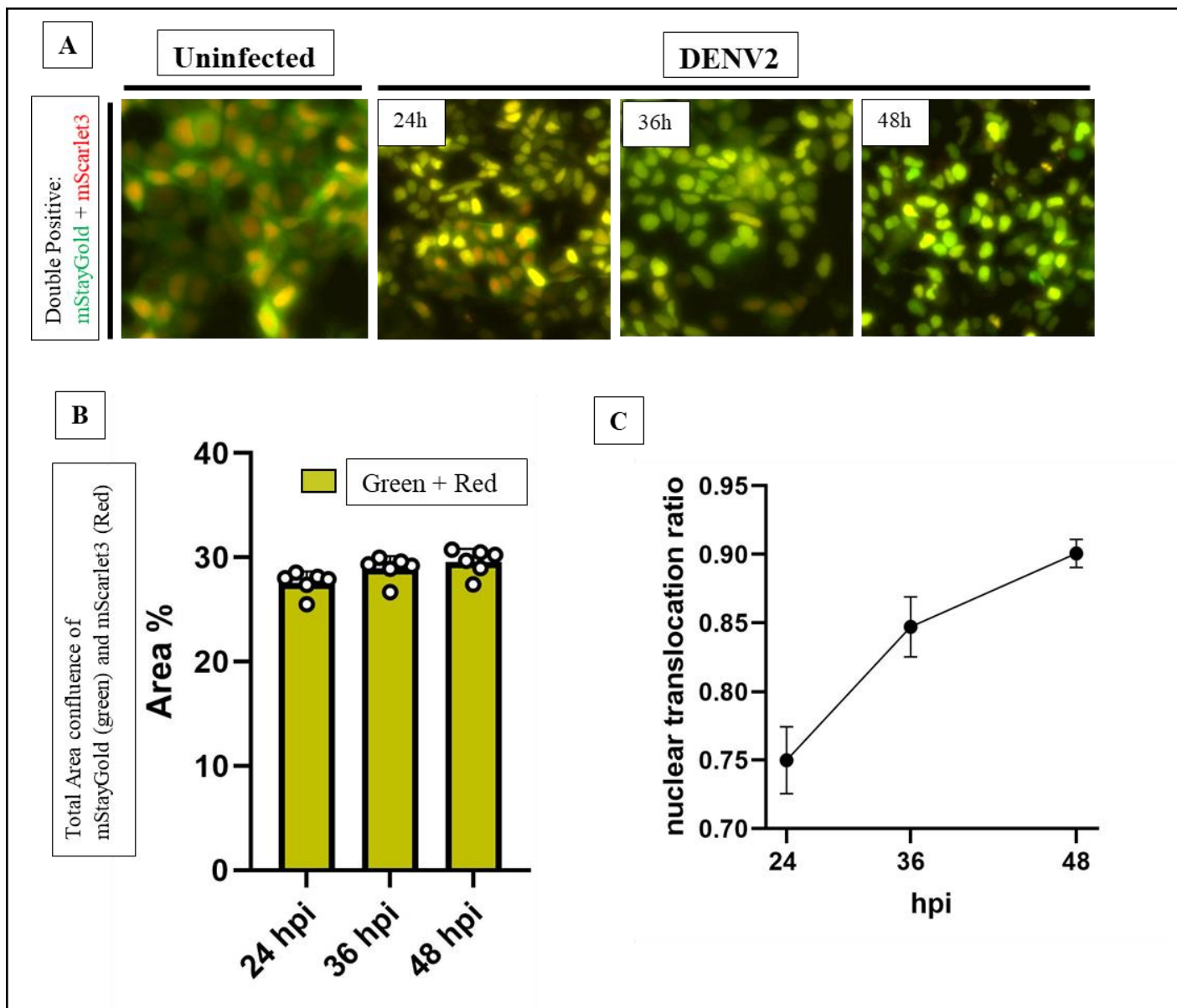


**Figure 3.7.2: DENV reporter system under uninfected and DENV2-infected conditions at 24h, 36h, and 48h postinfection (h.p.i).** (A) Uninfected cells showing ER-like cytoplasmic distribution of mStayGold without nuclear translocation, when infected, cells showed nuclear translocation of GFP with increase in nuclear fluorescence signal at 24h, 36h, and 48h postinfection representing the activation of viral protease through cleavage and translocation of GFP into the nucleus. (B) Quantification of images acquired in A. The total percentage area of double positive cells increase across time points, a sign that replication capacity of the reporter virus is higher within a time dependent manner. (C) Quantification of images acquired from experiment shown in A. Ratio of nuclear translocation for GFP localized in nucleus from cytoplasm. For each time points, ratio increases as increase in level of infection. Scale bar = 200µm. Note that this data was extracted from the same experiment described in Fig.3.7.1.

### **3.8 Immunofluorescence analysis of Dengue Virus Reporter Protease (DENVpr) shows activation of viral protease in infected versus uninfected cells.**

As mentioned in methodology section 2.2.3.3, the stable cell lines after WT dengue virus infection for 48hours, the activity of the reporter construct was further assessed by indirect immunofluorescence staining in both uninfected and infected cells to check how well the cell has respond to infection and GFP localization at a subcellular level. Cells were fixed and stained with primary antibody, secondary antibody as mentioned in materials section 2.1.5 and 2.1.6 and DAPI to visualize the viral envelope proteins in infected cells.

In stained cells (Figure 3.8 ‘top panel’), the nuclei stained with DAPI is shown in blue, Anti E AlexaFluor647-conjugated secondary antibody in red showed stable expression of reporter protein. These stained cells represent the morphology of the DAPI stained nuclei, distributed red fluorescence and minimal red fluorescent intensity. In contrast, the DENV2 infected cells (Figure 3.8 ‘bottom panel’) with merged (DAPI+ Anti E AlexaFluor647) signals expressing reporter constructs at MOI 1, MOI 2, MOI 3, and MOI 5 showed strong red fluorescence indicating the presence of viral envelope proteins with increasing in multiplicity of infection (MOIs). Cell expressing reporter construct at MOI 5 indicate highest infection level by clearly differentiating the active state of DENV reporter protease from inactive state following the dengue virus infection. However, lower number of the reporting cells were observed in reporter construct at MOI 5 in compared to cells in construct at MOI 1. Additionally, infection level in the cells expressing reporter constructs were associated with high virus infection, illustrating a dose-related activation of the reporter system. Moreover, by MOI 5, almost all the cells have progressive increase in red fluorescent intensity signal, which suggests that the antibody-based detection is specific and the high infection efficiency is dose-dependent with the production of more viral envelope proteins.

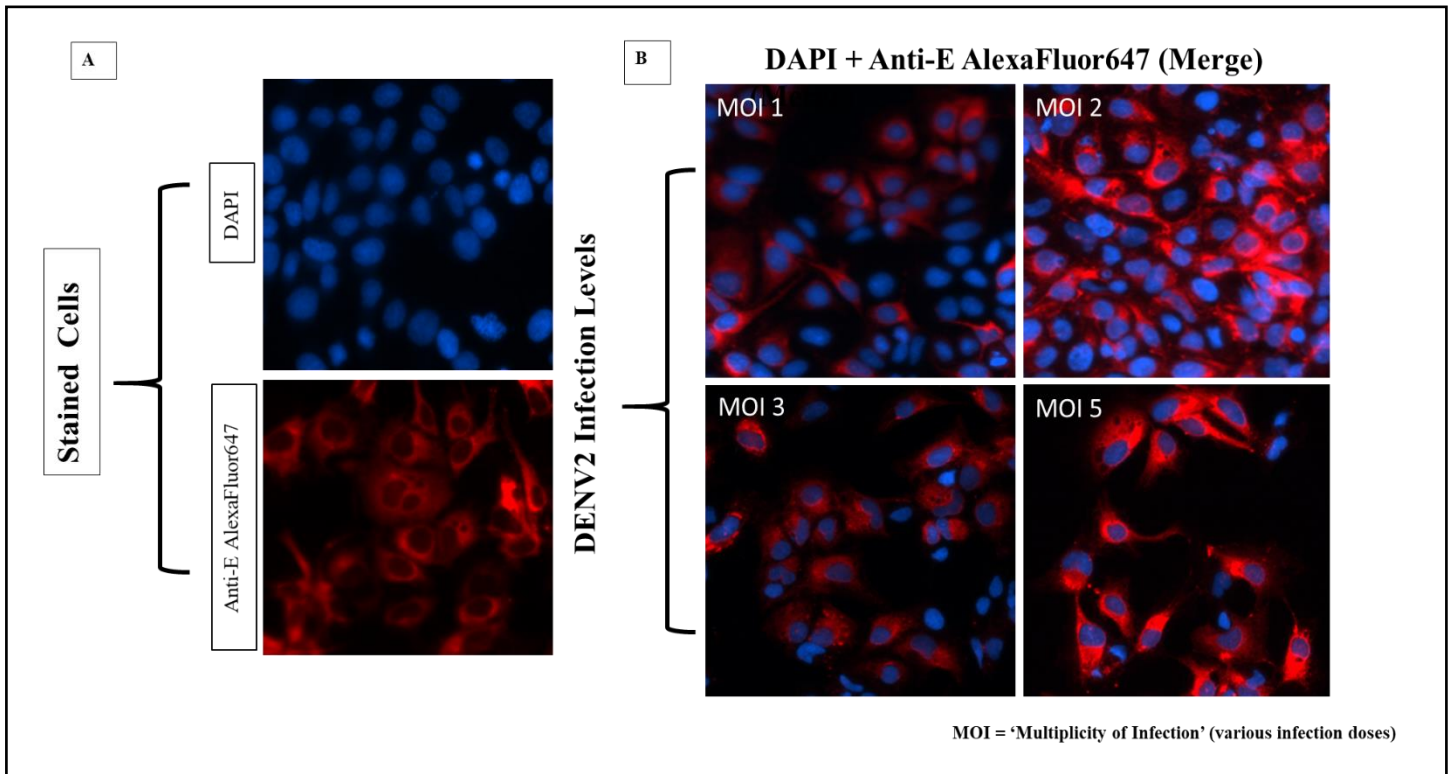


**Figure 3.8: Immunofluorescence imaging of DENV reporter protease using confocal microscopy to analyse reporter activity within uninfected and WT DENV infected conditions.** Cells were stained (Top panel) showed nuclei stained DAPI in blue and Anti E AlexaFluor647-conjugated secondary antibody in red. DENV Infected cells (bottom panel) in reporter constructs at MOI 1, 2, 3, and 5 signified progressive increase in red fluorescence confirming more infected cells and producing more viral envelope proteins in reporter constructs at MOI 5. Note that DENV-2 infections were performed by Dr. Nicholas Eyre.

### **3.9 Western Blot Analysis of Huh-7.5+eGFP DENVpr+pTRIPZ\_3XNLS\_mScarlet3 and Huh-7.5+eGFP ZIKVpr+pTRIPZ\_3XNLS\_mScarlet3 cell line showed the cleavage properties of reporter construct upon infection with Dengue and Zika viruses**

In this western blot study, the Huh-7.5+eGFP DENVpr+pTRIPZ\_3XNLS\_mScarlet3 and Huh-7.5+eGFP ZIKVpr+pTRIPZ\_3XNLS\_mScarlet3 cell line was used, which was previously generated by Dr. Nicholas Eyre. To validate the similar functioning of our reporter construct, western blot analysis was performed for the cell lysates prepared 48hours postinfection (h.p.i)

(Figure 3.9A, 3.9B). Among all the lanes, the Huh-7.5 cells was used as a control to compare with the DENV and ZIKV reporter proteases cleavage activity. As we can see in figure 3.9A, the green bands across all the lanes shows, the loading control ' $\beta$ -Actin' and red bands shows the reporter construct tagged with eGFP. The green  $\beta$ -Actin bands are uniform throughout all lanes with the molecular weight of ~40kDa confirming the equal protein sample loading across all lanes. Similarly, we could see very strong fluorescent uncleaved eGFP protein in uninfected cells in compare to infected cells and was predicted to have a molecular weight of ~34kDa, based on the reporter construct design (Figure 3.9A). In infected cells, we observed an additional band of eGFP with an approximately lower molecular weight (Figure 3.9A, red arrow). Upon DENV2 infection, the additional band of ~30kDa eGFP protein was detected in both lysates of DENVpr and ZIKVpr cells, without any additional band in Huh-7.5 cells as expected (Pahmeier et al., 2021). Consequently, in ZIKV infection, similar ~30kDa eGFP protein band was detected in both lysates of DENVpr and ZIKVpr cells, without any additional band in Huh-7.5 cells. This additional band of molecular weight ~30kDa was consistent with the predicted molecular weight of the DENVpr and ZIKVpr cleavage product after infection with dengue and zika viruses, respectively (Figure 3.9B). However, we noted a very faint fluorescent cleavage product of the eGFP proteins in DENVpr when infected with ZIKV, suggesting zika virus might not fully cleaved the DENV protease as compared to dengue virus active cleavage in ZIKV protease upon infection.

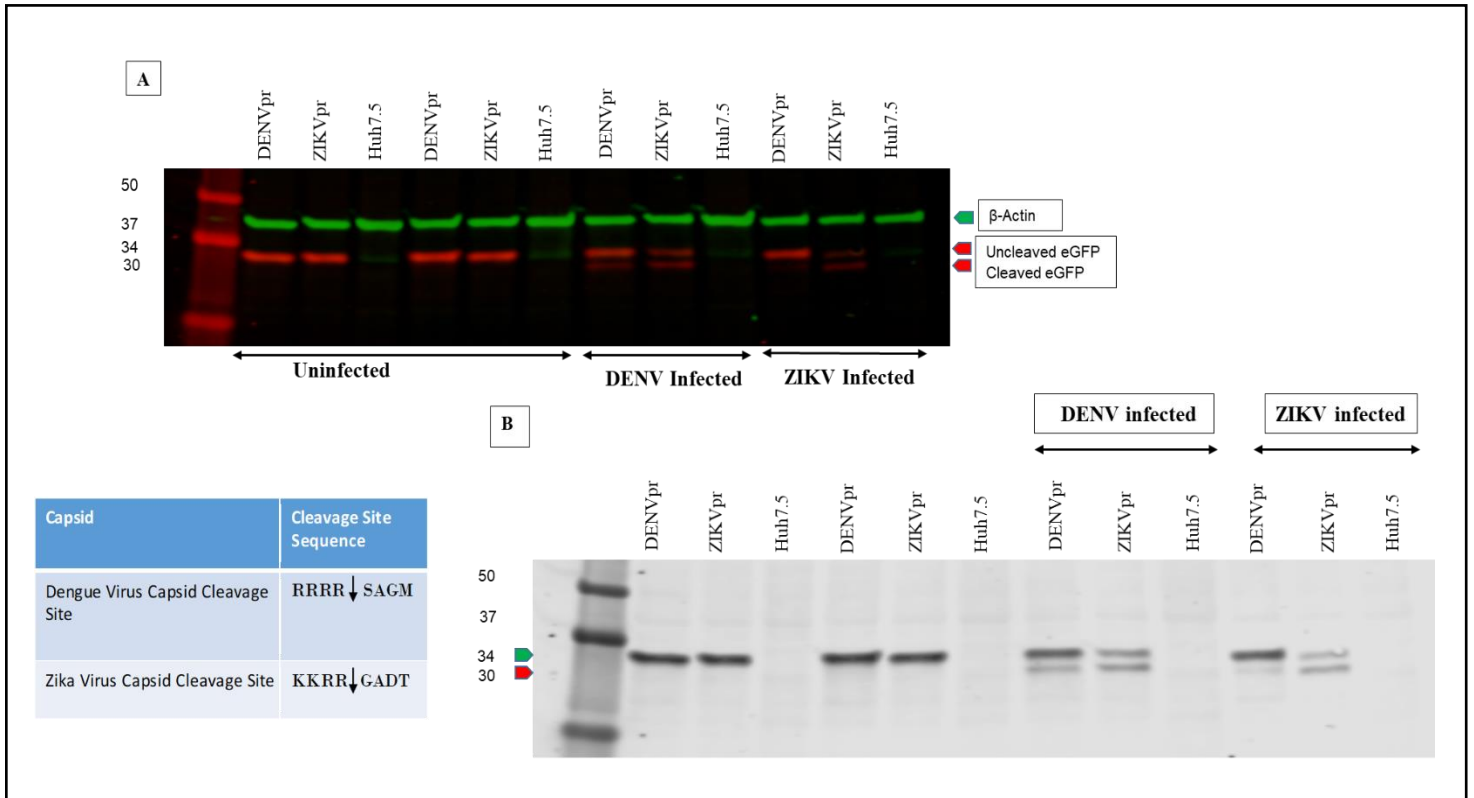


**Figure 3.9: Western Blot Analysis of Huh-7.5+eGFP DENVpr+pTRIPZ\_3XNLS\_mScarlet3 and Huh-7.5+eGFP ZIKVpr+pTRIPZ\_3XNLS\_mScarlet3 cell lysates prepared 48hpi (MOI=2) with DENV and ZIKV viruses.** At 48h.p.i, cell lysates were resolved by SDS-PAGE. The eGFP was detected with specific antibody. (A)  $\beta$ -Actin (green) served as a loading control and fluorescently tagged eGFP (red) with cleavage product (red arrow). (B) Green arrowheads, uncleaved reporter (~34kDa); red arrowhead, cleaved reporter (~30kDa) products. Note that DENV and ZIKV infections and lysate preparations were performed by Dr. Nicholas Eyre.

### 3.10 Time-course experiments confirms early nuclear translocation of the protease-dependent mStayGold reporter proteins after transient transfection following West Nile and Zika virus infection

As previously described in 2.2.5.1 the transient transfection of WNVpr and ZIKVpr was performed with HeLa cells and imaged at 24h.p.i. Here, we analysed the image showing nuclear GFP translocation in the uninfected and infected WNVpr and ZIKVpr reporter cell line. Cells were infected with either West Nile virus or Zika virus with respective protease reporter construct at MOI=1, and subsequently imaged using Incucyte SX5 live cell imaging system.

The uninfected WNV protease reporter cells already exhibited the nuclear GFP signal and in WNV infected cells expressing reporter construct, a noticeable increase of nuclear GFP was observed and even more accumulation of nuclear GFP upon WNV infection at 72 h.p.i (Figure 3.10A). The bar diagram showed total percentage of cells positive for both mStayGold and mScarlet3 at different time points following infection for West Nile Virus. 'Green bars' represent Infected WNV and 'White bars' represent uninfected WNV. As we can see at 24h.p.i, the total double positive cells is similar for both uninfected and infected cells with no clear difference in nuclear GFP localization following infection showing no any statistical significant difference (ns) between these cells. However, at 48h.p.i, there is a significant increase in double positive cells infected with WNV virus showing statistical significant difference (\*\*\*) between uninfected vs infected cells. Similarly, at 72h.p.i, significantly higher increase in double positive cells was observed which signify high nuclear GFP translocation due to activation of the WNV protease upon infection showed high statistical significant difference (\*\*\*\*) between uninfected vs infected cells (Figure 3.10A).

Comparatively, the uninfected ZIKV protease reporter cells exhibited ER-like localization of the GFP signals whereas, in infected cells expressing reporter construct, a noticeable increase in nuclear GFP was observed as early as 24 hours postinfection (Figure 3.10B) and even higher accumulation of nuclear GFP upon infection at 72 h. The bar diagram alongside represent total percentage of cells positive for both mStayGold and mScarlet3 at different time points following infection with Zika Virus. 'Green bars' represent Infected ZIKV and 'White bars' represent uninfected ZIKV. At 24h.p.i, the total double positive cells for both uninfected and infected cells showed clear difference in nuclear GFP localization following infection showed statistical significant difference (\*) between these cells. Similarly, at 48h.p.i, there is a strong significant increase in double positive cells infected with ZIKV virus showing high statistical significant difference (\*\*\*\*) between uninfected vs infected cells. Consequently, at 72h.p.i, similar higher increase in double positive cells was observed which signify high nuclear GFP translocation due to activation of the ZIKV protease upon infection showed high similar significant difference (\*\*\*\*) between uninfected vs infected cells (Figure 3.10B).

Importantly, increase in the percentage of double positive cells showed nuclear translocation of GFP (mStayGold) at 48 hours and 72 hours postinfection, respectively (Figure 3.10). Additionally, fewer double positive cells ~2% exhibited nuclear GFP localization even in the absence of reporter virus signal in both WNV and ZIKV protease reporter cells could be due

to overexpression of the fluorescent reporter protein following the transient transfection with HeLa cells.

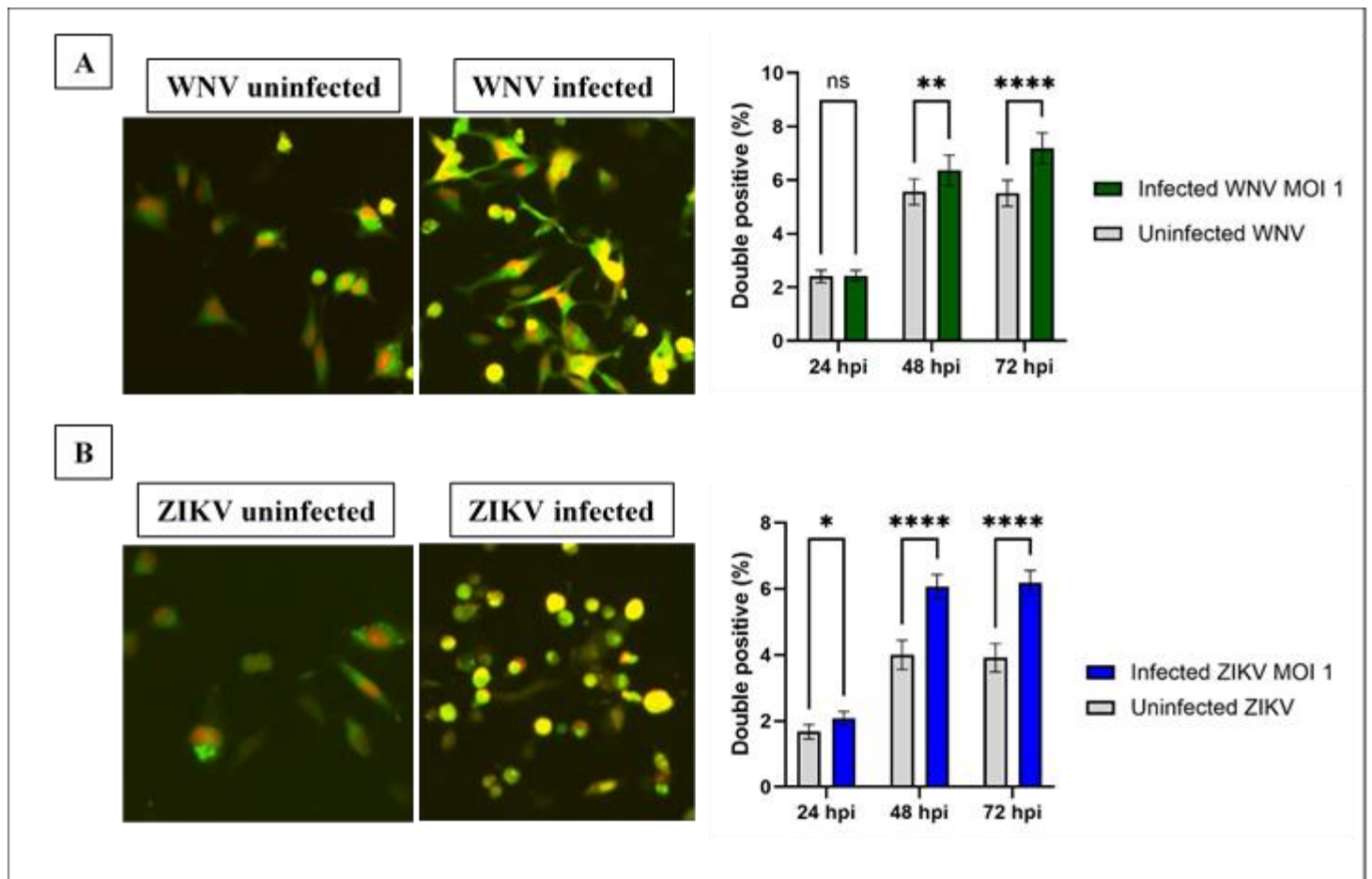


**Figure 3.10: Quantification of WNVpr and ZIKVpr reporter cell line following infection at different time points, 24hours, 48hours, and 72hours.** (A) Uninfected WNV (left) and infected WNV (right) with total percentage of cell positive for both mStayGold (green) and mScarlet3 (red) were quantified at 24, 48, and 72h.p.i. Similarly, (B) Uninfected ZIKV (left) and infected ZIKV (right) with total percentage of cell positive for both mStayGold (green) and mScarlet3 (red) were quantified at 24, 48, and 72h.p.i. Here, GFP localization is indicated by green fluorescence ‘GFP’ and nuclear staining by red fluorescence ‘mScarlet3’ for both Figure A, B. White bars are uninfected and green bars are infected cells (MOI 1). The statistical significance using paired *t-test* indicates; ns “not significant”, \* and \*\* “significant ( $p < 0.01$ )”, and \*\*\*\* “high significant ( $p < 0.0001$ )” shown at different time points reveals the experiment in a time dependent manner, providing evidence for nuclear GFP localization upon infection due to activation of viral reporter protein cleavage. Note that ZIKV and WNV (Kunjin)

infections were performed by Dr. Nicholas Eyre and assistance in imaging analysis was provided by Dr. Eva Hesping.

### **3.11 JNJ-A07 inhibits reporter-detected viral protease activity in infected cells validate the functioning of eGFP DENVpr reporter cell line for antiviral drug screening**

JNJ-A07 as a highly potent antiviral drug targets the viral proteins and has shown high action potential at the target region against all DENV serotypes thereby showing high antiviral efficacy (Goethals et al., 2023). JNJ-A07 had shown an outstanding efficacy against DENV infection by targeting DENV NS4B along with NS2B/NS3 helicase complex, thereby blocking the interaction and shows lower or no drug resistance (Kaptein et al., 2021). A proof-of-concept experiment to validate the reporter cell line generated in our laboratory settings was performed using JNJ-A07 with previously generated cell line i.e. Huh\_7.5+eGFP DENVpr\_pTRIPZ\_3XNLS\_mScarlet3 as mentioned in 2.2.9 which has very similar generation and characterisation to our generated cell line. The cells infected with WT DENV2 in a 96-well plate was loaded into Incucyte SX5 imaging system and imaged for 72 hours at every 2 hours. Representative images of DMSO 0.1% and JNJ-A07+infected cells are shown in Figure 3.11. Here, the DMSO treated infected cell display vibrant red and green fluorescence corresponding to the active viral infection and reporter construct expression (nuclear mScarlet3 with cytoplasmic mStayGold), whereas, JNJ-A07 treated with infected cell shows minimal fluorescence signal providing evidence to inhibit the active infection and viral protease activity (Figure 3.11A). As per our reporter construct design, the active fluorescent signal represent protease dependent cleavage of reporter construct resulting in nuclear GFP localization upon infection as described in 3.6.

In Figure 3.11B, the dose response curve of JNJ-A07 concentration in  $\mu\text{M}$  showing percentage of control value (DMSO treated controls) with time-course experiment presented by gradation of light blue (24h.p.i) to dark blue (72h.p.i). Based on the curve, JNJ-A07 showed minimal effect at the lower concentration ( $10^{-6}$  to  $10^{-4}$   $\mu\text{M}$ ) and we could see a sharp drop-off from  $10^{-3}$  to  $10^{-2}$   $\mu\text{M}$  in JNJ-A07 concentration showing highly potent antiviral action within this range

started to show inhibitory effect from 48h.p.i to maximal effect at 72h.p.i. At the concentration of  $>10^{-2}$   $\mu\text{M}$  and above, the infection was almost completely inhibited (% control  $\sim 0\%$ ), showing high efficacy. Overall data showed time-course dependent antiviral effect where inhibition was seemed to be greater in the later time-points 72h.p.i (thicker lines) indicating sustained inhibition. These data of incucyte imaging experiment confirms fewer infected cells after JNJ-A07 treatment, thereby decreasing the viral infection in a dose and time-dependent manner.

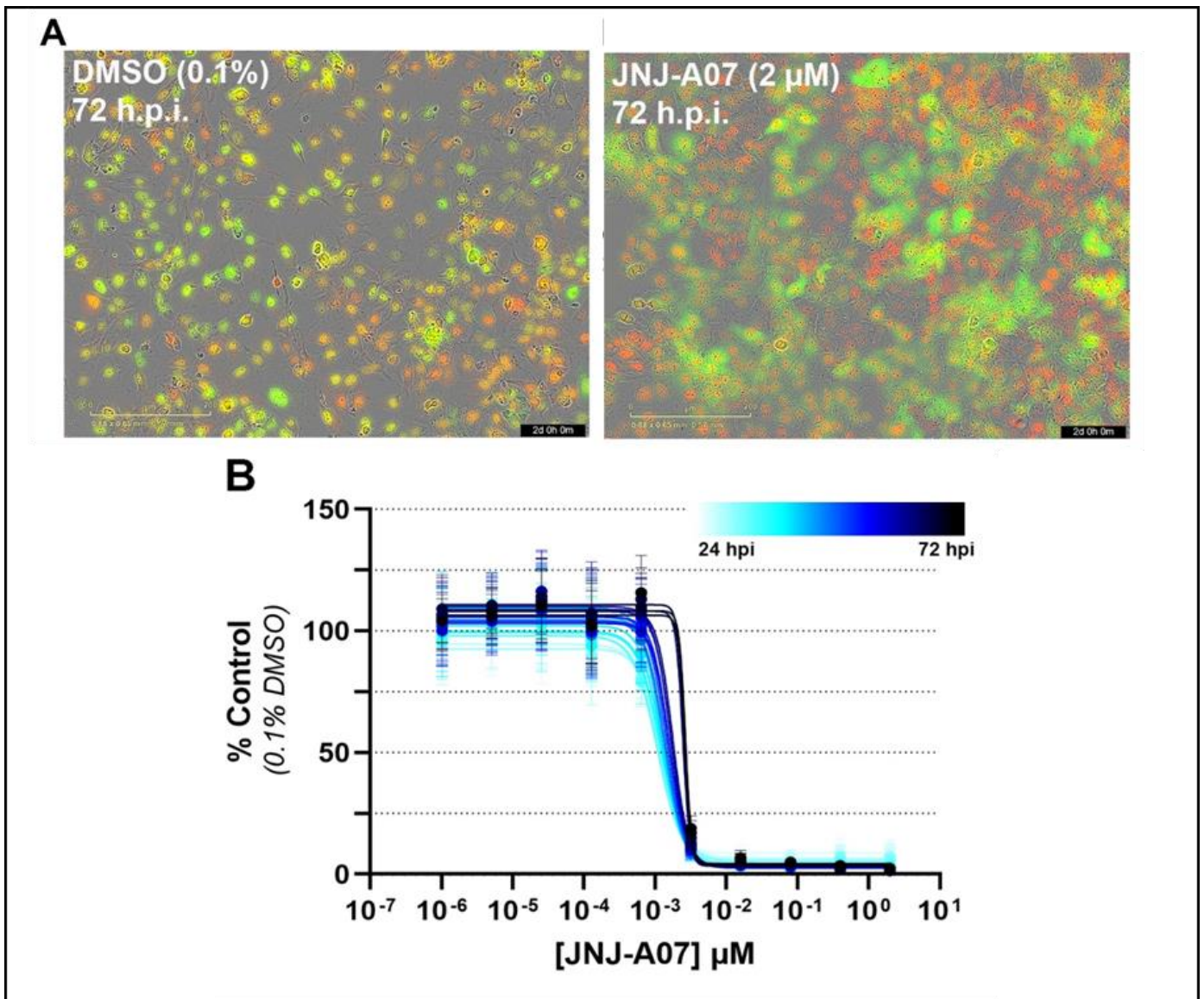


**Figure 3.11: Antiviral effect of JNJ-A07 antiviral drug in a DENV2 infection.** (A) infected cell fluorescence at 72 h.p.i, represents DMSO treated infected cells (left panel) and JNJ-A07 treated infected cells (right panel). In compared to DMSO-treated cells with JNJ-A07 treatment at 72h.p.i, fluorescence intensity was decreased in JNJ-A07 treated infected cells preferentially

in green channel suggesting the inhibition of viral protease activity and therefore the viral infection. (B) Dose response curve of JNJ-A07 concentration in  $\mu\text{M}$  showing minimal effect at the lower concentration ( $10^{-6}$  to  $10^{-4}$   $\mu\text{M}$ ) (24h.p.i) and a sharp drop-off from  $10^{-3}$  to  $10^{-2}$   $\mu\text{M}$  in JNJ-A07 concentration at 48h.p.i providing evidence of highly potent antiviral action within this range started to show inhibitory effect from 48h.p.i to maximal effect at 72h.p.i. Note that DENV infections, drug treatments and data analysis was performed by Dr. Nicholas Eyre.

## Chapter Four: Discussion

Orthoflaviviruses such as Dengue Virus, West Nile Virus, and Zika Virus, are among the most harmful single-stranded positive sense RNA viruses causing significant concerns in regions where they are highly prevalent (Wu et al., 2019). Clinical evidence of the disease caused by infection of these orthoflaviviruses are life threatening to global health posing intense illness and increased rates of transmission (Pierson & Diamond, 2020). Regardless of their impact, no universal antiviral therapies or vaccines have been approved scientifically in clinical settings for prevention and treatment of the infections caused by DENV, WNV, and ZIKV (Liang & Dai, 2024). Traditional microscopy-based studies of infection and ER remodelling in infected cells have used imaging of fixed cells, which are limited to provide only static views, which hinder the evidences for real-time monitoring of the viruses (Liu et al., 2020). Currently monitoring the viral infections in real time and finding suitable system to develop treatment options against the infection are minimal. However, real-time visualization of the virus infection is possible with the help of reporter systems that track the activity of viral protease that provides deeper insight into virus infection kinetics and interaction of virus with host cells (Pahmeier et al., 2021). In addition to this, reliability of the reporter system can be performed for screening and testing antiviral compounds to facilitate studies and screening of new antiviral-drug like compounds for treatment purpose (Chaudhuri et al., 2018; Komarasamy et al., 2022). While numerous researches have been performed utilizing the fluorescent reporter system to monitor infection in case of dengue and zika virus showing the virus-dependent changes to the host cell endoplasmic reticulum (McFadden et al., 2018; Medin et al., 2015). However, the ability to identify the DENV, WNV, and ZIKV infected cells by distinguishing infected cells from uninfected cells in real-time is yet challenging, which often fails (Corliss et al., 2022).

To address this knowledge gap, this project intends to further use an alternative approach to generate novel viral protease-dependent engineered fluorescent reporter proteins based on the reporter system models to be stably expressed in living cells, which can be altered upon virus infection (Li et al., 2016; Pahmeier et al., 2021; Van den Elsen et al., 2021). This study describes the generation and characterisation of reporter construct consisting of a green fluorescent protein (GFP 'mStayGold') fused with three nuclear localization signal (NLS) sequence, ER membrane anchored TM domain of sec61 $\beta$  protein, and specific linker region

containing viral NS2B/NS3 protease cleavage sequence for DENVpr, WNVpr, and ZIKVpr within the linker region connecting ER and fluorescent protein. Upon infection, the viral protease cleaves the linker of the reporter construct design releasing GFP from cytoplasm of the ER to the nucleus providing a visual indication of viral infection (Figure 3.6).

To achieve the study's aim, fluorescence activated cell sorting; live fluorescence cell imaging, fixed cell imaging, and western blotting were performed. Moreover, utilizing reporter cell lines for its reliability and validity with antiviral compounds allows a rapid analysis of various antiviral drug-like compounds (like JNJ-A07 for dengue virus inhibitor used in this study), which were designed from high-throughput screening. Importantly, this study performed with investigating the generated protease-dependent reporter cell lines of DENVpr, WNVpr, and ZIKVpr for screening antiviral drug compounds. This further ensured the novel experiments implemented and completed during this master's project, which is relevant to improving our understanding of virus-host interaction and antiviral drugs screening (Cihlova et al., 2021; Kaptein et al., 2021; Kiemel et al., 2024). The live cell monitoring of orthoflaviviruses upon infected vs uninfected state remains mostly unclear from the literature. For example, 4B5-EGFP has been reported to exhibit green signal in both infected and uninfected cells, making it difficult to distinguish (Medin et al., 2015). However, performing fluorescence activated cell sorting (FACS) (Figure 3.5) after transduction that only sort the positive cells has shown high green fluorescence in nucleus upon infection leading to selectively isolate infected cells from uninfected cells (Figure 3.7.1A and 3.7.2A).

In some studies for DENV reporter constructs, high GFP translocation were observed already during uninfected or absence of viral protease which is unlikely (Lennemann et al., 2020; McFadden et al., 2018; Medin et al., 2015). In context to our Aim 1, study for the DENV protease reporter construct (cell line previously generated by Dr. Nicholas Eyre) (Figure 3.7.1A) showed ER-like pattern represented by mStayGold (GFP) in cytoplasm and mScarlet3 in nucleus in uninfected cells. Whereas, in DENV2 infected cells (Figure 3.7.1B) at MOI of 2, the percentage of total double positive (Green and Red proteins) showed the noticeable increase in the GFP translocation from cytoplasm into the nucleus and even higher nuclear GFP accumulation at increasing infection levels i.e. (MOI 0.25), (MOI 1), and (MOI 2) respectively. Among all the constructs that were tested for DENV2 infection, infected cells expressing the reporter constructs at MOI 1 and MOI 2 showed relatively higher nuclear GFP localization and very minimal cytoplasmic GFP. This revealed the completion of nuclear GFP localization at

MOI 2, showing that the experiment is dose dependent and upon infection, GFP translocate into nucleus from cytoplasm indicate the activation of viral protease. Interestingly, it can be seen at MOI 0 (uninfected), very few  $\sim 0.6$  (nuclear translocation ratio) cells already showed some nuclear GFP signal which stated the onset of GFP localization into nucleus (Figure 3.7.1C). This could be due to very high expression of the fluorescent reporter proteins leading to unspecific cleavage or masking the cleavage and relocation of nuclear GFP (Arias-Arias et al., 2020; Pahmeier et al., 2021). Comparatively, a very clear difference in nuclear GFP upon DENV2 infection with gradual increase in nuclear translocation ratio  $\sim 0.65$  at MOI 0.25 following rigorous nuclear GFP localization ratio  $\sim 0.9$  at MOI 1 and MOI 2 (Figure 3.7.1C) was observed. Similarly, in uninfected vs infected cells over different time point, overall number of the double positive cells (mStayGold and mScarlet3) expressing GFP nuclear localization was higher at 48h postinfection as compared to infected cells after 24h and 36 hours postinfection (Figure 3.7.2B). Additionally, nuclear GFP localization ratio i.e. 0.75 with early detection at 24hours postinfection followed by higher ratio i.e. 0.90 at 48h.p.i was observed providing evidence for nuclear GFP translocation from cytoplasm to nucleus with increase in green fluorescent signal in a time dependent manner (Figure 3.7.2A and 3.7.2C). A possible explanation of this result could be the correlation of double positive cells with the nuclear translocation ratio is dose dependent and time course experiments (different hours postinfection) confirmed early detection of nuclear GFP signal showing promising good indication to validate our DENV protease reporter stable cell line.

The immunofluorescence imaging of DENV reporter protease to analyse reporter activity upon infection using confocal microscopy were also explored. The existing literature showed no clear difference in nuclear GFP signal among some reporter cell lines upon DENV2 infection, which limits to provide details about subcellular GFP localization in infected versus uninfected cells (Amarilla et al., 2021; Cortese et al., 2017; Garcia-Blanco et al., 2016). We sought not only to separate infected from uninfected cells but also to check how well the cell have respond with the infection by indirect immunofluorescence staining in infected cells. Confocal microscopy showed stained cells representing the morphology of the DAPI stained nuclei, distributed red fluorescence which marks the viral envelope proteins. In contrast, the DENV2 infected cells with merged (DAPI+ Anti E AlexaFluor647) signals expressing reporter constructs showed a progressive strong red fluorescence, most notably accumulating at the perinuclear region (Figure 3.8). This increase in red fluorescence intensity becomes more stronger and denser closer to the nucleus, particularly at MOI 3 and 5 which is consistent with

higher viral replication activity and indicates a clear difference between the active state of DENV reporter protease leading to cleavage of the reporter construct from inactive state following the high virus infection. However, lower number of the reporting cells were observed at MOI 5 in compared to MOI 1. This decline observed in positive cells could be due to high expression of the positive cells and might have achieved a high protease activity. Overall, this results confirms that our antibody-based detection is specific and dose-related activation of the reporter system by successfully imaging the progression of DENV infection with the production of more viral proteins (Zhang et al., 2011).

Analysis of reporter system for orthoflavivirus detection revealed either cytosolic or ER anchored viral non-structural proteins (Fernandes et al., 2020; Hsieh et al., 2017; Van den Elsen et al., 2021; Wahaab et al., 2021), where, majority utilizes expression of large viral proteins (McFadden et al., 2018; Medin et al., 2015) leading to introduce unwanted pleiotropic effect. In contrast, as our reporter construct carries only the cleavage site-specific sequence from viral sequences, it is less likely to interfere with cellular processes. The reliability conferred by our reporter design with DENV protease as we discussed above makes it easy to adapt the reporter system to other viruses such as WNV and ZIKV that have proteases functioning close to ER membranes (Caldas et al., 2020; Cassidy et al., 2021). This enabled us to quickly employ the system for detection of WNV and ZIKV infection within living cells by performing transient transfection with Hela cells expressing WNVpr and ZIKVpr constructs for real-time live cell imaging of the infection in cells. Here, the purpose of transient transfection with Hela cells allowed rapid and robust plasmid expression to check the functionality of the reporter construct and if cleavage activity occurs upon infection. The reason behind not investing time to make a stable cell lines, given that, we were able to achieve lower production of lentiviral titre capable of transducing huh7.5 cells resulting in almost no any viable cells might be due to poor quality of the lentiviral packaging plasmids (psPAX2 and pMD2.G). These plasmids were capable to detect the fluorescent reporter protein, however, unable to produce high lentiviral titre in the meantime as evident in 3.4. In context to our aim 1, nuclear GFP translocation in the infected WNVpr and ZIKVpr reporter cell line was analysed in this study. Like in uninfected DENV protease reporter cell lines, the uninfected WNV and ZIKV protease reporter cells also exhibited the double positive signal with nuclear GFP (Figure 3.10A and 3.10B), given that high green fluorescent protein expression after transient transfection masking cleavage. The fewer translocation of GFP from cytoplasm into nucleus even during absence of virus infection with WNV and ZIKV protease reporter cell line further support this. Although this does not

fully supports in case of ZIKV protease reporter cell line, where we could see a noticeable significant difference (\*) between (double positive cells) uninfected and infected cells shows clear difference in nuclear GFP localization at 24h.p.i ( $*p < 0.01$ ). This might be due to more optimized cleavage site in the ZIKV reporter construct (Table 3.2), thereby showing more efficient cleavage of the reporter substrate upon infection leading to higher nuclear GFP signal accumulation (Dos Santos Nascimento et al., 2022; McFadden et al., 2018; Nunes et al., 2022).

On the contrary, in WNVpr reporter cells upon infection (MOI 1) caused an increase in double-positive cells over time i.e. 48h.p.i, and 72h.p.i (Figure 3.10A), reflecting nuclear GFP localization due to cleavage mediated by viral WNV protease. This was particularly evident at 48h.p.i and 72h.p.i, when a significant difference (\*\*,  $p < 0.01$ , and \*\*\*\*,  $p < 0.0001$ , respectively) between uninfected and infected cells were observed. However, no any significant difference (ns) at 24h.p.i was seen which referred to our previous explanation of unspecific cleavage happening due to high fluorescence protein expression during transfection (Pahmeier et al., 2021). These findings substantiate the lack of appropriate cleavage proficiency of WNV-capsid site (Table 3.2), which can result in less effective viral replication and reporter protease expression for induction of nuclear GFP.

Unlike the modular nature of reporter construct in uninfected WNVpr reporter cells, ZIKVpr reporter cells upon infection, showed similar and even higher significant difference (\*\*,  $p < 0.01$ , and \*\*\*\*,  $p < 0.0001$ , respectively) between uninfected and infected cells at 24h.p.i, 48h.p.i, and 72h.p.i with early and significant nuclear GFP detection within 24h.p.i. This result of early detection of GFP signal in nucleus upon infection provide an evidence of ZIKV NS2B/NS3 protease efficiently recognizing the ZIKV-specific capsid cleavage site (Table 3.2) which was not clearly explored in literatures (Caldas et al., 2020; Liang & Dai, 2024; McFadden et al., 2018; Sharma & Lal, 2017). This significant difference correlation with difference in cleavage activity of DENV, WNV, and ZIKV reporter systems is likely due to the virus-specific protease recognition efficiency exhibited at their respective capsid cleavage sites. The double positive cells appearance with high nuclear GFP signal over time for cells being infected manifest the accuracy of our reporter system to distinguish between uninfected and infected cells within a time-dependent and dose-dependent manner. Additionally, our study showed that ZIKV reporter construct was more sensitive and reliable in early detection of viral infection making it more applicable for future experiments of antiviral screening assays.

Due to repeated experiments of lentivirus transduction with WNV and ZIKV protease reporter as mentioned in 3.4 that lead into limited time, our experiments to generate stable cell lines for WNV and ZIKV protease-dependent reporter constructs was prevented from being completed. However, we aim to utilize the previously generated eGFP (green fluorescent protein) tagged DENVpr and eGFP (green fluorescent protein) tagged ZIKVpr reporter cell lines stably transduced with Huh7.5 cells to assess the cleavage activity of reporter proteins in DENV2 and ZIKV infected cells using western blot analysis of cell lysates prepared at 48h.p.i (Shiryaev et al., 2023). In addition to this, a reason behind using this stable cell lines was also to show the similar cleavage activity and functionality of our engineered WNVpr and ZIKVpr reporter construct, besides there weren't any previously generated eGFP tagged WNVpr reporter cell lines in our Molecular Virology Group. The engineered reporter constructs where eGFP-NLS attached with ER and separated by virus-specific cleavage site (similar to our reporter construct design), upon infection, viral NS2B/NS3 proteolytic activity was expected to cut the reporter construct linker at a specific protease cleavage site, releasing the GFP for nuclear localization (Li et al., 2016; Malaikah, 2018; Wu et al., 2015).

As confirmed by Figure 3.9, the uncleaved eGFP-NLS fusion protein with molecular weight of ~34kDa was observed in uninfected cells. In both DENV and ZIKV infected cells, however, an additional band with molecular weight ~30kDa, was seen for GFP, consistent with the expected size for cleaved product. This cleaved product released from ER anchor for GFP-NLS by DENV and ZIKV viral protease activity accounts similar protease-dependent fluorescent reporter systems as seen for other researches (Low et al., 2023; Suphatrakul et al., 2018). The strong cleaved GFP band in the DENVpr and ZIKVpr cells infected with dengue virus relative to uninfected controls (Figure 3.9), confirmed effective cleavage by DENV NS2B/NS3 protease targeting the dibasic residues within the viral polyprotein cleavage junctions showing its appropriate functioning in both infected DENVpr and ZIKVpr reporter cell lines (Choudhry et al., 2019; Hill et al., 2018). A similar cleavage was seen with ZIKV-infected ZIKVpr cells, however, in DENVpr cells, the appearance of the cleaved band was faint which was unlikely. This variation in the intensity of the cleaved band might be the result of amino acid sequence at the C terminus of cleavage product or post-translational modification by intracellular enzymes (Arias-Arias et al., 2020; Li et al., 2020; Pahmeier et al., 2021).

These findings were consistent with previous research by Pahmeier et al. (2021), when western blot experiments revealed additional band of cleaved GFP expressing equivalent reporter constructs in cells infected with DENV. Pahmeier et al., in their study correlated the differential

band intensities for cleavage to the variation observed for cleavage site recognition and processing by host proteases. Similarly, the molecular weight of cleaved product found in our study might be due to sequence-dependent changes or further host enzyme trimming after cleavage by the host protease (Bera et al., 2007; Wahaab et al., 2021). These results together establish that the cleavage of reporter constructs are specifically virus-dependent and a validation of the live-cell imaging approach demonstrated the nuclear translocation of GFP following infection. This dual verification at imaging and fluorescent protein levels solidifies the reporter system effectiveness for real-time monitoring of DENV, WNV, and ZIKV infection in living cells. The differences in cleavage activity between DENV and ZIKV reporter cells after infection also provides a clear insights into virus-specific protease activity, which may assist in future experiments in optimizing the design for antiviral drug screening and host factor discovery (Anindita et al., 2024; Pierson & Diamond, 2020).

As we discussed how well the live cell imaging discovered that DENV, WNV, and ZIKV infected cells can be detected as early as 24hour postinfection (Figure 3.7.2A and Figure 3.10A and 3.10B). In current state, real-time identification of DENV-infected cells is carried out mainly by generating a plasmid-based reporter for all DENV serotypes (Medin et al., 2015). In case of WNV-infected cells, a fluorescence-based system for analysing catalytic activity of WNV RNA-dependent RNA polymerase has been developed (Garcia-Zarandieta et al., 2023). Similarly, for ZIKV-infected cell, real-time monitoring is performed by developing a fluorescent reporter system, which determine induce apoptosis in ZIKV infected cells in a cell-autonomous manner through the protease activity of non-structural proteins marking virus-infected cells (McFadden et al., 2018). While these studies report strong and definitive findings of DENV, WNV, and ZIKV infected cells, our engineered reporter cell line has major superiority in various context. The use of our reporter cell line detected infected cells in real time with observable protease-dependent nuclear translocation of the fluorescence signal within hours of infection. Some studies have shown detection of orthoflavivirus-infected cells with recombinant reporter viruses that express fluorescent proteins (Pierson & Diamond, 2020; Shan et al., 2016). However, this requires availability of infectious molecular clones and the stability of this reporter virus can be compromised in long run since high recombination rates might result in deletion or mutation of inserted reporter gene (Arias-Arias et al., 2020; Pahmeier et al., 2021). Conversely, our protease-dependent reporter cell lines, without any modification, through careful inclusion of NS2B/NS3 protease processing sites in reporter construct is responsive to authentic virus protease function. This allow real-time imaging of

the infection dynamics and clear understanding of virus-host interactions avoiding the instability of reporter virus.

In this study, the antiviral activity of JNJ-A07 (2 $\mu$ M) was tested with a previously generated viral protease-dependent fluorescence reporter cell line to confirm the reliability and suitability of our reporter system for screening antiviral drugs as mentioned previously in 2.2.8. JNJ A07, a potent dengue virus inhibitor that targets DENV NS4B protein and NS2B/NS3 helicase complex, disrupting the virus replication and has demonstrated minimal resistance in several DENV serotypes (Goethals et al., 2023; Kaptein et al., 2021; Kiemel et al., 2024). Cells when treated with DMSO control showed high red (mScarlet3) and green (mStayGold) fluorescence in nucleus at 72h.p.i. indicative of active viral protease and efficient cleavage of the reporter construct. In contrast, JNJ-A07-treated infected cells showed dramatic decreased in green fluorescence, reflecting inhibition of viral protease activity and associated decreased replication (Figure 3.11A), which is closer to the findings reported in literature (Kiemel et al., 2024; Rosales-Rosas et al., 2024; Wang et al., 2015). The high sensitivity of the reporter construct showing functional verification of the design in which protease-mediated cleavage is responsible for inducing eGFP translocation from cytoplasm to nucleus – a marker for infection status. In addition to this, quantitative analysis (Figure 3.11B) further supports this. The dose-response curve indicates JNJ-A07 has minimal antiviral effect in concentrations ranging from  $10^{-6}$  to  $10^{-4}$   $\mu$ M, whereas there was a drop off in infection rates from  $10^{-3}$   $\mu$ M, with nearly complete inhibition at concentrations  $>10^{-2}$   $\mu$ M. It is important to note that, application of a time-course-colour gradient (24h.p.i to 72h.p.i in Figure 3.11B) in this study showed inhibition was increasingly potent with time, resulting maximum inhibition being observed at 72h.p.i indicating the experiment is dose and time dependent.

Nevertheless, JNJ-A07 to exhibit antiviral activity in our eGFP DENVpr reporter construct should be explored with ZIKVpr and WNVpr reporter construct in future experiments to further validate by such time-course experiments or viral quantifications. Overall, the findings from our study confirms the utility of engineered reporter system two broad applications: real-time analysis of viral infection in case of all orthoflaviviruses, host-factor investigations, and safe as well effective antiviral drug screening. The construct allows for dynamic visualization and quantification of viral protease activity, and it is thus a sensitive and powerful tool for screening drugs in live-cell. Because of these advantages in identifying new antivirals that act on DENV,

it enables potentially to act on other orthoflaviviruses that use similar proteolytic processes like WNV and ZIKV.

In conclusion, our study described a reporter system as powerful tools allows for real-time monitoring of orthoflavivirus like DENV, WNV, and ZIKV infected cells and help to fill critical gaps in understanding orthoflavivirus-host interactions and finding targets for antiviral-drug candidate activity. This reporter system, which we generate in our laboratory settings, is reliable and easy to handle. These advanced tools will ultimately contribute to the development and testing of experimental antiviral drug compounds for treatment purposes.

# Bibliography

- Amarilla, A. A., Sng, J. D. J., Parry, R., Deerrain, J. M., Potter, J. R., Setoh, Y. X., Rawle, D. J., Le, T. T., Modhiran, N., Wang, X., Peng, N. Y. G., Torres, F. J., Pyke, A., Harrison, J. J., Freney, M. E., Liang, B., McMillan, C. L. D., Cheung, S. T. M., Guevara, D., . . . Khromykh, A. A. (2021). A versatile reverse genetics platform for SARS-CoV-2 and other positive-strand RNA viruses. *Nat Commun*, 12(1), 3431. <https://doi.org/10.1038/s41467-021-23779-5>
- Anindita, P. D., Otsuka, Y., Lattmann, S., Ngo, K. H., Liew, C. W., Kang, C., Harris, R. S., Scampavia, L., Spicer, T. P., & Luo, D. (2024). A high-throughput cell-based screening method for Zika virus protease inhibitor discovery. *SLAS Discov*, 29(5), 100164. <https://doi.org/10.1016/j.slasd.2024.100164>
- Arias-Arias, J. L., MacPherson, D. J., Hill, M. E., Hardy, J. A., & Mora-Rodriguez, R. (2020). A fluorescence-activatable reporter of flavivirus NS2B-NS3 protease activity enables live imaging of infection in single cells and viral plaques. *J Biol Chem*, 295(8), 2212-2226. <https://doi.org/10.1074/jbc.RA119.011319>
- Arias, C. F., Preugschat, F., & Strauss, J. H. (1993). Dengue 2 virus NS2B and NS3 form a stable complex that can cleave NS3 within the helicase domain. *Virology*, 193(2), 888-899. <https://doi.org/https://doi.org/10.1006/viro.1993.1198>
- Aynekulu Mersha, D. G., van der Sterren, I., van Leeuwen, L. P. M., Langerak, T., Hakim, M. S., Martina, B., van Lelyveld, S. F. L., & van Gorp, E. C. M. (2024). The role of antibody-dependent enhancement in dengue vaccination. *Trop Dis Travel Med Vaccines*, 10(1), 22. <https://doi.org/10.1186/s40794-024-00231-2>
- Barbier, V., Lang, D., Valois, S., Rothman, A. L., & Medin, C. L. (2017). Dengue virus induces mitochondrial elongation through impairment of Drp1-triggered mitochondrial fission. *Virology*, 500, 149-160. <https://doi.org/10.1016/j.virol.2016.10.022>
- Bera, A. K., Kuhn, R. J., & Smith, J. L. (2007). Functional characterization of cis and trans activity of the Flavivirus NS2B-NS3 protease. *J Biol Chem*, 282(17), 12883-12892. <https://doi.org/10.1074/jbc.M611318200>
- Beutner, E. H. (1961). Immunofluorescent Staining: The Fluorescent Antibody Method. *Bacteriol Rev*, 25(1), 49-76. <https://doi.org/10.1128/br.25.1.49-76.1961>
- Biolabs, N. E. (2013). *High Efficiency Transformation for NEB® Stable Competent E. coli (C3040H)*. NEB. <https://www.neb.com/en-au/protocols/2013/10/30/high-efficiency->

[transformation-protocol-  
c3040h?srsId=AfmBOooCiwD1tnaozIFmMv2ZvnUIIdLG9hSY8t60QTR\\_usGWT-  
hUvCfQ](#)

- Bouzidi, H. S., Sen, S., Piorkowski, G., Pezzi, L., Ayhan, N., Fontaine, A., Canivez, T., Geulen, M., Amaral, R., Grard, G., Durand, G. A., de Lamballerie, X., Touret, F., & Klitting, R. (2024). Genomic surveillance reveals a dengue 2 virus epidemic lineage with a marked decrease in sensitivity to Mosnodenvir. *Nat Commun*, *15*(1), 8667. <https://doi.org/10.1038/s41467-024-52819-z>
- Burleson, F. G., Chambers, T. M., & Wiedbrauk, D. L. (2014). *Virology: a laboratory manual*. Elsevier. <https://books.google.co.vi/books?id=5s3SBQAAQBAJ&printsec=copyright>
- Caldas, L. A., Azevedo, R. C., da Silva, J. L., & de Souza, W. (2020). Microscopy analysis of Zika virus morphogenesis in mammalian cells. *Sci Rep*, *10*(1), 8370. <https://doi.org/10.1038/s41598-020-65409-y>
- Campeau, E., Ruhl, V. E., Rodier, F., Smith, C. L., Rahmberg, B. L., Fuss, J. O., Campisi, J., Yaswen, P., Cooper, P. K., & Kaufman, P. D. (2009). A versatile viral system for expression and depletion of proteins in mammalian cells. *PloS one*, *4*(8), e6529. <https://doi.org/https://doi.org/10.1371/journal.pone.0006529>
- Carrington, L. B., & Simmons, C. P. (2014). Human to mosquito transmission of dengue viruses. *Front Immunol*, *5*, 290. <https://doi.org/10.3389/fimmu.2014.00290>
- Cassedy, A., Parle-McDermott, A., & O'Kennedy, R. (2021). Virus Detection: A Review of the Current and Emerging Molecular and Immunological Methods. *Front Mol Biosci*, *8*, 637559. <https://doi.org/10.3389/fmolb.2021.637559>
- Chaudhuri, S., Symons, J. A., & Deval, J. (2018). Innovation and trends in the development and approval of antiviral medicines: 1987-2017 and beyond. *Antiviral Res*, *155*, 76-88. <https://doi.org/10.1016/j.antiviral.2018.05.005>
- Chauhan, N., Gaur, K. K., Asuru, T. R., & Guchhait, P. (2024). Dengue virus: pathogenesis and potential for small molecule inhibitors. *Biosci Rep*, *44*(8), BSR20240134. <https://doi.org/10.1042/BSR20240134>
- Chen, Y. P., Becnel, J. J., & Valles, S. M. (2012). RNA viruses infecting pest insects. *Insect pathology*(5), 133-170. <https://doi.org/http://dx.doi.org/10.1016/B978-0-12-384984-7.00005-1>
- Chong, M. K., Chua, A. J., Tan, T. T., Tan, S. H., & Ng, M. L. (2014). Microscopy techniques in flavivirus research. *Micron*, *59*, 33-43. <https://doi.org/https://doi.org/10.1016/j.micron.2013.12.006>

- Choudhry, H., Alzahrani, F. A., Hassan, M. A., Alghamdi, A., Abdulaal, W. H., Bakhrebah, M. A., Zamzami, M. A., Helmi, N., Bokhari, F. F., Zeyadi, M., Baothman, O. A., Kamal, M. A., Warsi, M. K., Ali, A., Jarullah, B., & Jamal, M. S. (2019). Zika Virus Targeting by Screening Inhibitors against NS2B/NS3 Protease. *Biomed Res Int*, 2019(1), 3947245. <https://doi.org/10.1155/2019/3947245>
- Cihlova, B., Huskova, A., Boserle, J., Nencka, R., Boura, E., & Silhan, J. (2021). High-Throughput Fluorescent Assay for Inhibitor Screening of Proteases from RNA Viruses. *Molecules*, 26(13), 3792. <https://doi.org/10.3390/molecules26133792>
- Corliss, L., Holliday, M., & Lennemann, N. J. (2022). Dual-fluorescent reporter for live-cell imaging of the ER during DENV infection. *Front Cell Infect Microbiol*, 12, 1042735. <https://doi.org/10.3389/fcimb.2022.1042735>
- Cortese, M., Goellner, S., Acosta, E. G., Neufeldt, C. J., Oleksiuk, O., Lampe, M., Haselmann, U., Funaya, C., Schieber, N., Ronchi, P., Schorb, M., Pruunsild, P., Schwab, Y., Chatel-Chaix, L., Ruggieri, A., & Bartenschlager, R. (2017). Ultrastructural Characterization of Zika Virus Replication Factories. *Cell Rep*, 18(9), 2113-2123. <https://doi.org/10.1016/j.celrep.2017.02.014>
- Dalby, B., Cates, S., Harris, A., Ohki, E. C., Tilkins, M. L., Price, P. J., & Ciccarone, V. C. (2004). Advanced transfection with Lipofectamine 2000 reagent: primary neurons, siRNA, and high-throughput applications. *Methods*, 33(2), 95-103. <https://doi.org/10.1016/j.ymeth.2003.11.023>
- De Clercq, E., & Li, G. (2016). Approved Antiviral Drugs over the Past 50 Years. *Clin Microbiol Rev*, 29(3), 695-747. <https://doi.org/10.1128/CMR.00102-15>
- Dehghani, M., Skerlos, L., Shean, J., & Bevan, N. (2024). Real Time Ev Uptake Characterization Using Incucyte Live Cell Imaging System. *Cytotherapy*, 26(6), S88-S88. <Go to ISI>://WOS:001282333600215
- Ding, B., & Kilpatrick, D. L. (2013). Lentiviral vector production, titration, and transduction of primary neurons. In *Neural development: methods and protocols* (pp. 119-131). Springer. [https://doi.org/https://doi.org/10.1007/978-1-62703-444-9\\_12](https://doi.org/https://doi.org/10.1007/978-1-62703-444-9_12)
- Diosa-Toro, M., Prasanth, K. R., Bradrick, S. S., & Garcia Blanco, M. A. (2020). Role of RNA-binding proteins during the late stages of Flavivirus replication cycle. *Viol J*, 17(1), 60. <https://doi.org/10.1186/s12985-020-01329-7>
- Donaldson, J. G. (2015). Immunofluorescence Staining. *Curr Protoc Cell Biol*, 69(1), 4.3.1-4.3.7. <https://doi.org/10.1002/0471143030.cb0403s69>

- Dos Santos Nascimento, I. J., da Silva Rodrigues, E. E., da Silva, M. F., de Araujo-Junior, J. X., & de Moura, R. O. (2022). Advances in Computational Methods to Discover New NS2B-NS3 Inhibitors Useful Against Dengue and Zika Viruses. *Curr Top Med Chem*, 22(29), 2435-2462. <https://doi.org/10.2174/1568026623666221122121330>
- Fernandes, R. S., Freire, M., Bueno, R. V., Godoy, A. S., Gil, L., & Oliva, G. (2020). Reporter Replicons for Antiviral Drug Discovery against Positive Single-Stranded RNA Viruses. *Viruses*, 12(6), 598. <https://doi.org/10.3390/v12060598>
- Garcia-Blanco, M. A., Vasudevan, S. G., Bradrick, S. S., & Nicchitta, C. (2016). Flavivirus RNA transactions from viral entry to genome replication. *Antiviral Res*, 134, 244-249. <https://doi.org/10.1016/j.antiviral.2016.09.010>
- Garcia-Zarandieta, M., Quesada, E., Martinez-Jimenez, M. I., Newnes, C. V., Fernandez-Cabello, V., Saez-Alvarez, Y., Blazquez, A. B., Escribano-Romero, E., Saiz, J. C., Del Aguila, C., Martin-Acebes, M. A., Perez-Perez, M. J., & Agudo, R. (2023). Identification of West Nile virus RNA-dependent RNA polymerase non-nucleoside inhibitors by real-time high throughput fluorescence screening. *Antiviral Res*, 212, 105568. <https://doi.org/10.1016/j.antiviral.2023.105568>
- gene, A. (2025). *Lentiviral Guide*. addgene. <https://www.addgene.org/guides/lentivirus/>
- Goethals, O., Vogt, N. V., Kesteleyn, B., Chaltin, P., Jinks, T., De Marez, T., Koul, A., Draghia-Akli, R., Neyts, J., & Van Loock, M. (2023). A pan-serotype antiviral to prevent and treat dengue: A journey from discovery to clinical development driven by public-private partnerships. *Antiviral Res*, 210, 105495. <https://doi.org/10.1016/j.antiviral.2022.105495>
- Gong, E. Y. (2013). *Antiviral methods and protocols* (Vol. 452). Springer. <https://doi.org/10.1007/978-1-62703-484-5>
- Gupta, A. (2020). *Identification of Host-Targeting Antiviral Drug Combinations and Targets*. Stanford University. <https://www.proquest.com/dissertations-theses/identification-host-targeting-antiviral-drug/docview/2426517543/se-2?accountid=10910>
- Guzman, M. G., Gubler, D. J., Izquierdo, A., Martinez, E., & Halstead, S. B. (2016). Dengue infection. *Nat Rev Dis Primers*, 2(1), 16055. <https://doi.org/10.1038/nrdp.2016.55>
- Hadpech, S., & Thongboonkerd, V. (2024). Proteomic investigations of dengue virus infection: key discoveries over the last 10 years. *Expert Rev Proteomics*, 21(7-8), 281-295. <https://doi.org/10.1080/14789450.2024.2383580>
- Hannemann, H. (2020). Viral replicons as valuable tools for drug discovery. *Drug Discov Today*, 25(6), 1026-1033. <https://doi.org/10.1016/j.drudis.2020.03.010>

- Hill, M. E., Kumar, A., Wells, J. A., Hobman, T. C., Julien, O., & Hardy, J. A. (2018). The Unique Cofactor Region of Zika Virus NS2B-NS3 Protease Facilitates Cleavage of Key Host Proteins. *ACS Chem Biol*, *13*(9), 2398-2405. <https://doi.org/10.1021/acscchembio.8b00508>
- Hsieh, M. S., Chen, M. Y., Hsieh, C. H., Pan, C. H., Yu, G. Y., & Chen, H. W. (2017). Detection and quantification of dengue virus using a novel biosensor system based on dengue NS3 protease activity. *PloS one*, *12*(11), e0188170. <https://doi.org/10.1371/journal.pone.0188170>
- Invitrogen, G. (2014). Cell culture basics. *Thermo Fisher Scientific*. <https://www.thermofisher.com/au/en/home/references/gibco-cell-culture-basics.html>
- Kaptein, S. J., Goethals, O., Kiemel, D., Marchand, A., Kesteleyn, B., Bonfanti, J.-F., Bardiot, D., Stoops, B., Jonckers, T. H., & Dallmeier, K. (2021). A pan-serotype dengue virus inhibitor targeting the NS3–NS4B interaction. *Nature*, *598*(7881), 504-509. <https://doi.org/https://doi.org/10.1038/s41586-021-03990-6>
- Kiemel, D., Kroell, A. H., Denolly, S., Haselmann, U., Bonfanti, J. F., Andres, J. I., Ghosh, B., Geluykens, P., Kaptein, S. J. F., Wilken, L., Scaturro, P., Neyts, J., Van Loock, M., Goethals, O., & Bartenschlager, R. (2024). Pan-serotype dengue virus inhibitor JNJ-A07 targets NS4A-2K-NS4B interaction with NS2B/NS3 and blocks replication organelle formation. *Nat Commun*, *15*(1), 6080. <https://doi.org/10.1038/s41467-024-50437-3>
- Komarasamy, T. V., Adnan, N. A. A., James, W., & Balasubramaniam, V. R. (2022). Finding a chink in the armor: Update, limitations, and challenges toward successful antivirals against flaviviruses. *PLoS Negl Trop Dis*, *16*(4), e0010291. <https://doi.org/10.1371/journal.pntd.0010291>
- Lanigan, T. M., Rasmussen, S. M., Weber, D. P., Athukorala, K. S., Campbell, P. L., Fox, D. A., & Ruth, J. H. (2020). Real time visualization of cancer cell death, survival and proliferation using fluorochrome-transfected cells in an IncuCyte((R)) imaging system. *J Biol Methods*, *7*(2), e133. <https://doi.org/10.14440/jbm.2020.323>
- Latanova, A., Starodubova, E., & Karpov, V. (2022). Flaviviridae Nonstructural Proteins: The Role in Molecular Mechanisms of Triggering Inflammation. *Viruses*, *14*(8), 1808. <https://doi.org/10.3390/v14081808>
- Lennemann, N. J., Evans, A. S., & Coyne, C. B. (2020). Imaging-Based Reporter Systems to Define CVB-Induced Membrane Remodeling in Living Cells. *Viruses*, *12*(10), 1074. <https://doi.org/10.3390/v12101074>

- Li, L. H., Kaptein, S. J. F., Schmid, M. A., Zmurko, J., Leyssen, P., Neyts, J., & Dallmeier, K. (2020). A dengue type 2 reporter virus assay amenable to high-throughput screening. *Antiviral Res*, *183*, 104929. <https://doi.org/10.1016/j.antiviral.2020.104929>
- Li, Y., Li, L. F., Yu, S., Wang, X., Zhang, L., Yu, J., Xie, L., Li, W., Ali, R., & Qiu, H. J. (2016). Applications of Replicating-Competent Reporter-Expressing Viruses in Diagnostic and Molecular Virology. *Viruses*, *8*(5), 127. <https://doi.org/10.3390/v8050127>
- Liang, Y., & Dai, X. (2024). The global incidence and trends of three common flavivirus infections (Dengue, yellow fever, and Zika) from 2011 to 2021. *Front Microbiol*, *15*, 1458166. <https://doi.org/10.3389/fmicb.2024.1458166>
- Liu, S. L., Wang, Z. G., Xie, H. Y., Liu, A. A., Lamb, D. C., & Pang, D. W. (2020). Single-Virus Tracking: From Imaging Methodologies to Virological Applications. *Chem Rev*, *120*(3), 1936-1979. <https://doi.org/10.1021/acs.chemrev.9b00692>
- Low, K., Moller, R., Stegmann, C., Becker, M., Rehburg, L., Obernolte, H., Schaudien, D., Oestereich, L., Braun, A., Kunz, S., & Gerold, G. (2023). Luminescent reporter cells enable the identification of broad-spectrum antivirals against emerging viruses. *J Med Virol*, *95*(11), e29211. <https://doi.org/10.1002/jmv.29211>
- Macherey-Nagel. (2019). *Plasmid DNA purification*. Takara-Bio. [https://www.takarabio.com/documents/User%20Manual/NucleoBond%20Xtra%20Plasmid%20DNA%20Purification%20User%20Manual\\_Rev\\_15.pdf?srsId=AfmBOorVmcSpUPirCm-grvIgZWAs1hYQ3Avq1\\_jD4XITxSotIMmKswg](https://www.takarabio.com/documents/User%20Manual/NucleoBond%20Xtra%20Plasmid%20DNA%20Purification%20User%20Manual_Rev_15.pdf?srsId=AfmBOorVmcSpUPirCm-grvIgZWAs1hYQ3Avq1_jD4XITxSotIMmKswg)
- Malaïkah, M. K. (2018). *Monitoring Proteolytic Activity of West Nile Virus in a Cell-Based Assay for Novel Drug Discovery* (Publication Number 10933699) San Diego State University]. United States -- California. <https://www.proquest.com/dissertations-theses/monitoring-proteolytic-activity-west-nile-virus/docview/2119693310/section2?accountid=10910>
- Marecki, J. C., Belachew, B., Gao, J., & Raney, K. D. (2021). RNA helicases required for viral propagation in humans. *The Enzymes*, *50*, 335-367. <https://doi.org/https://doi.org/10.1016/bs.enz.2021.09.005>
- Matthew, A. N., Leidner, F., Lockbaum, G. J., Henes, M., Zephyr, J., Hou, S., Rao, D. N., Timm, J., Rusere, L. N., Ragland, D. A., Paulsen, J. L., Prachanronarong, K., Soumana, D. I., Nalivaika, E. A., Kurt Yilmaz, N., Ali, A., & Schiffer, C. A. (2021). Drug Design Strategies to Avoid Resistance in Direct-Acting Antivirals and Beyond. *Chem Rev*, *121*(6), 3238-3270. <https://doi.org/10.1021/acs.chemrev.0c00648>

- McFadden, M. J., Mitchell-Dick, A., Vazquez, C., Roder, A. E., Labagnara, K. F., McMahon, J. J., Silver, D. L., & Horner, S. M. (2018). A Fluorescent Cell-Based System for Imaging Zika Virus Infection in Real-Time. *Viruses*, *10*(2), 95. <https://doi.org/10.3390/v10020095>
- Meads, M. B., & Medveczky, P. G. (2009). Application of western blotting to diagnosis of viral infections. *Clinical Virology Manual*, 150-155. <https://doi.org/https://doi.org/10.1128/9781555815974.ch13>
- Medin, C. L., Valois, S., Patkar, C. G., & Rothman, A. L. (2015). A plasmid-based reporter system for live cell imaging of dengue virus infected cells. *J Virol Methods*, *211*, 55-62. <https://doi.org/10.1016/j.jviromet.2014.10.010>
- Mohsin, N. U., Irfan, M., & Qamar, S. (2023). Current Advancements for New Drug Discovery Against Dengue Virus: A Review (2015-2020). *Pharmaceutical Chemistry Journal*, *57*(6), 932-951. <https://doi.org/10.1007/s11094-023-02969-z>
- Morita, E., & Suzuki, Y. (2021). Membrane-Associated Flavivirus Replication Complex-Its Organization and Regulation. *Viruses*, *13*(6), 1060. <https://doi.org/10.3390/v13061060>
- Motulsky, H., & GraphPad Software, I. (2003). *GraphPad Prism : Version 4.0 user's guide: clearly the fastest, easiest way to organize, analyze and graph scientific data*. GraphPad Software. <https://doi.org/https://doi.org/10.1093/oso/9780195171792.003.0050>
- Murugesan, A., & Manoharan, M. (2020). Dengue virus. In *Emerging and reemerging viral pathogens* (pp. 281-359). Elsevier. <https://doi.org/https://doi.org/10.1016/B978-0-12-819400-3.00016-8>
- Nguyen-Tien, T., Lundkvist, Å., & Lindahl, J. (2019). Urban transmission of mosquito-borne flaviviruses—a review of the risk for humans in Vietnam. *Infection ecology & epidemiology*, *9*(1), 1660129. <https://doi.org/https://doi.org/10.1080/20008686.2019.1660129>
- Nunes, D. A. d. F., Santos, F. R. d. S., da Fonseca, S. T. D., de Lima, W. G., Nizer, W. S. d. C., Ferreira, J. M. S., & De Magalhães, J. C. (2022). NS2B-NS3 protease inhibitors as promising compounds in the development of antivirals against Zika virus: A systematic review. *Journal of Medical Virology*, *94*(2), 442-453. <https://doi.org/https://doi.org/10.1002/jmv.27386>
- O'Kelly, E. (1998). Cell culture and diagnostic virology. In *Animal Cell Culture Techniques* (pp. 13-37). Springer. [https://doi.org/https://doi.org/10.1007/978-3-642-80412-0\\_2](https://doi.org/https://doi.org/10.1007/978-3-642-80412-0_2)

- Oceguera, L. F., 3rd, Patiris, P. J., Chiles, R. E., Busch, M. P., Tobler, L. H., & Hanson, C. V. (2007). Flavivirus serology by Western blot analysis. *Am J Trop Med Hyg*, 77(1), 159-163. <https://www.ncbi.nlm.nih.gov/pubmed/17620648>
- Pahmeier, F., Neufeldt, C. J., Cerikan, B., Prasad, V., Pape, C., Laketa, V., Ruggieri, A., Bartenschlager, R., & Cortese, M. (2021). A Versatile Reporter System To Monitor Virus-Infected Cells and Its Application to Dengue Virus and SARS-CoV-2. *J Virol*, 95(4), 10.1128/jvi.01715-01720. <https://doi.org/10.1128/JVI.01715-20>
- Pierson, T. C., & Diamond, M. S. (2020). The continued threat of emerging flaviviruses. *Nat Microbiol*, 5(6), 796-812. <https://doi.org/10.1038/s41564-020-0714-0>
- Preugschat, F., Yao, C.-W., & Strauss, J. H. (1990). In vitro processing of dengue virus type 2 nonstructural proteins NS2A, NS2B, and NS3. *Journal of virology*, 64(9), 4364-4374. <https://doi.org/https://doi.org/10.1128/jvi.64.9.4364-4374.1990>
- Pruijssers, A. J., George, A. S., Schafer, A., Leist, S. R., Gralinski, L. E., Dinnon, K. H., 3rd, Yount, B. L., Agostini, M. L., Stevens, L. J., Chappell, J. D., Lu, X., Hughes, T. M., Gully, K., Martinez, D. R., Brown, A. J., Graham, R. L., Perry, J. K., Du Pont, V., Pitts, J., . . . Sheahan, T. P. (2020). Remdesivir Inhibits SARS-CoV-2 in Human Lung Cells and Chimeric SARS-CoV Expressing the SARS-CoV-2 RNA Polymerase in Mice. *Cell Rep*, 32(3), 107940. <https://doi.org/10.1016/j.celrep.2020.107940>
- Qiu, D., Tannock, G. A., Barry, R. D., & Jackson, D. C. (1992). Western blot analysis of antibody responses to influenza virion proteins. *Immunol Cell Biol*, 70 ( Pt 3)(3), 181-191. <https://doi.org/10.1038/icb.1992.23>
- Rasmussen, S. A., Meaney-Delman, D. M., Petersen, L. R., & Jamieson, D. J. (2017). Studying the effects of emerging infections on the fetus: Experience with West Nile and Zika viruses. *Birth Defects Res*, 109(5), 363-371. <https://doi.org/10.1002/bdr2.1006>
- Rosales-Rosas, A. L., Goossens, S., Chiu, W., Majumder, A., Soto, A., Masyn, S., Stoops, B., Wang, L., Kaptein, S. J. F., Goethals, O., & Delang, L. (2024). The antiviral JNJ-A07 significantly reduces dengue virus transmission by *Aedes aegypti* mosquitoes when delivered via blood-feeding. *Sci Adv*, 10(48), eadr8338. <https://doi.org/10.1126/sciadv.adr8338>
- Roy, S. K., & Bhattacharjee, S. (2021). Dengue virus: epidemiology, biology, and disease aetiology. *Can J Microbiol*, 67(10), 687-702. <https://doi.org/10.1139/cjm-2020-0572>
- Samrat, S. K., Xu, J., Li, Z., Zhou, J., & Li, H. (2022). Antiviral Agents against Flavivirus Protease: Prospect and Future Direction. *Pathogens*, 11(3), 293. <https://doi.org/10.3390/pathogens11030293>

- Scientific, T. *Improve Lentiviral Production Using Lipofectamine 3000 Reagent*. Thermofisher Scientific Biotechnology Company. <https://www.thermofisher.com/au/en/home/life-science/cell-culture/cell-culture-learning-center/cell-culture-resource-library/cell-culture-transfection-application-notes/improve-lentiviral-production-using-lipofectamine-3000-reagent.html>
- Shan, C., Xie, X., Muruato, A. E., Rossi, S. L., Roundy, C. M., Azar, S. R., Yang, Y., Tesh, R. B., Bourne, N., Barrett, A. D., Vasilakis, N., Weaver, S. C., & Shi, P. Y. (2016). An Infectious cDNA Clone of Zika Virus to Study Viral Virulence, Mosquito Transmission, and Antiviral Inhibitors. *Cell Host Microbe*, 19(6), 891-900. <https://doi.org/10.1016/j.chom.2016.05.004>
- Sharma, A., & Lal, S. K. (2017). Zika Virus: Transmission, Detection, Control, and Prevention. *Front Microbiol*, 8, 110. <https://doi.org/10.3389/fmicb.2017.00110>
- Shiryaev, S. A., Cieplak, P., Cheltsov, A., Liddington, R. C., & Terskikh, A. V. (2023). Dual function of Zika virus NS2B-NS3 protease. *PLoS Pathog*, 19(11), e1011795. <https://doi.org/10.1371/journal.ppat.1011795>
- Sinare, A. B., & Barkade, G. D. (2023). Dengue: A mosquito borne disease. *World Journal of Biology Pharmacy and Health Sciences*, 14(2), 251-261. <https://doi.org/https://doi.org/10.30574/wjbphs.2023.14.2.0218>
- Sinha, S., Singh, K., Ravi Kumar, Y. S., Roy, R., Phadnis, S., Meena, V., Bhattacharyya, S., & Verma, B. (2024). Dengue virus pathogenesis and host molecular machineries. *J Biomed Sci*, 31(1), 43. <https://doi.org/10.1186/s12929-024-01030-9>
- Srisawat, N., Thisyakorn, U., Ismail, Z., Rafiq, K., Gubler, D. J., & Committee, A.-I. W. D. D. (2022). World Dengue Day: A call for action. *PLoS Negl Trop Dis*, 16(8), e0010586. <https://doi.org/10.1371/journal.pntd.0010586>
- Stancheva, V. G., & Sanyal, S. (2024). Positive-strand RNA virus replication organelles at a glance. *J Cell Sci*, 137(17). <https://doi.org/10.1242/jcs.262164>
- Suphatrakul, A., Duangchinda, T., Jupatanakul, N., Prasittisa, K., Onnome, S., Pengon, J., & Siridechadilok, B. (2018). Multi-color fluorescent reporter dengue viruses with improved stability for analysis of a multi-virus infection. *PloS one*, 13(3), e0194399. <https://doi.org/10.1371/journal.pone.0194399>
- Thomas, S. J., Martinez, L. J., & Endy, T. P. (2023). Flaviviruses: yellow fever, japanese b, west Nile, and others. In *Viral infections of humans: epidemiology and control* (pp. 1-62). Springer. [https://doi.org/https://doi.org/10.1007/978-1-4899-7448-8\\_16](https://doi.org/https://doi.org/10.1007/978-1-4899-7448-8_16)

- Troupin, A., & Colpitts, T. M. (2016). Overview of West Nile Virus Transmission and Epidemiology. *Methods Mol Biol*, 1435, 15-18. [https://doi.org/10.1007/978-1-4939-3670-0\\_2](https://doi.org/10.1007/978-1-4939-3670-0_2)
- van den Elsen, K., Chew, B. L. A., Ho, J. S., & Luo, D. (2023). Flavivirus nonstructural proteins and replication complexes as antiviral drug targets. *Current opinion in virology*, 59, 101305. <https://doi.org/https://doi.org/10.1016/j.coviro.2023.101305>
- Van den Elsen, K., Quek, J. P., & Luo, D. (2021). Molecular insights into the flavivirus replication complex. *Viruses*, 13(6), 956. <https://doi.org/https://doi.org/10.3390/v13060956>
- Wahaab, A., Mustafa, B. E., Hameed, M., Stevenson, N. J., Anwar, M. N., Liu, K., Wei, J., Qiu, Y., & Ma, Z. (2021). Potential Role of Flavivirus NS2B-NS3 Proteases in Viral Pathogenesis and Anti-flavivirus Drug Discovery Employing Animal Cells and Models: A Review. *Viruses*, 14(1), 44. <https://doi.org/10.3390/v14010044>
- Wang, Q. Y., Dong, H., Zou, B., Karuna, R., Wan, K. F., Zou, J., Susila, A., Yip, A., Shan, C., Yeo, K. L., Xu, H., Ding, M., Chan, W. L., Gu, F., Seah, P. G., Liu, W., Lakshminarayana, S. B., Kang, C., Lescar, J., . . . Shi, P. Y. (2015). Discovery of Dengue Virus NS4B Inhibitors. *J Virol*, 89(16), 8233-8244. <https://doi.org/10.1128/JVI.00855-15>
- Williams, D. T., Mackenzie, J. S., & Bingham, J. (2019). Flaviviruses. *Diseases of swine*, 530-543. <https://doi.org/https://doi.org/10.1016/b978-0-323-82501-6.00005-0>
- Wright, J. F. (2009). Transient transfection methods for clinical adeno-associated viral vector production. *Hum Gene Ther*, 20(7), 698-706. <https://doi.org/10.1089/hum.2009.064>
- Wu, H., Bock, S., Snitko, M., Berger, T., Weidner, T., Holloway, S., Kanitz, M., Diederich, W. E., Steuber, H., Walter, C., Hofmann, D., Weissbrich, B., Spannaus, R., Acosta, E. G., Bartenschlager, R., Engels, B., Schirmeister, T., & Bodem, J. (2015). Novel dengue virus NS2B/NS3 protease inhibitors. *Antimicrob Agents Chemother*, 59(2), 1100-1109. <https://doi.org/10.1128/AAC.03543-14>
- Wu, P., Yu, X., Wang, P., & Cheng, G. (2019). Arbovirus lifecycle in mosquito: acquisition, propagation and transmission. *Expert Rev Mol Med*, 21, e1. <https://doi.org/10.1017/erm.2018.6>
- Xie, X., Muruato, A. E., Zhang, X., Lokugamage, K. G., Fontes-Garfias, C. R., Zou, J., Liu, J., Ren, P., Balakrishnan, M., Cihlar, T., Tseng, C. K., Makino, S., Menachery, V. D., Billello, J. P., & Shi, P. Y. (2020). A nanoluciferase SARS-CoV-2 for rapid

- neutralization testing and screening of anti-infective drugs for COVID-19. *Nat Commun*, 11(1), 5214. <https://doi.org/10.1038/s41467-020-19055-7>
- Yang, X., Quam, M. B. M., Zhang, T., & Sang, S. (2021). Global burden for dengue and the evolving pattern in the past 30 years. *J Travel Med*, 28(8), taab146. <https://doi.org/10.1093/jtm/taab146>
- Zhang, S., He, Y., Wu, Z., Wang, M., Jia, R., Zhu, D., Liu, M., Zhao, X., Yang, Q., Wu, Y., Zhang, S., Huang, J., Ou, X., Gao, Q., Sun, D., Zhang, L., Yu, Y., Chen, S., & Cheng, A. (2023). Secretory pathways and multiple functions of nonstructural protein 1 in flavivirus infection. *Front Immunol*, 14, 1205002. <https://doi.org/10.3389/fimmu.2023.1205002>
- Zhang, S., Tan, H. C., & Ooi, E. E. (2011). Visualizing dengue virus through Alexa Fluor labeling. *J Vis Exp*(53), e3168. <https://doi.org/10.3791/3168>

# Appendices

1.

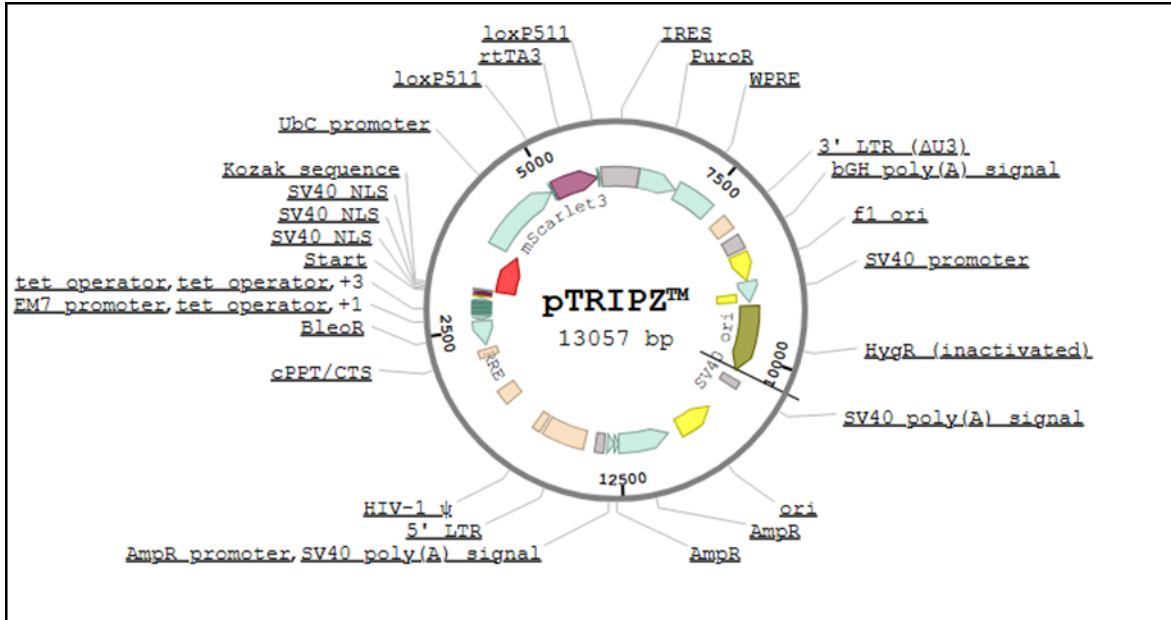


**Figure Appendices 1: pTRIPZ\_3XNLS\_mScarlet3 Plasmid Map.** The circular plasmid map of pTRIPZ\_3XNLS\_mScarlet3 vector shown is a lentiviral inducible expression system with gene expression, employed in the production of stable cell lines with 13,057 base pairs (bp) in size.

2.

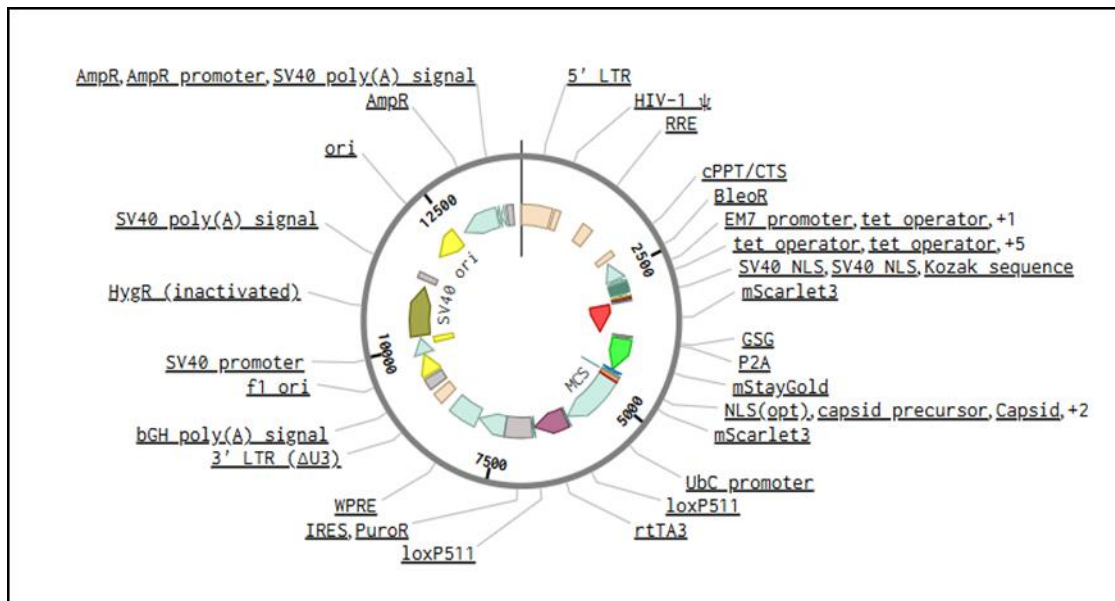


**Figure Appendices 2: pTRIPZ\_3XNLS\_mScarlet3\_DENVpr\_mStayGold Plasmid Map.**

This showed the lentiviral-based reporter construct with fluorescent reporter proteins, which is about 13000bp in size and includes number of aspects essential for regulation, gene expression and selection.

3.

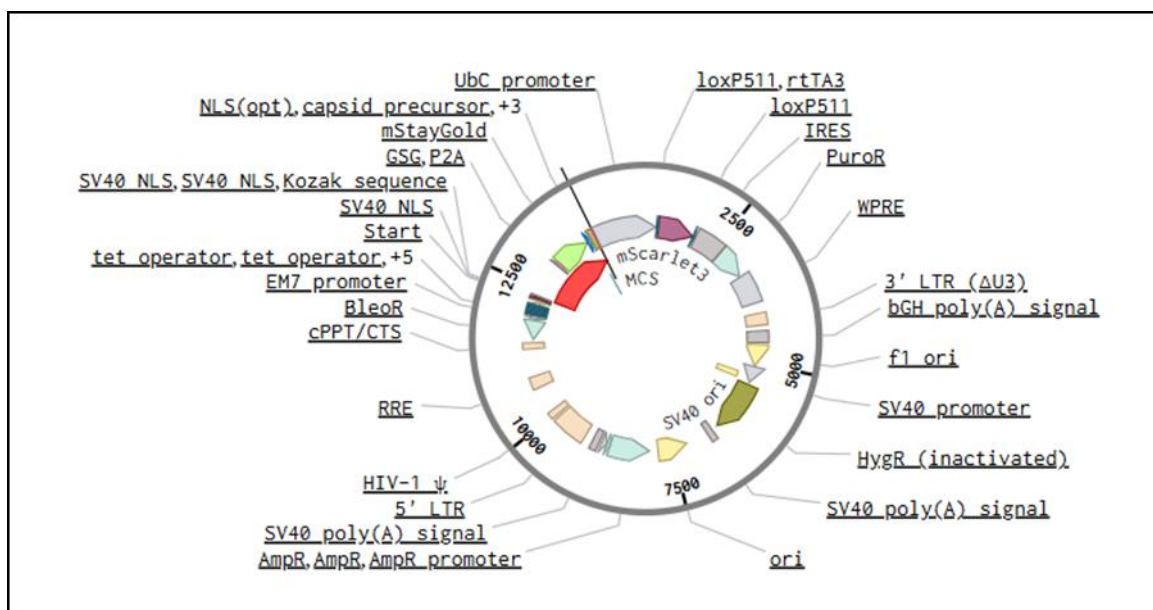


**Figure Appendices 3: pTRIPZ\_3XNLS\_mScarlet3\_WNVpr\_mStayGold Plasmid Map.**

This plasmid map showed the lentiviral expression vector designed for monitoring WNVpr with fluorescent readouts.

4.

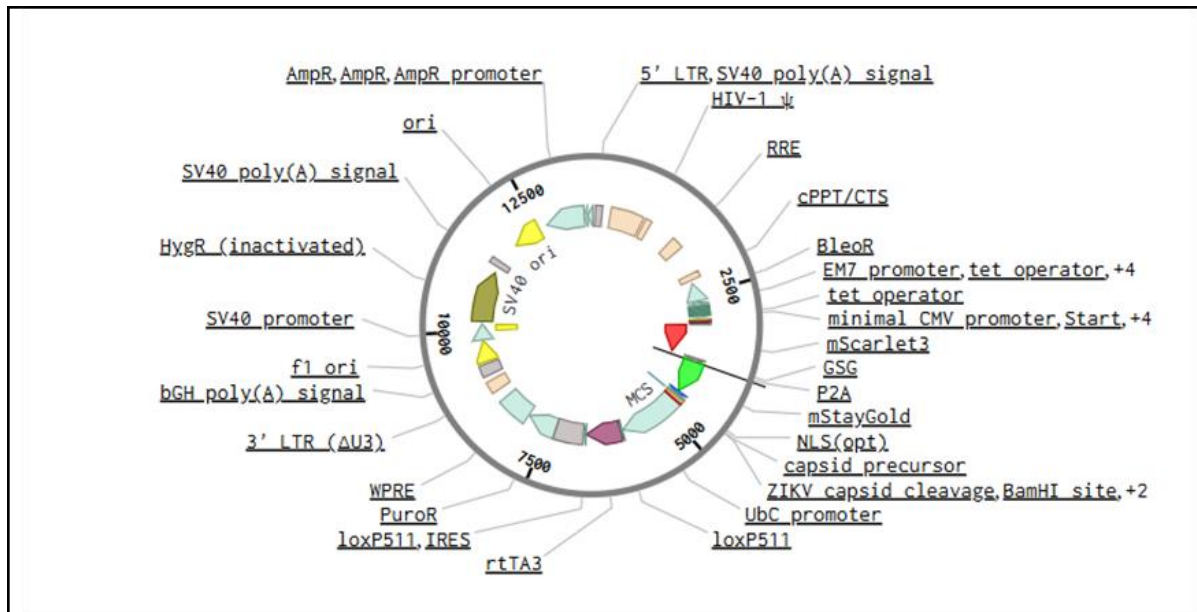


**Figure Appendices 4: pTRIPZ\_3XNLS\_mScarlet3\_ZIKVpr\_mStayGold Plasmid Map.**

A lentiviral vector used to monitor activity of ZIKVpr through redistribution of fluorescent signals and constructed from pTRIPZ plasmid backbone.

5.



**Figure Appendices 5: Nucleotide Alignment for DENV, WNV, and ZIKV capsid cleavage site.** The nucleotide sequences of DENV, WNV, and ZIKV capsid cleavage sites are displayed herein, which are inserted in the reporter construct design and are placed between Multiple Cloning Sites (MCS) and Nuclear Localization Signal (NLS).

6.

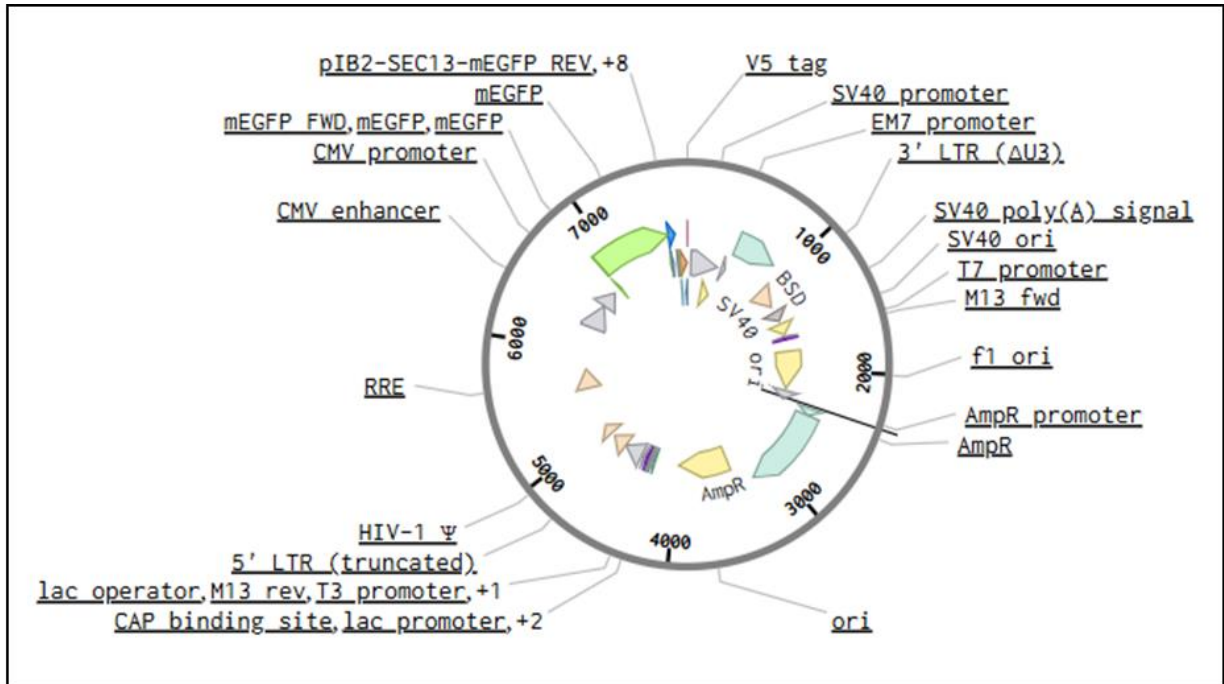


**Figure Appendices 6: Plasmid map of pLenti6\_eGFP\_DENVCapsidCleavage (7755bp).** The map showed the lentiviral expression vector used for eGFP tagged with a recognition site for DENV capsid cleavage. This plasmid vector was used for generating Huh7.5+eGFP\_DENVpr\_pTRIPZ\_3XNLS\_mScarlet3 cell line to detect the activation of viral protease cleavage for eGFP DENV reporter construct.

7.

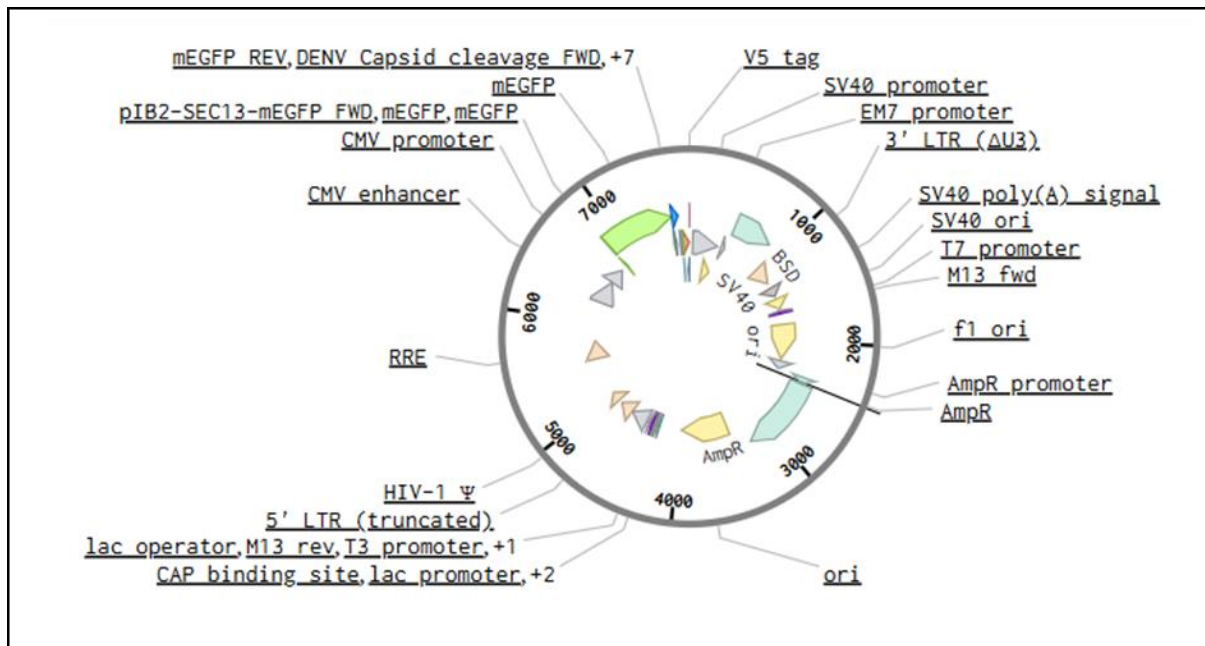


**Figure Appendices 7: Plasmid map of pLenti6\_eGFP\_ZIKVCapsidCleavage (7755bp).**

This lentiviral vector expression construct used for expression of eGFP tagged with a recognition site for ZIKV capsid protease cleavage, allowing detection of ZIKV protease activity in infected cells. This plasmid vector was employed for the construction of Huh7.5+eGFP\_ZIKVpr\_pTRIPZ\_3XNLS\_mScarlet3 cell line to detect the activation of viral protease cleavage for eGFP ZIKV reporter construct.